The Journal of Gemmology

2014 / Volume 34 / No. 4

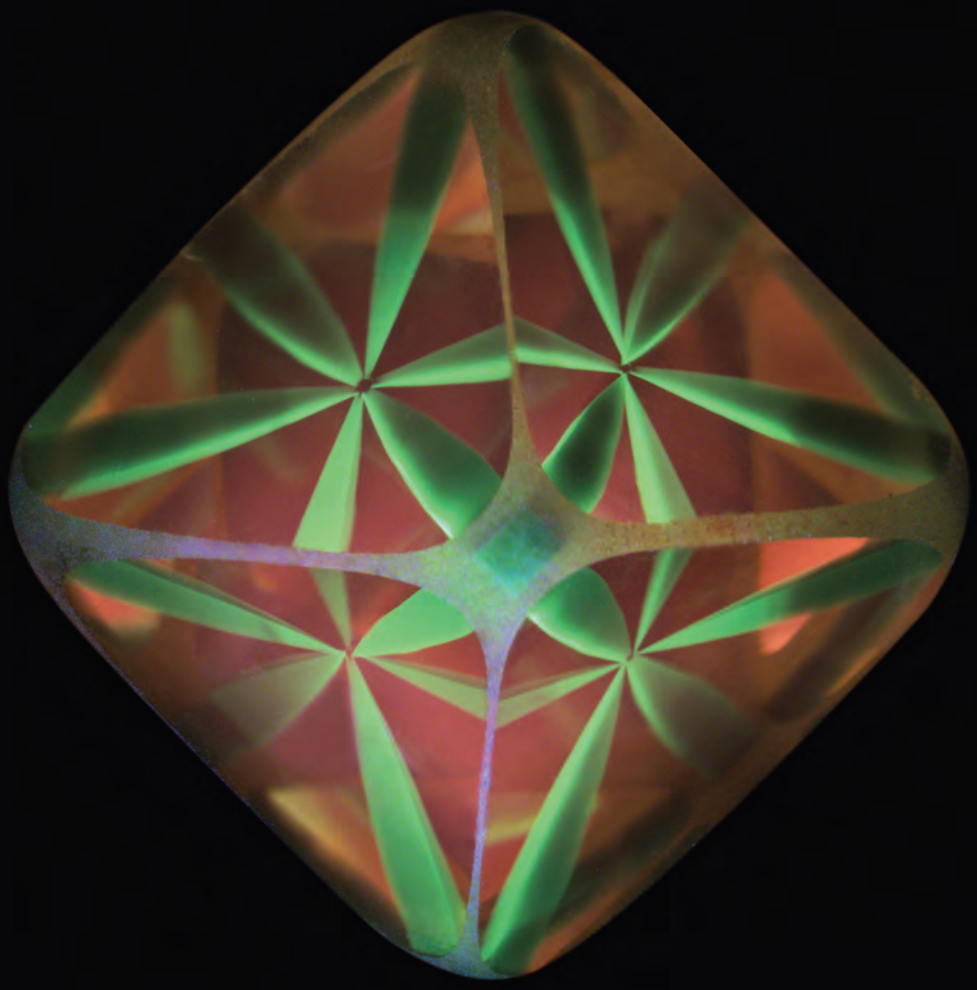

SSEF SCHWEIZERISCHES GEMMOLOGISCHES INSTITUT SWISS GEMMOLOGICAL INSTITUTE INSTITUT SUISSE DE GEMMOLOGIE

Gem-A THE GEMMOLOGICAL ASSOCIATION OF GREAT BRITAIN

The Gemmological Association of Great Britain

Gem-A

THE GEMMOLOGICAL ASSOCIATION
OF GREAT BRITAIN

Polish your knowledge

A good understanding of diamond grading is essential for the buying, selling and trading of diamond. Our **Diamond Diploma** is recognized as one of the most comprehensive and valuable diamond qualifications worldwide — the ultimate education in diamonds. Graduates of our Diamond Diploma can apply for Diamond Membership, allowing you to use the letters 'DGA' after your name — a mark of excellence in the trade.

Sign up now and receive our **NEW** fully illustrated Diamond Diploma course notes — updated to include the most current information and research on diamonds, as well as everything you need to get you started.

For more information or to book contact **education@gem-a.com.**

Understanding Gems

Join us.

The Gemmological Association of Great Britain, 21 Ely Place, London, EC1N 6TD, UK. T: +44 (0) 20 7404 3334 F: +44 (0) 20 7404 8843. Registered charity no. 1109555. A company limited by guarantee and registered in England No. 1945780. Registered Office: 3rd Floor, 1-4 Argyll Street, London W1F 7LD.

The Journal of Gemmology
2014 / Volume 34 / No. 4

COLUMNS

Cover Photo: An 11.38 ct diamond with an asteriated hydrogen cloud is photographed under 250–350 nm broadband UV excitation. See article by Thomas Hainschwang, Franck Notari and Erik Vadaszi on pages 306–315. Photo by T. Hainschwang.

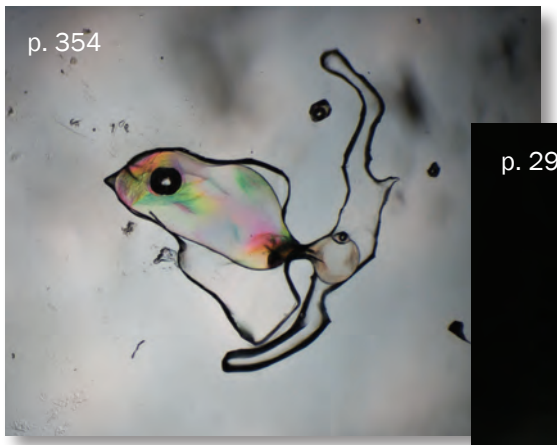

ARTICLES

Feature Articles

Gemmological Brief

The Journal is published by Gem-A in collaboration with SSEF and with the support of AGL and GIT.

ISSN: 1355-4565, http://dx.doi.org/10.15506/JoG.2014.34.4

The Journal of Gemmology

Content Submission

The Editor-in-Chief is glad to consider original articles, news items, conference/excursion reports, announcements and calendar entries on subjects of gemmological interest for publication in *The Journal of Gemmology*. A guide to the preparation of manuscripts is given at www.gem-a.com/publications/journal-of-gemmology.aspx, or contact the Production Editor.

Subscriptions

Gem-A members receive *The Journal* as part of their membership package, full details of which are given at www.gem-a.com/membership.aspx. Laboratories, libraries, museums and similar institutions may become Direct Subscribers to *The Journal* (see www.gem-a.com/publications/subscribe.aspx).

Advertising

Enquiries about advertising in *The Journal* should be directed to the Marketing Consultant. For more information, see www.gem-a.com/publications/journal-of-gemmology/advertising-in-the-journal.aspx.

Copyright and Reprint Permission

The Journal of Gemmology is published quarterly by Gem-A, The Gemmological Association of Great Britain. Any opinions expressed in *The Journal* are understood to be the views of the contributors and not necessarily of the publisher.

Printed by DG3 (Europe) Ltd.

ISSN: 1355-4565

Gem-A
THE GEMMOLOGICAL ASSOCIATION OF GREAT BRITAIN

21 Ely Place
London EC1N 6TD
UK

t: +44 (0)20 7404 3334
f: +44 (0)20 7404 8843
e: information@gem-a.com
w: www.gem-a.com

Registered Charity No. 1109555
Registered office: Palladium House, 1–4 Argyll Street, London W1F 7LD

What's New

INSTRUMENTS AND TECHNIQUES

GemmoFtir

The GemmoFtir, a new Fourier-transform infrared spectrometer developed specifically for gemmological analysis, was unveiled on 1 November 2014 at the Gem-A Conference in London. The instrument uses a gold-coated DRIFT sampling module and employs user-friendly software that follows the manufacturer's philosophy of providing a consistent platform for all of its spectrometer products. The user interface contains easy-to-follow acquisition wizards and includes searchable spectral libraries for important gem species and their color variations. The software also enables interactive peak labelling and features applications for facilitating spectral interpretation. The GemmoFtir was designed and

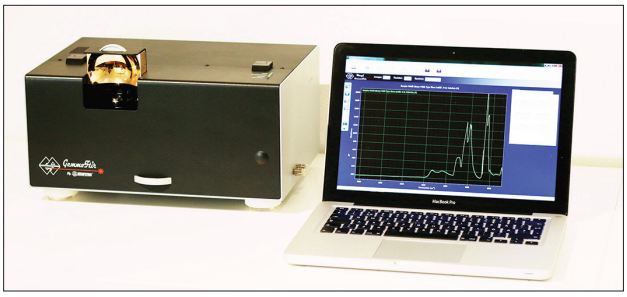

manufactured together with Interspectrum, an Estonian company that has supplied spectrometers for space stations. For more information, visit www.gemmoraman.com/GemmoFtir.aspx.

Alberto Scarani and Mikko Åström
info@gemmoraman.com
M&A Gemological Instruments
Rome, Italy and Järvenpää, Finland

NEWS AND PUBLICATIONS

GSJ Abstracts

Abstract of papers presented at the 2014 Annual Meeting of the Gemmological Society of Japan are available for free download at www.jstage.jst.go.jp/browse/gsj. The website also hosts papers from previous GSJ conferences dating back to 2001.

Making polycrystalline diamond under very high pressure: Synthesis and application of ultrahard nano-polycrystalline diamond (Hime-diamond).

Tetsuo Irifune

Geodynamics Research Center, Ehime University; Earth-Life Science Institute, Tokyo Institute of Technology

We succeeded to synthesize pure polycrystalline diamond by direct conversion from graphite at very high pressure and high temperature using Kawai-type multianvil apparatus (KMA), which was found to be made of nano-sized crystals with peculiar fine textures and have extraordinary high hardness. Thus synthesized nano-polycrystalline diamond (NPD or " Hime-diamond ") has following features in addition to its outstanding hardness: higher fracture toughness, higher thermal resistance, and relatively low thermal conductivity, etc., relative to single crystal diamond. NPD is highly transparent, but exhibits rather yellowish in color due to absorption of optical lights in shorter wave lengths, probably because of grain boundary scattering/absorption of sintered diamond crystals. Application of NPD to various high-pressure apparatus has been attempted in addition to its industrial applications, yielding some promising results particularly in higher pressure generation using diamond anvil cell with relatively large culet size. X-ray absorption studies at high pressure combined with synchrotron radiation, and high pressure generation in multianvil apparatus. The techniques to synthesize NPD are also applied to synthesize high-pressure phases, yielding some novel polycrystalline materials, such as nano-polycrystalline stishovite, nano-polycrystalline cubic BN, and nano- to micro-polycrystalline garnets, some of which are highly transparent and named as "poly-crystalline gems (poly gems). Thus, the KMA has opened a new field of making novel functional

Historical Facet Designs

Year corrected from 2014 to 2013.

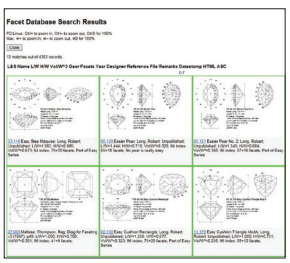

Facet Database Search Results

In June 2013, www.facetdiagrams.org was launched to make a comprehensive collection of faceting diagrams freely available to the hobbyist or professional gem cutter. Users can view nearly 3,900 historical designs that date back to 1902.

ICGL Newsletter

The International Consortium of Gem-Testing Laboratories has released Newsletter No. 4, Fall 2014, available at http://icglabs.org. The theme of the newsletter is sapphire, and it includes reports on HPHT-treated blue sapphires; pink sapphires from Batakundi, Pakistan, showing blue adularescence; cobalt-doped glass-filled blue sapphires; Punsiri-type heat treatment of blue sapphires done in Khambat, India; and heat-treated sapphires from the Nigeria-Cameroon area.

NEWSLETTER
Fall 2014
ISSUE No. 4 / 2014

Appearance of new treatment method on sapphire using HPHT apparatus

By Hyun-min Choi, Sun-kil Kim and Young-chool Kim
Hanmi Gemological Institute & Laboratory (GIGL), Seoul, Korea

Margaritologia Pearl Newsletter

A new pearl newsletter prepared by Elisabeth Strack debuted in October 2014, titled *Margaritologia*. It is intended to cover all aspects of natural and cultured pearls, from their history to new developments, including farming, grading, testing procedures, pricing and market trends. The inaugural issue (No. 1, 2014) focuses on cultured pearls from Vietnam; pearl presentations at the International Gemmological Conference in Hanoi, Vietnam; DNA fingerprinting of pearls; *Spondylus* pearls; cultured pearl necklaces produced by Mikimoto in the 1950s; and a report on an exhibition at the Schwerin Museum in Mecklenburg, Germany. The newsletter is published quarterly, in both English and German, and an annual subscription costs €70. To sign up, visit www.strack-gih.de.

Pearl Presentations

Videos of presentations from pearl forums that took place at the Inhorgenta Munich jewellery show (14–17 February 2014) and the Hong Kong Jewelry & Gem Fair (21 June 2014) are freely downloadable at www.sustainablepearls.org/about-contact/events. In addition, a pearl presentation from an earlier Hong Kong Jewellery & Gem Fair (12 September 2013) is available at www.hinatatrading.com/hongkong.pdf.

Proceedings of the Santa Fe Symposium

Papers from this important conference on jewellery manufacturing technology are available for free download at www.santafesymposium.org/papers/year.html. The most recent Symposium proceedings are from 2013, with earlier papers dating back to 1999.

Silver Jewellery Buying Trends

A survey conducted by National Jeweler on behalf of the Silver Institute's Silver Promotion Service showed very strong sales of silver jewellery in the USA in 2013. The report, released in March 2014, is available at www.silverinstitute.org/site/2014/03/18.

OTHER RESOURCES

Pueblo Gem & Mineral Show Lectures

BlueCap Productions has released audio recordings of presentations given at the 2014 Pueblo Gem & Mineral Show in Tucson, Arizona, USA. The podcasts can be heard directly from the website (www.buzzsprout.com/35310) or downloaded as MP3 files.

What's New provides announcements of new instruments/technology, publications, online resources and more. Inclusion in What's New does not imply recommendation or endorsement by Gem-A. Entries are prepared by Brendan Laurs unless otherwise noted.

Visual Optics and the Birefringence/ Dispersion Ratio of Gemstones

Alan Hodgkinson

Gemmologists are familiar with the concepts of birefringence (the maximum double refraction of a gem material) and dispersion (the difference in the refractive index for red and violet light). The latter optical phenomenon is generally beyond the measuring capability of gemmologists, and yet both of these factors are easily accessible to the unaided eye.

In most anisotropic gems, double refraction is easily seen with a 10× loupe. However, to see its effect at maximum will involve some manoeuvring of the stone, and this can be even more difficult with biaxial gems, where the maximum doubling may not be fully visible depending on the orientation of the optic axes in the faceted gem.

Dispersion (fire) catches the eye unsolicited when we are in the proximity of lead-crystal domestic ware, or light crossing the threshold of a glass panel with a bevelled edge. In a faceted gemstone, dispersion typically is seen as flashes of colour that come from various crown facets. These flashes are seen when the gem, or the light source, is moved. While some gem species have more dispersion than others, there are also situations when two gems of the same identity appear to show contrasting fire—a result of differences in their crown and pavilion facet angles. The size of the facets also has a bearing on the apparent fire of a gemstone, but this is purely subjective: the larger the facet, the greater the width of the spectrum seen. However, the constant measure of dispersion is the length of the spectrum from the red to violet extremities of white light.

There is a simple procedure to evaluate the birefringence and dispersion of a gem without any instrumentation. If a faceted gemstone (loose or mounted) is held with the table facet close to the eye and the culet pointed toward a distinct light source (e.g. a fibre-optic light, penlight, candle or even the moon), the light passes through the stone and enters the eye to register on the retina as an array of spectral images, each one corresponding to a pavilion facet, as for the zircon shown in Figure 1. This procedure I christened 'Visual Optics' (Hodgkinson, 1978). The concept appealed to Dr William Hanneman, and in 1980 he authored an article that explored the method further and introduced the concept of the birefringence/dispersion (B/D) ratio—which is obtained simply by dividing the birefringence by the dispersion. A later article explored the Visual Optics principle in more detail (Hanneman, 1982). The method was later taken up and pursued by Dr Don Hoover (1998), who subsequently collaborated with Trevor Linton to provide an extensive list of dispersion measurements and B/D ratios (Hoover and Linton, 2000; Linton, 2005).

Figure 1: The Visual Optics method was used to produce this trio of doubled primaries from a faceted high-type round-cut zircon, which has a B/D ratio of 1.5. Photo by A. Hodgkinson.

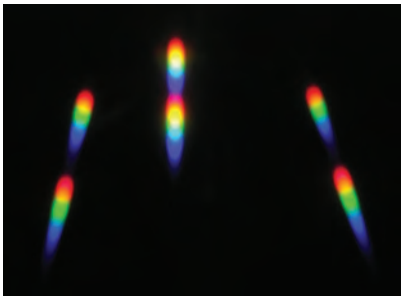

For doubly refractive gemstones, each of the multitude of spectral images seen with Visual Optics will consist of two spectra (corresponding to the birefringent rays) that show various amounts of separation or more commonly superimposition. Double refraction will be evident in some of the images more than in others—seen as a linear separation of the two spectra—dependent on the facet angle to the optic axis. Some will of course be single images, where the direction follows the optic axis.

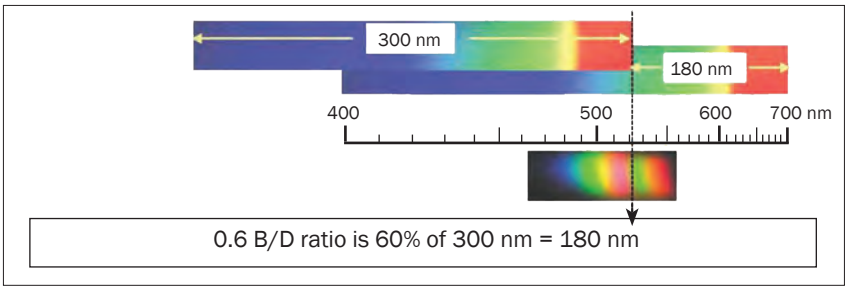

Figure 2: The B/D ratio of quartz is 0.6, which corresponds to the 60% overlap in the doubled primaries seen with Visual Optics. Photo by A. Hodgkinson.

When observing the kaleidoscopic pattern seen with Visual Optics, the B/D ratio is manifested in the widest spacing between the doubled spectral images. For practical purposes, the beginner looks at the gap between the red components of the two images. To see the doubled spectral primary images ('primaries') at their maximum separation, the observer should first locate an image which is obviously doubled, even if the spectral images are partially superimposed. Concentrate on this doubled primary, and then tilt the gem in various directions to coax the doubled primaries to their widest separation. With this spacing, and thus an idea of the B/D ratio, much can be learned instantly in terms of a gemstone's identity, or more commonly, the elimination of possible identities. As this observation can be performed on the spot, wherever the user happens to be (indoors or outdoors), this method provides the gemmologist with useful information—even before reaching for a loupe, which is not always instantly available.

The transparent quartz varieties of amethyst, citrine, smoky quartz and rock crystal are easily accessible to the gemmologist and provide good examples for observing and practising Visual Optics. Figure 2 displays the B/D ratio of quartz (0.6), but what exactly does this number convey? When a faceted quartz is observed with the Visual Optics technique, in no case will the doubled images separate completely. Where doubled, they will always be partially superimposed. By studying one such doubled image and tilting the stone, the partial superimposition will close or open until the B/D ratio 0.6 is seen. This is demonstrated in Figure 2, which shows a photo of a doubled spectral image and the corresponding positions of the superimposed spectra. Bear in mind that the spectral images observed are of a prism format (not a linear diffraction format), as the light has to pass through a faceted gemstone which is an assemblage of prisms. With a B/D ratio of 0.6 (60%), the outer primary spectrum commences at 180 nm (60% of the 300 nm–wide visible spectrum) from the 700 nm red end of the inner spectrum—that is, near the blue-green boundary at 520 nm (700 nm minus 180 nm).

Tourmaline also provides a useful Visual Optic example. With the price escalation of the 'electric' blue and 'neon' green Paraíba-type tourmalines, it is surely useful to have an instant method to check the claimed identity of such a gem—even if it seems an innocent gesture of eyeballing the stone to further enjoy its colour. Dividing the typical tourmaline birefringence (0.02) by its dispersion (0.02), the resultant B/D ratio is 1.0. The significance of this is that when the eye's retina perceives the doubled spectral primary images of a tourmaline at their widest separation, the violet of the inner spectrum of the pair is followed immediately by the red of the outer primary to form a continuous linear repeated spectrum (Figure 3).

Gem dealers initially greeted the amazing Paraíba tourma-

Figure 3: The Visual Optics view of tourmaline shows an outer primary image immediately following the inner primary with no separation or superimposition, corresponding to the B/D ratio of 1.0. The image on the left is from a brightly coloured Paraiba-type gem, while the one on the right is derived from a darker colour-saturated tourmaline (and therefore shows a dimmer outer spectrum that corresponds to the ordinary ray). Photos by A. Hodgkinson.

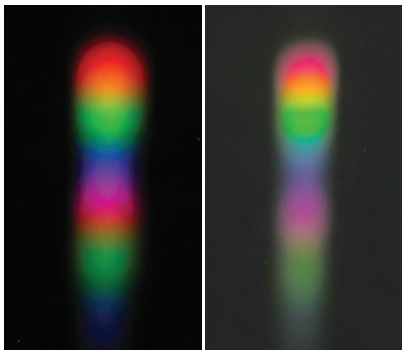

lines with nothing short of incredulity. By an extraordinary quirk of nature, the trade was simultaneously confronted by finds of apatite that showed very similar bright colours (after heat treatment). However the B/D ratio of apatite is very small—with a typical birefringence of 0.003 and dispersion of 0.013, the B/D ratio is only 0.23. This produces a Visual Optic image which is so superimposed that it is quite difficult to see its doubled nature—a problem familiar to the user of a 10× loupe when searching for doubling of the back facets of an apatite.

In all of the darker colour-saturated tourmalines, a further corroboration of the mineral's identity is revealed by the comparative absorption factor of the ordinary and extraordinary rays. The outer image of the spectral pair is the ordinary ray, and it is more heavily absorbed and therefore appears dimmer (Figure 3, right).

The challenge of measuring dispersion explains the rather limited listing of this property in gem reference books. Nevertheless, this 'no-go area' has been vigorously pursued by Hoover and Linton (2000). The measurement of dispersion using a Hanneman/Hodgkinson air refractometer is also described in a forthcoming book by the author titled *Gem Testing Techniques*, due for release mid-2015.

References

Hanneman W.W., 1980. Educating the eyeball—The Hodgkinson Method. *Lapidary Journal,* **34**, 1498–1519.

Hanneman W.W., 1982. Understanding the Hodgkinson Method. *Journal of Gemmology*, **18**(3), 221–228.

Hodgkinson A., 1978. Visual Optics. *Journal of Gemmology,* **16**(5), 301–309.

Hoover D.B., 1998. The Hodgkinson method, a.k.a. the eye and prism method: Some further adaptations. *Australian Gemmologist,* **20**(1), 20–33.

Hoover D.B. and Linton T., 2000. Dispersion measurement with the gemmologist's refractometer. *Australian Gemmologist,* **20**(12), 506–516.

Linton T., 2005. Practical application for measuring dispersion on the refractometer. *Australian Gemmologist,* **22**(8), 330–344.

Alan Hodgkinson FGA DGA is a gemmology instructor and lecturer from Ayrshire, Scotland. E-mail: alan-hodgkinson@talktalk.net

Thank You, Guest Reviewers

The following individuals served as guest reviewers during the past publication year. The editors extend their special thanks to all of them for lending their expertise to reviewing manuscripts submitted to *The Journal*. Together with the Associate Editors, these individuals have enhanced the quality of *The Journal* through their knowledge and professionalism.

Dr Ahmadjan Abduriyim
Gemological Institute of America, Tokyo, Japan

Hai An Nguyen Bui
University of Nantes, France

Frank Notari
GGTL Laboratories, Geneva, Switzerland

Al Gilbertson
Gemological Institute of America, Carlsbad, California, USA

Dr George Harlow
American Museum of Natural History, New York, New York, USA

Alan Hodgkinson
Ayrshire, Scotland

Yoichi Horikawa
Central Gem Laboratory, Tokyo, Japan

Richard W. Hughes
Lotus Gemology Co. Ltd., Bangkok, Thailand

Laura Otter
Johannes Gutenberg-Universität Mainz, Germany

Maggie Campbell Pedersen
Organic Gems, London

Dr Andy H. Shen
China University of Geosciences, Wuhan, P.R. China

Dr William B. 'Skip' Simmons
University of New Orleans, Louisiana, USA

Dr Cédric Simonet
Akili Minerals Services, Lavington, Kenya

Mark H. Smith
Thai Lanka Trading, Bangkok, Thailand

Thomas E. Tashey Jr.
Professional Gem Sciences Laboratory, Chicago, Illinois, USA

Dr Ursula Wehrmeister
Johannes Gutenberg-Universität Mainz, Germany

An innovator in gemstone reporting

• Identification of colored gemstones • Country of origin determination • Full quality and color grading analysis

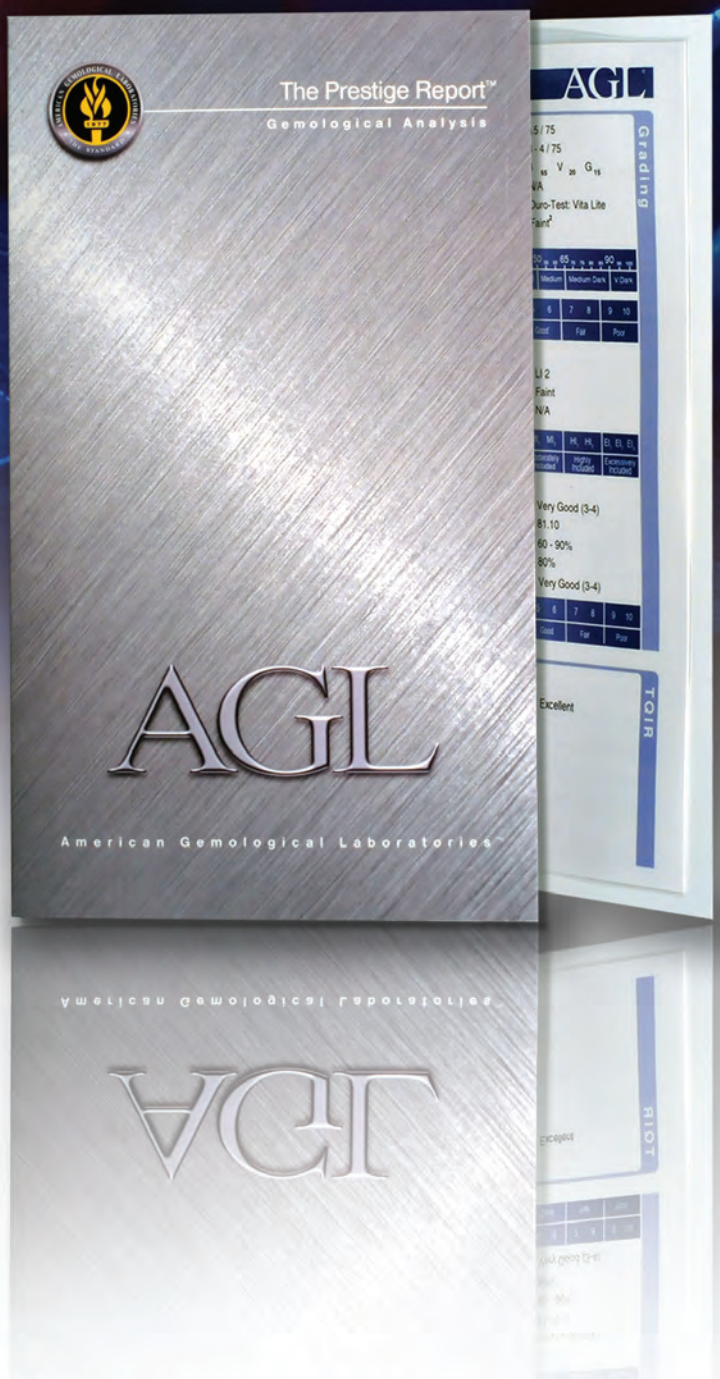

AMERICAN GEMOLOGICAL LABORATORIES AGL

580 5th Ave • Suite 706 • New York, NY 10036, USA
www.aglgemlab.com • +1 (212) 704 - 0727

SSEF

SCHWEIZERISCHES GEMMOLOGISCHES INSTITUT
SWISS GEMMOLOGICAL INSTITUTE
INSTITUT SUISSE DE GEMMOLOGIE

ORIGIN DETERMINATION · TREATMENT DETECTION

DIAMOND GRADING · PEARL TESTING

EDUCATION · RESEARCH

THE SCIENCE OF GEMSTONE TESTING©

Aeschengraben 26, CH-4051 Basel, Switzerland Tel. +41 61 262 06 40 Fax + 41 61 262 06 41 admin@ssef.ch www.ssef.ch

Gem Notes

COLOURED STONES

Almandine from Erving, Massachusetts

At the Springfield Gem and Mineral Show (Massachusetts, USA) in August 2014, a new production of almandine debuted (see, e.g., www.minerals.net/news/post/2014/09/11/Garnet-from-Red-Embers-Mine-Erving-MA.aspx). The garnets were mined from an area near Erving, Massachusetts, by Jason Baskin of Jay's Minerals (Flemington, New Jersey). Currently named the Red Embers mine, Baskin has been secretly working the deposit with hand tools since 2008. Baskin has heard that a major retailer of fine coloured stone jewellery once sourced garnets from this deposit around the turn of the 20th century, but this has yet to be confirmed. The authors first viewed these garnets in 2009, but due to confidentiality agreements with the owner of the property, no announcements could be made at that time.

According to Baskin, mining these garnets will 'leave their mark' on you. The almandine is hosted by a layer of biotite-graphite schist, and Baskin wears a protective suit (Tyvek; see Figure 1) during the digging process since everything gets coated with a dark, slick layer of graphite. This tough and dirty work would thwart most hobbyist prospectors.

Figure 1: At the Red Embers mine, Jason Baskin wears a Tyvek suit while digging for garnets within graphite-rich schist. Courtesy of Red Embers Mining.

Much of the garnet production consists of attractive mineral specimens (e.g. Figures 2 and 3). Baskin prepares the specimens by carefully removing the matrix from both sides of garnet-bearing schist slabs using an air abrasion tool equipped with plastic media. Light can then be transmitted through the garnets to show their deep red colour (Figure 3). Indeed, with proper lighting one can see how appropriate the 'Red Embers' name is. Most of the specimens contain multiple garnets, while some feature only a single crystal; the largest garnet found to date measures 21.36 mm in diameter. Embedded along the foliation within the graphite of some of the specimens (e.g. Figure 2) are dark needles that have been identified as dravite. Gems up to 4.74 ct (Figure 4) have been faceted from the garnets, although most are less than 0.80 ct (5.5 mm in diameter). Numerous stones have been cut into calibrated sizes.

Eight mineral specimens and 28 cut samples (0.20–4.74 ct) were examined for this report. The faceted material showed a saturated red colour, with faint brown tones seen in some of the gems; none exhibited bluish tones. RI was over the limit of the refractometer, but based on other measured properties, it is estimated at just over 1.81 (cf. Hoover et al., 2008). SG was measured hydrostatically as 4.24, and the magnetic susceptibility of these garnets was determined by D. Hoover as 32.8 SI (see Hoover et al., 2008, for an explanation of magnetic data). Raman spectroscopy indicated the garnet to be predominantly almandine with some spessartine and minor pyrope components. Chemical analysis by energy-dispersive X-ray fluorescence (EDXRF) spectroscopy showed a

Figure 2: This slab of graphite schist (10 × 8 cm) from the Red Embers mine contains several almandine crystals and dravite needles. Photo by B. Williams.

Figure 3: Transmitted lighting shows the ember-like appearance of the garnets in this multi-crystal specimen (16 × 11 cm). Photo by B. Williams.

Figure 4: The largest almandine cut to date from the Red Embers mine is this 4.74 ct round brilliant. The other cut stone (5 mm in diameter) displays the red colour typical of most of the smaller faceted stones. Photo by B. Williams.

high Fe content, consistent with almandine. There was also significant Mn and a minor amount of Ca. However, Mg (being a relatively light element) was below the detection limit of the instrument. Crystal inclusions were plentiful in many of the stones, and although they were not positioned where they could be identified by Raman analysis, most appeared to be apatite, with dark mica (probably biotite) also present. The results obtained from the current samples matched those of the specimens we first examined five years ago.

While the cut stones provided good material for gem testing and inclusion observations, it was the matrix specimens that were our favourite. The red glow of the garnets against the matte silver of the biotite-graphite schist makes for very attractive display pieces, especially when multiple crystals are present.

Cara and Bear Williams (info@stonegrouplabs.com)
Stone Group Laboratories
Jefferson City, Missouri, USA

Reference

Hoover D.B., Williams C., Williams B. and Mitchell C., 2008. Magnetic susceptibility, a better approach to defining garnets. *Journal of Gemmology*, **31**(3/4), 91–103, http://dx.doi.org/10.15506/jog.2008.31.3.91.

Observations of Pegmatitic Amethyst from São Paulo State, Brazil

In many parts of the world, construction can be halted by the discovery of ancient ruins or burial sites. In July 2006, during road construction in a rural area of southern São Paulo State in Brazil, an interruption occurred for a different reason—the discovery of a rich deposit of amethyst hosted by granitic pegmatites (see www.cprm.gov.br/publique/media/evento_1776.pdf). The site was rapidly overtaken by *garimpeiros* (Brazilian artisanal miners), causing the government to close the area, which lies approximately 90 km from the city of São Paulo. Due to the local poor economic conditions, the deposit may be reopened to the miners in the future as a potential source of income. However, environmental legislation would require that any future digging be done in a responsible manner.

Recently submitted for analysis by George Williams, a senior buyer for Jewelry Television (Knoxville, Tennessee, USA), was a selection of 39 amethyst gemstones reportedly obtained from this locale. Several of them were quite large, weighing more than 100 ct (e.g. Figures 5 and 6). Standard gemmological testing yielded results that were expected for single-crystal quartz (RI of 1.543–1.552 and hydrostatic SG of 2.65). The samples were a medium strong purple, and straight and angular colour zoning was prominent when they were viewed in certain orientations (Figure 6), which is not unusual for amethyst. No twinning was seen in the samples, which is consistent with the reported pegmatitic origin (Guzzo, 1992). Viewed with darkfield illumination, some of the stones contained numerous, evenly spaced, undulating dotted lines of fluid droplets that were oriented in various directions (Figure 7). Of the 39 stones examined, all but seven contained these inclusions. While fluid inclusions are common in all varieties of quartz, this type and arrangement has not been previously observed by the authors, and a literature search did not reveal any such inclusions in amethyst.

The presence of abundant molecular H_2O was detected with Fourier-transform infrared

Figure 5: These large amethysts (113.79 and 114.15 ct) are from southern São Paulo State in Brazil. Photo by B. Williams.

Figure 6: Straight and angular colour zoning is evident in this 113.79 ct São Paulo amethyst. Photo by B. Williams.

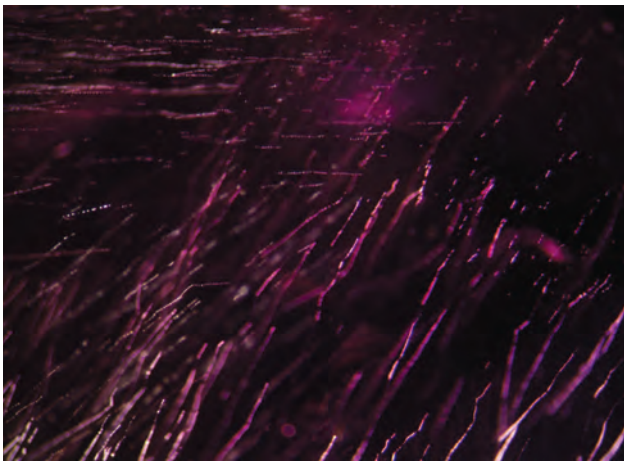

Figure 7: Undulating dotted lines of fluid inclusions such as these were present in most of the São Paulo amethysts examined. Photomicrograph by B. Williams; magnified 35×.

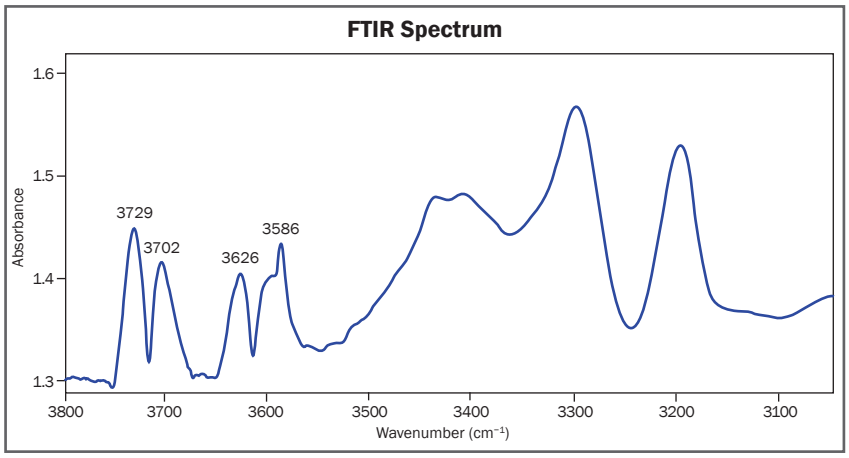

Figure 8: FTIR spectroscopy showed an unusually high water content in the amethyst. The four bands in the 3750–3550 cm^{-1} region correspond to molecular H_2O within the fluid inclusions of this pegmatitic amethyst.

spectroscopy (FTIR; see Figure 8, cf. Fukuda, 2012). This water was trapped in the fluid inclusions described above.

Determining provenance for any material as plentiful and diverse as amethyst is problematic at best, but the unusual fluid inclusions could help differentiate material from this São Paulo locality. In addition to these inclusions, the pegmatitic origin of this amethyst makes it an interesting gem for collectors.

Cara and Bear Williams

References

Fukuda J., 2012. Water in rocks and minerals—Species, distributions, and temperature dependencies. In T. Theophanides, Ed., *Infrared Spectroscopy—Materials Science, Engineering and Technology*, InTech, Rijeka, Croatia, 77–96, http://tinyurl.com/ma8yw89.

Guzzo P.L., 1992. Characterization of the Structures, Impurities and Defects Centers Related to Al and OH in Natural Quartz. PhD dissertation, Mechanical Engineering Department, University of Campinas, Brazil.

Apatite from Kenya

In September 2013, gem dealer Dudley Blauwet (Dudley Blauwet Gems, Louisville, Colorado, USA) received a 35.1 g parcel of rough green apatite from his supplier in Nairobi. The material was obtained from local dealers who confirmed that it came from the Machakos area in south-central Kenya, but did not want to give more specific location information to protect their source. The parcel consisted of 39 pieces, and after cutting Blauwet obtained 54 stones totalling 30.93 carats that ranged from 0.10 to 3.78 ct each.

Blauwet loaned two of the apatites (1.28 and 3.78 ct; Figure 9) to this author for examination. Their colours were a medium-dark to dark, moderately strong, slightly yellowish green. Refractive indices varied between 1.638 and 1.644, with a birefringence of 0.003–0.005, and the hydrostatic SG of both stones was 3.17. These values are consistent with apatite. Both stones showed remarkably strong dichroism, in bluish green and greenish yellow. No fluorescence was observed under UV radiation, and neither stone showed any well-defined features when viewed with a prism spectroscope. They were moderately included, with growth tube–like inclusions oriented parallel to the c-axis that looked

Figure 9: These apatites (3.78 and 1.28 ct) are reportedly from Kenya. Photomicrograph by Dirk van der Marel.

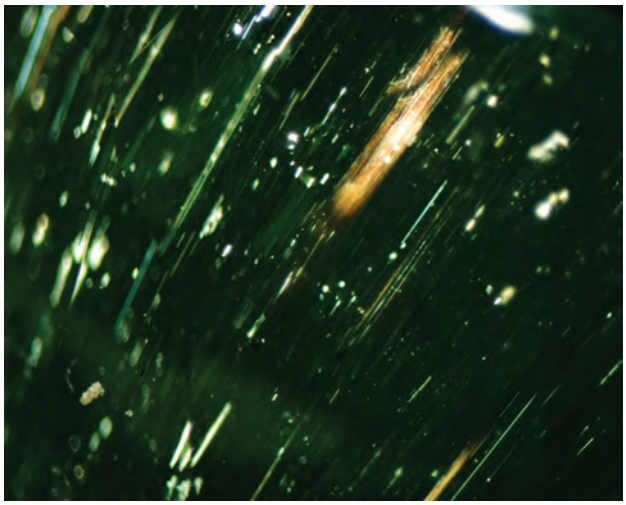

Figure 10: The Kenyan apatites contain long tube-like inclusions that show red-brown reflections in certain orientations. Photomicrograph by J. C. Zwaan; image width 3.5 mm.

transparent or brownish in transmitted light, and in certain directions produced bright red-brown reflections (Figure 10). Oriented at 120° to these features were shorter tubes and long prismatic mineral inclusions. None of the inclusions could be identified by Raman spectroscopy due to the strong fluorescence generated by the apatite when excited by the laser. However, Raman spectra of the host gemstone did give close matches with reference spectra for fluorapatite, $Ca_5(PO_4)_3F$.

EDXRF spectroscopy showed Ca and P as the main elements, and also revealed traces of Mn (~0.1 wt.% MnO) and Fe (~0.05 wt.% FeO). FTIR spectroscopy recorded a relatively weak but significant band at about 3550 cm^{-1} (Figure 11), which indicated the presence of some hydroxyl groups (OH). It is known that varying percentages of F can be replaced by OH in fluorapatite (Shi et al., 2003; Rodrigo, 2005). The presence of a band at 3540 cm^{-1} confirms that the main crystal structure corresponds to fluorapatite with trace substitutions of hydroxyl groups (OH-F pairs), while a small but clear band at 3494 cm^{-1} indicates minor replacement of Cl by OH (Tacker, 2004). Hydroxyl groups of pure hydroxyapatite (OH-OH pairs) show a peak at 3573 cm^{-1} (e.g. Rodrigo, 2005). In the present apatites, the position of the main peak at 3550 cm^{-1}—which is also seen in fluorapatite from other localities (e.g. Durango, Mexico, and Tamil Nadu, India)—could be due to a combination of OH-F with the edges of the OH-OH peak, which shifts the apparent maximum from 3540 cm^{-1} to higher wavenumbers (cf. Tacker, 2004).

J. C. (Hanco) Zwaan (hanco.zwaan@naturalis.nl)
National Museum of Natural History 'Naturalis'
Leiden, The Netherlands

References

Rodrigo C.P., 2005. Synthesis and Characterization of Strontium Fluorapatite. M.Sc. thesis, University of Nevada, Las Vegas, USA, 63 pp.

Shi J., Klocke A., Zhang M. and Bismayer U., 2003. Thermal behavior of dental enamel and geologic apatite: An infrared spectroscopic study. *American Mineralogist*, **88**, 1866–1871.

Tacker R.C., 2004. Hydroxyl ordering in igneous apatite. *American Mineralogist*, **89**, 1411–1421.

Figure 11: FTIR spectroscopy of both stones indicated that they are fluorapatite, with a diagnostic peak at 3550 cm^{-1}, mainly indicating replacement of F by OH, and a minor peak at 3494 cm^{-1}, showing that some Cl has been replaced by OH.

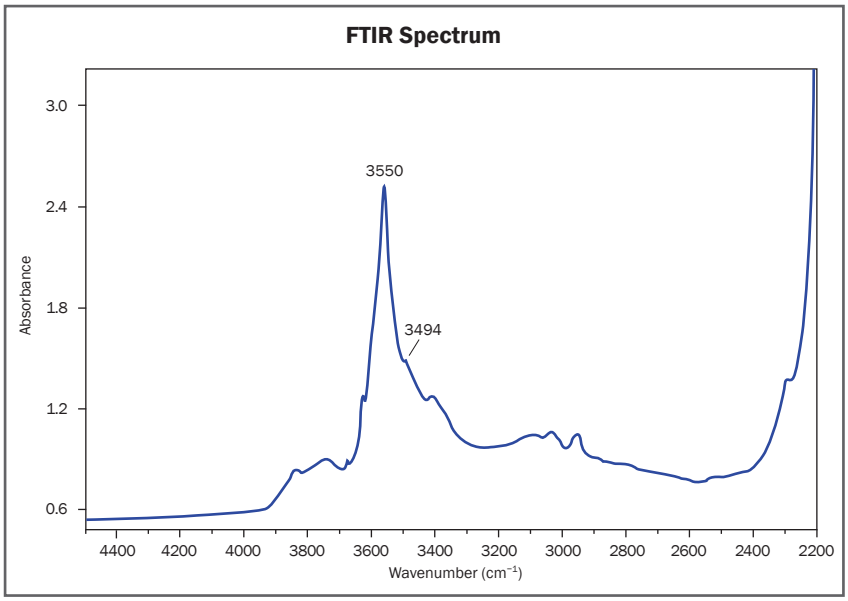

Colourless to Near-colourless Diopside from Canada and Kenya

Diopside, a calcium-magnesium clinopyroxene ($CaMgSi_2O_6$) and Mg-rich end-member of the diopside-hedenbergite series (Deer et al., 2013), is rather unusual as a gem material. It is commonly greenish brown (mostly due to iron impurities) to dark brown (typically as cabochons displaying asterism), but its most attractive gem variety is emerald-green Cr-diopside from Russia.

Gem-quality colourless to near-colourless (thus chemically rather pure) diopside has been described from the Mogok Stone Tract in Myanmar (Themelis, 2008), Tanzania (Milisenda and Wehr, 2009) and Kenya (Renfro and Shen, 2012), in rather small sizes (generally <2 ct). These gems reportedly formed in contact-metamorphosed Ca-rich sediments (e.g. skarns) and silica-enriched marbles (Themelis, 2008; Deer et al., 2013).

Recently the author had the opportunity to examine five samples of colourless diopside from an additional locality—Canada—and compare them to some from Kenya (e.g. Figure 12). The samples were supplied by gem dealer Brad Payne (The Gem Trader, Cave Creek, Arizona, USA). He obtained the Canadian samples at the 2014 Tucson gem shows in Arizona, USA, from Brad Wilson (Coast-to-Coast Rare Stones International, Kingston, Ontario, Canada). Wilson stated that the gems were cut from old rough material that was mined more than 20 years ago in Cawood, Quebec. He had around 20–30 carats of cut stones in the 0.25–1.5 ct range. The Kenyan samples were selected by Payne at the 2010 Tucson gem shows from approximately 100–200 faceted pieces that mostly weighed less than 0.50 ct (larger stones were rather included).

Analysed for this report were two stones from Canada (0.64–0.91 ct) that were absolutely colourless, and three samples from Kenya (0.13–0.25 ct) that were very pale yellow. Raman analyses of all five samples revealed spectra that perfectly matched our diopside references. The properties measured for one sample each from Canada (0.91 ct) and Kenya (0.25 ct) fit well with reported values in the literature (Deer et al., 2013): RIs of 1.667–1.695 and 1.670–1.695, birefringence of 0.028 and 0.025, and hydrostatic SG of 3.28 and 3.30, respectively. The properties obtained for the Kenyan sample were consistent with those reported by Renfro and Shen (2012). The EDXRF chemical compositions of the two samples showed slight differences in Fe content (0.24 wt.% FeO in the colourless Canadian diopside and 0.40 wt.% FeO in the very pale yellow Kenyan sample; Table I). The Canadian diopside contained a marked concentration of Na (2.23 wt.% Na_2O), but this element was below the detection limit in the Kenyan sample.

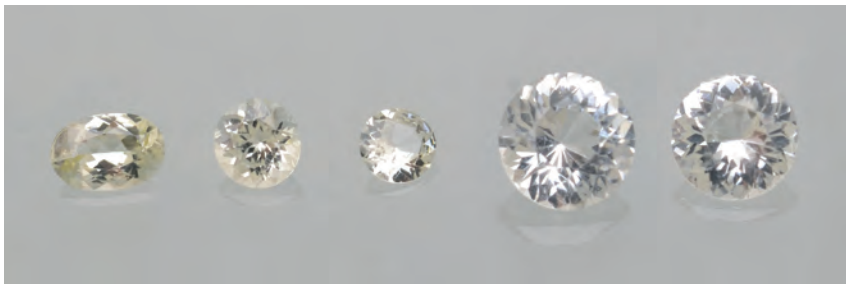

Figure 12: Studied for this report were these three near-colourless diopsides from Kenya (0.25, 0.24 and 0.13 ct from left to right) and two colourless diopsides from Canada (0.91 and 0.64 ct). The slightly higher Fe concentration in the samples from Kenya is responsible for their very pale yellow colour. Photo © M. S. Krzemnicki, SSEF.

*Table I: Chemical composition of the analysed diopside samples.**

Location	Kenya	Canada
Weight (ct)	0.25	0.91
Colour	Very pale yellow	Colourless
Long-wave UV	Inert	Orange
Oxide (wt.%)		
SiO_2	47.4	47.0
TiO_2	0.11	0.08
MgO	22.9	23.3
MnO	0.01	0.05
FeO	0.40	0.24
CaO	28.7	26.7
Na_2O	nd	2.23
K_2O	0.08	0.07
Total	**99.6**	**99.7**

* V and Cr were analyzed for, but not detected. Abbreviation: nd = not detected.

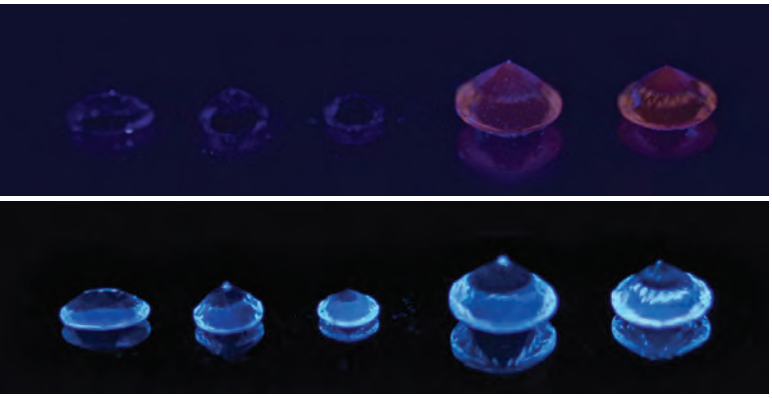

Figure 13: The three samples from Kenya (left side) and the two larger diopsides from Canada (right side) are shown under long-wave (top image) and short-wave (bottom image) UV radiation. The orange reaction of the Canadian diopsides under long-wave UV is quite marked. Photos © M. S. Krzemnicki, SSEF.

Microscopically, all five investigated samples contained a few tiny fluid inclusions and partially healed fissures ('fingerprints'). One of the Canadian specimens additionally had some slightly curved hollow tubes. All samples showed a characteristic strong doubling effect under the microscope due to their high birefringence.

Interestingly, the studied diopsides from these two different localities showed distinctly different reactions to long-wave UV radiation (Figure 13). The samples from Canada exhibited a distinct orange reaction, whereas those from Kenya were inert. This difference in fluorescence was also noted in their PL spectra (taken with 514 nm laser excitation); the sample from Canada had a distinct and broad PL band centred at about 580 nm (Figure 14). When exposed to short-wave UV radiation, all of the samples showed an equally bluish white reaction. This observation of varying UV reactions for diopside has been previously reported in the literature (Henkel, 1988–1989). In this case, however, this property allows a quick separation of these diopsides from Kenya and Canada. Nevertheless, not all Kenyan diopside shows the same fluorescence: the colourless samples studied by Renfro and Shen (2012) fluoresced a strong chalky greenish yellow to short-wave UV radiation and were inert to long-wave UV.

Michael S. Krzemnicki (michael.krzemnicki@ssef.ch)
Swiss Gemmological Institute SSEF
Basel, Switzerland

References

Deer W.A., Howie R.A. and Zussman J., 2013. *An Introduction to the Rock-forming Minerals*, 3rd edn. The Mineralogical Society, London, 510 pp.

Henkel G., 1988–1989. The Henkel glossary of fluorescent minerals. *Journal of the Fluorescent Mineral Society*, **15**, 91 pp.

Milisenda C.C. and Wehr K., 2009. Gemmologie Aktuell: Kornerupine and diopside from Tanzania. *Gemmologie: Zeitschrift der Deutschen Gemmologischen Gesellschaft*, **58**(3/4), 78–80.

Renfro N. and Shen A.H., 2012. Gem News International: Diopside from Kenya. *Gems & Gemology*, **48**(1), 63–64.

Themelis T., 2008. *Gems & Mines of Mogok*. Self-published, 352 pp.

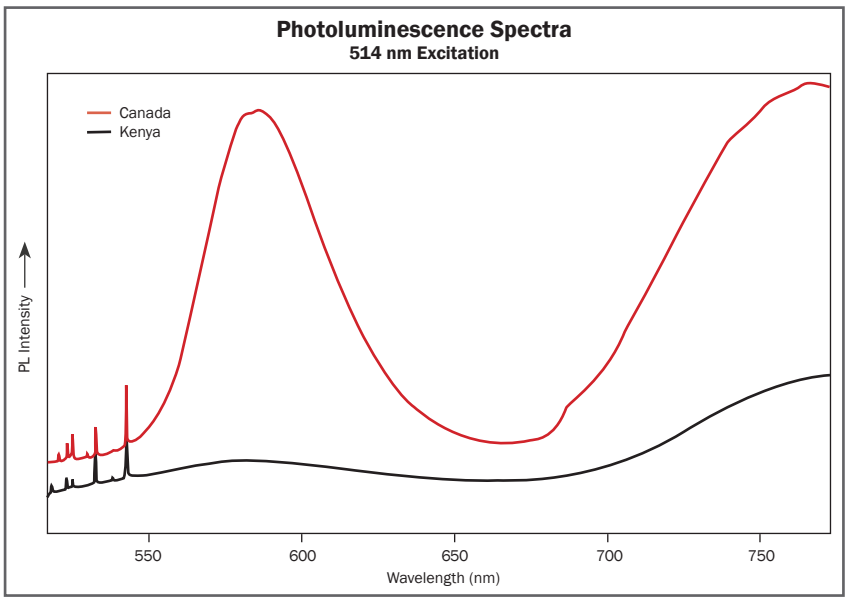

Figure 14: PL spectra (using 514 nm laser excitation) of two selected diopsides from Kenya and Canada show distinct differences. The Canadian diopside has a strong PL band (at about 580 nm), whereas the sample from Kenya exhibits only very weak PL emission.

Hessonite from Somalia

Somalia is not often reported as a source of gem materials, although small amounts of beryl (emerald and aquamarine), quartz and pyrope are known from there (Eliezri and Kremkow, 1994). Recently, another gem was found there—hessonite. According to gem dealer Dudley Blauwet, his supplier encountered the rough garnet in July or August 2011 in Nairobi, Kenya, where there is a large population of Somalis. He obtained about 10 pieces of rough ranging from orange to 'honey'-tan to red-brown, and Blauwet had them faceted into stones weighing 0.18–1.05 ct. His supplier is not aware of any additional production of this garnet.

Figure 15: This 1.05 ct hessonite, reportedly from Somalia, shows an attractive orange colour and good transparency. Photo by Bilal Mahmood.

Blauwet loaned a 1.05 ct orange faceted hessonite (Figure 15) to the American Gemological Laboratories for examination. The RI of 1.741 and faint band at 430 nm in the absorption spectrum were consistent with grossular (Stockton and Manson, 1985). This identification was confirmed by FTIR and EDXRF spectroscopy. Microscopic examination showed small flake-like inclusions as well as transparent needle-like and tabular crystals. The roiled appearance that is typical of some hessonite was not obvious in this sample.

It is always interesting to see gem varieties that reportedly come from new sources, and this hessonite from Somalia is no exception.

Bryan Clark (bclark@aglgemlab.com)
American Gemological Laboratories
New York, New York, USA

References

Eliezri I.Z. and Kremkow C., 1994. The 1995 ICA world gemstone mining report. *ICA Gazette*, December, pp. 1, 12–19.

Stockton C.M. and Manson D.V., 1985. A proposed new classification for gem-quality garnets. *Gems & Gemology*, **21**(4), 205–218, http://dx.doi.org/10.5741/gems.21.4.205.

Polycrystalline Kyanite from Tanzania

Recently the Swiss Gemmological Institute SSEF received two samples of a blue translucent material from Tanzania for examination (Figure 16). They consisted of a sawn waterworn pebble and a 1.72 ct faceted stone that was cut from the same piece. The pebble was obtained by gem dealer Farooq Hashmi in December 2013 while on a buying trip in Arusha. The person who sold him the stone was unaware of its identity, but noted that it was very hard.

Testing of both samples revealed an anisotropic polycrystalline optic character (i.e. always bright in the polariscope). As a consequence of this, it was difficult to obtain a precise RI value on the refractometer; the faceted sample showed an indistinct reading of approximately 1.72. SG was

Figure 16: These translucent blue samples proved to be polycrystalline kyanite. The sawn pebble (7.48 ct) is what remains after cutting of the pear-shape gem (1.72 ct). Photo © M. S. Krzemnicki, SSEF.

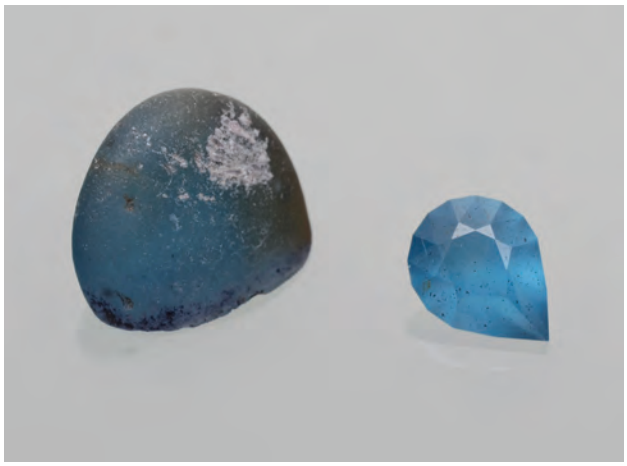

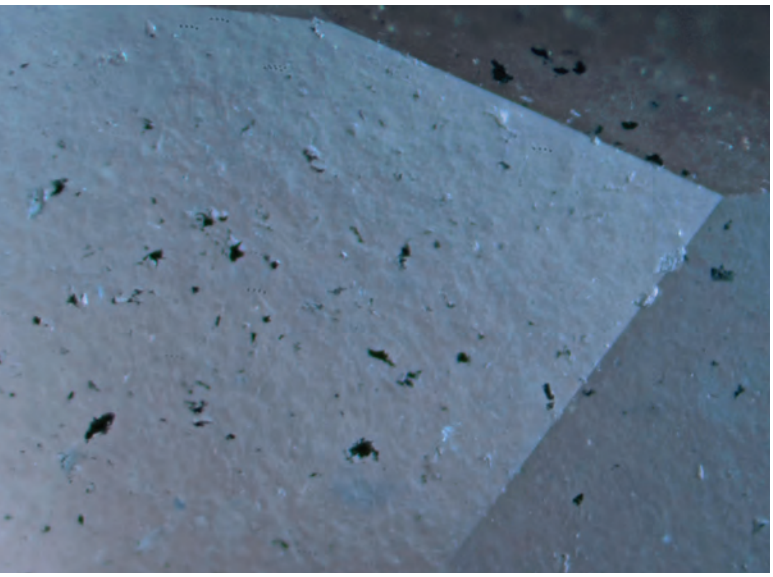

Figure 17: Viewed with the microscope, the faceted polycrystalline kyanite showed a treacle-like appearance and numerous black residues of polishing powder in small cavities on the polished surface. Photomicrograph © M. S. Krzemnicki, SSEF; magnified 60×.

determined to be 3.67 for both samples using a hydrostatic balance. They were inert to long- and short-wave UV radiation. Since the identity of the material was still not evident after this initial testing, it was analysed by Raman spectroscopy, which revealed a distinct kyanite spectrum. This identification was also in agreement with the RI and SG values. Chemical analysis confirmed that it was kyanite, showing Al and Si as main constituents, with small amounts of Fe and Ti, as well as traces of Cr, V, and a few alkaline earths. The blue colour of kyanite is most commonly linked to intervalence charge transfer of Ti^{4+}-Fe^{2+} (elements present in this sample) through the replacement of two Al^{3+} ions on adjacent crystal sites (Platonov et al., 1998; Henn and Schollenbruch, 2012; Krzemnicki, 2013); this mechanism is also well known in blue sapphire.

Microscopic observation revealed an interesting treacle-like appearance (Figure 17), similar to polycrystalline hessonite, created by an abundance of tiny fluid inclusions along kyanite grain boundaries. As a consequence of its microgranular nature and the directional hardness of kyanite, polishing of this material obviously was quite difficult, resulting in numerous black accumulations of polishing powder in small cavities on the surface of the faceted stone (again, see Figure 17).

To the author's knowledge, this is the first time that polycrystalline kyanite of gem quality has been reported. Hashmi has not encountered any other examples of this material on previous or subsequent buying trips.

Michael S. Krzemnicki

References

Henn U. and Schollenbruch K., 2012. Saphirblauer Disthen (Kyanit) aus Nepal. *Gemmologie: Zeitschrift der Deutschen Gemmologischen Gesellschaft*, **61**(3-4), 91–98 (in German).

Krzemnicki M., 2013. Some uncommon sapphire "imitations": Blue Co-zirconia, kyanite & blue dumortierite. *Journal of the Gemmological Association of Hong Kong*, **34**, 62–64.

Platonov A.N., Tarashchan A.N., Langer K., Andrut M., Partzsch G. and Matsyuk S.S., 1998. Electronic absorption and luminescence spectroscopic studies of kyanite single crystals: Differentiation between excitation of FeTi charge transfer and Cr^{3+} dd transitions. *Physics and Chemistry of Minerals*, **25**(3), 203–212, http://dx.doi.org/10.1007/s00269 0050104.

Green Daylight-Fluorescent Hyalite Opal from Mexico

At the 2014 Tucson gems shows, some interesting rough specimens of transparent hyalite opal from Mexico entered the market (Moore, 2014). The material shows noticeable green fluorescence in daylight (e.g. Figures 18 and 19-left), but when viewed in incandescent light there is almost no body colour (Figure 19-right). Although production of this opal is quite limited, one of the authors (PM) obtained several pieces of rough material, and five faceted stones ranging from 0.83 to 3.84 ct were cut by Michael Gray of Coast-to-Coast Rare Stones, Fort Bragg, California. In October 2014, author PM visited the opal deposit in the mountains of western Zacatecas State (Figure 20) and obtained more material from the miners. The opal occurs as botryoidal coatings or crusts within iron oxide-filled fractures cutting a quartz-rich devitrified rhyolite welded tuff.

Twelve rough specimens and three faceted stones (0.83–1.81 ct) were examined by one of us (EF). RI was approximately 1.45 (measured with white light), and hydrostatic SG ranged from 2.12 to 2.16; these values are typical for opal. The absorption-related body colour was light to very light yellow (near-colourless). When properly faceted, the gem may concentrate the daylight fluorescence to display a brilliant green appearance. The green emission is much less noticeable in weak lighting and in incandescent light. A UV lamp causes intense green luminescence, generally slightly brighter in short-wave than long-wave, which is also classic behaviour for opal.

Raman spectra of 10 samples were collected using a Bruker RFS100 Fourier-transform Raman spectrometer equipped with a 1064 nm near-infrared Nd:YAG laser (400 mW power), at a resolution of 4 cm^{-1}. The main feature was a broad band with an apparent maximum at about 450 cm^{-1}, indicating that the material is opal-A (*A* for amorphous). Narrower bands were present at approximately 1550, 1075, 975 and 790 cm^{-1}, all characteristic of opal (Ostrooumov et al., 1999). However, this material has a very different appearance from typical opal-A from Australia. The transparency and botryoidal morphology indicate that it is most likely opal-AN (i.e. amorphous with a network- or glass-like structure). Often called hyalite in gemmology, this is probably the rarest gem opal variety.

A Horiba Jobin-Yvon FluoroLog-3 spectrofluorimeter was used to gather both emission and excitation spectra of three opal samples. The green luminescence is a typical uranyl emission, with a wide band that extends from about 400 nm (end of the blue range) to slightly past 600 nm (red region). There were four maxima, with the strongest at about 524 nm (in the green region, as expected).

Figure 18: This specimen (4 cm tall) of daylight-fluorescent opal from Mexico shows the typical botryoidal appearance of this material. P. Megaw specimen; photo by Jeff Scovil.

The excitation spectrum (which measures the wavelengths that excite a given luminescence) showed a broad band from about 400 to 440 nm, with an apparent maximum at about 420 nm, all in the violet region. This maximum explains why daylight, which contains violet wavelengths, so effectively excites the luminescence.

The presence of uranium was confirmed by EDXRF analysis on three samples using a Rigaku NEX CG spectrometer, which showed approximately 2,000–4,000 ppmw UO_2 (an estimated range since the water content of the

Figure 19: The green appearance of the 3.44 ct opal trilliant (left, photo by Tino Hammid) is due to its daylight fluorescence. The 2.81 ct oval (right, photo by Michael Gray) shows the near-colourless body colour of the opal when viewed in incandescent light. Both gems were cut by Michael Gray and are courtesy of P. Megaw.

Figure 20: In western Zacatecas State, miners dig shallow trenches (indicated by the arrow) along the base of a hill in search of opal. They follow iron-oxide-filled fractures cutting a rhyolite welded tuff. Photo by P. Megaw.

opal is unknown). Nevertheless, a study of these three faceted samples at the School of Mines in Nantes showed that their radioactivity was not dangerous. Their dose rate was measured with a Canberra Inspector 1000 instrument (NaI detector) for approximately one-half hour. The samples were measured together (total weight ~4 ct), yielding a dose rate that fell within background levels of 0.052–0.065 µSv/h.

This new Mexican gem, currently marketed as 'Electric Opal', is a rare example of opal-AN that is thick and transparent enough to be faceted. Usually such material is cut into flat cabochons, such as 'Satin Flash Opal' from Utah. It is also one of the rare gems that is almost exclusively coloured by luminescence.

Emmanuel Fritsch (Emmanuel.Fritsch@cnrs-imn.fr)
Institut des Matériaux Jean Rouxel
CNRS, Team 6502, University of Nantes, France

Tyler Spano-Franco
University of Notre Dame, Indiana, USA

Peter Megaw
IMDEX Inc., Tucson, Arizona, USA

References

Moore T.P., 2014. What's new: Tucson show 2014. *Mineralogical Record*, **45**(3), 345–375.

Ostrooumov M., Fritsch E., Lasnier B. and Lefrant S., 1999. Spectres Raman des opales: Aspect diagnostique et aide à la classification. *European Journal of Mineralogy*, **11**(5), 899–908, http://dx.doi.org/10.1127/ejm/11/5/0899.

Quartz with Radiating Fibres, Sold as 'Trapiche' Quartz

Rock crystal is well known for containing a wide variety of inclusions. However, it is rare for these inclusions to create interesting optical effects.

During the 2014 Tucson gem shows, dealer German Salazar (Bogotá, Colombia) had some interesting tablets of colourless 'trapiche quartz' from Colombia. He stated that the quartz was found in 2011 in the Boyacá and southern Santander Departments, about 300 km (190 miles) north of Bogotá by road. Artisanal miners produced ~300 kg of quartz crystal clusters, but only 6 kg showed the optical phenomenon,

which is restricted to areas near the base of the specimens. The optically interesting areas were not visible from the outside of the specimens, but only after they were sawn in a direction perpendicular to the c-axis of the quartz crystals. The tablets were cut from phenomenal portions measuring 10–45 mm in diameter and up to 40 mm thick, so large amounts of quartz had to be processed to find the areas of interest.

Salazar kindly donated a 25.18 ct tablet to Gem-A, and it was examined by one of the authors (MSK) for this report. The hexagonal cross-section was cut perpendicular to the main c-axis of a quartz crystal, and was polished as a slightly domed cabochon (Figure 21, top). It exhibited very fine and slightly curved fibres (presumably hollow) that extended radially from a nearly inclusion-free central part of the quartz crystal (Figure 22). A closer look with the microscope revealed that these fibres were not continuous, but rather 'dotted'. They emerged in bundles from a slightly milky zone (presumably due to sub-microscopic hollow fibres) at the spiky interface with the relatively clean core.

The fibres appear to represent growth channels that formed perpendicular to the growing prism faces (parallel to the growth direction), similar to the so-called comet structures seen, for example, in corundum (Gübelin and Koivula, 2008). Much less probable is that these features are hollow remnants of dissolved fibrous minerals that originally grew syngenetically with the prism faces of the quartz crystal. It was not possible to identify any mineral phase within these fibrous structures by Raman microspectroscopy. The irregular and spiky interface between the fibrous quartz and the nearly inclusion-free core may be due to an initial episode of deep natural etching by a corrosive fluid. This would have then been followed by a second stage of quartz growth that was intensely disturbed by growth perturbances, resulting in the fibrous channels.

The radiating structure of this quartz is particularly noticeable when viewed in cross-polarized light (Figure 21, bottom). Although this pattern is reminiscent of the trapiche growth phenomenon shown by some minerals (e.g.

Figure 21: This 25.18 ct tablet of quartz shows a fine radiating fibrous structure (top), which is particularly noticeable when viewed between crossed polarizers (bottom). Gift of German Salazar; photos © L. Phan, SSEF (top) and by B. M. Laurs (bottom).

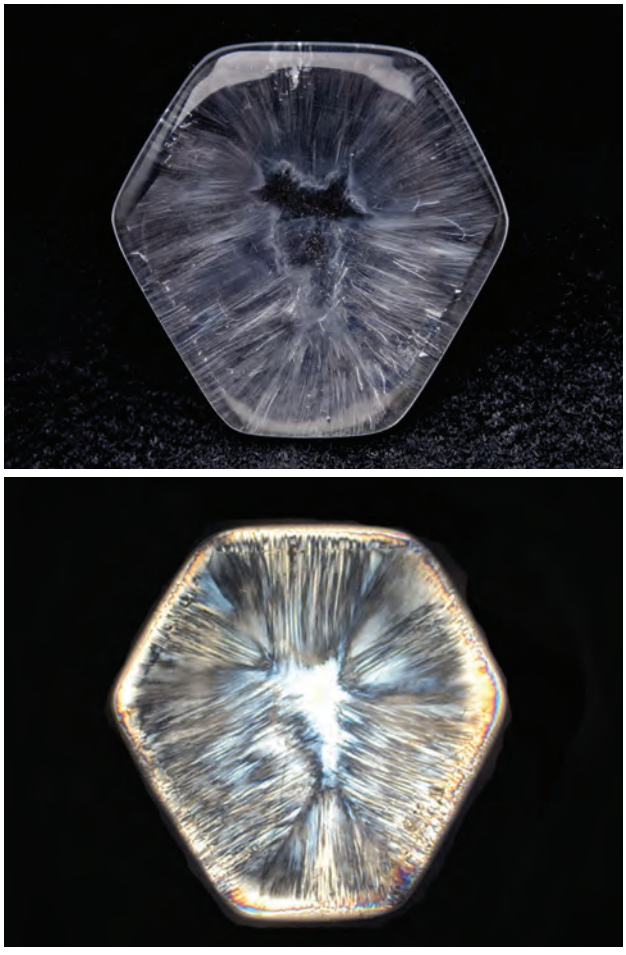

Figure 22: This closer view of the studied quartz shows the nearly inclusion-free core with an irregular spiky outline that is overgrown by a second quartz generation containing a fine fibrous pattern. The fibres are presumably hollow, and they are interpreted as growth channels due to perturbances at the growing prism faces. Photo © M. S. Krzemnicki, SSEF; image width 13 mm.

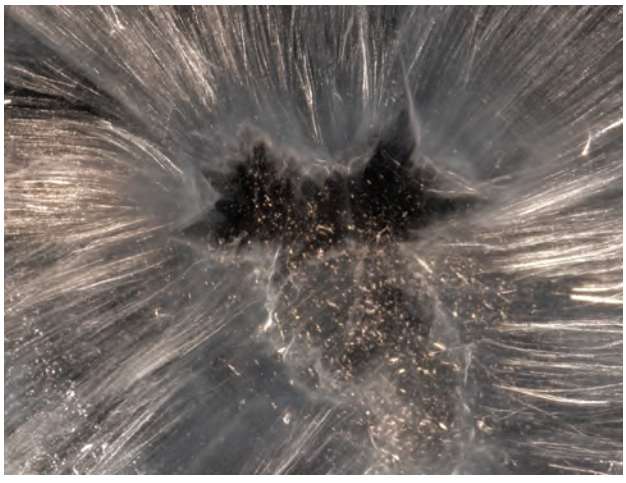

Figure 23: The skeletal crystal growth pattern in the two trapiche rubies at the bottom right shows distinct differences from the quartz studied for this report. Photo © L. Phan, SSEF.

ruby), the observed phenomenon is not the result of growth dynamics responsible for the trapiche pattern, and is also quite different in appearance (e.g. Figure 23). Previous studies have attributed the trapiche structure to skeletal crystal growth during which the edges of certain crystal planes grew much faster than the faces themselves (e.g. Schmetzer et al., 1996; Sunagawa, 2005).

Nowadays, the term *trapiche* is widely used in the gem trade for any material showing a fixed star-like pattern. Based on the fact that *trapiche* should be used only to describe material showing a skeletal growth pattern, one of the authors (MSK) suggests using another name for fixed star-like patterns of other origins. One possibility is the term *Polaris* (also known as the North Star, which is a fixed star in the northern hemisphere). Therefore 'Polaris Quartz' could be a poetic option for this interesting material that shows a fixed-star pattern.

Michael S. Krzemnicki

Brendan M. Laurs

References

Gübelin E.J. and Koivula J.I., 2008. *Photoatlas of Inclusions in Gemstones*, Vol. 3. Opinio Publishers, Basel, Switzerland.

Schmetzer K., Hänni H.A., Bernhardt H.-J. and Schwarz D., 1996. Trapiche rubies. *Gems & Gemology*, **32**(4), 242–250.

Sunagawa I., 2005. *Crystals—Growth, Morphology and Perfection*. Cambridge University Press, Cambridge, UK, 295 pp.

Yellow Scheelite from Khaplu, Pakistan

In early 2012, gem dealer Dudley Blauwet obtained a large piece of rough 'golden' yellow scheelite that reportedly came from the Khaplu area, Ghanche District, Gilgit-Baltistan (formerly Northern Areas), Pakistan. He first encountered scheelite from this locality in the 1990s, and most of it was orange-brown although rare pieces were red and weighed 7+ ct after faceting. The sample he obtained in 2012 weighed 102 g, but only a small part of it was cuttable. In January 2014 his cutting factory returned 34 stones weighing a total of 19.56 carats, which ranged up to 4.28 ct.

Blauwet loaned the 4.28 ct oval brilliant cut to this author for examination. It showed a light, slightly brownish, yellow colour with a high lustre and strong dispersion, somewhat similar to diamond (Figure 24). Doubling of the pavilion facets was readily seen when looking through the table with low magnification, which indicated a rather strong birefringence (the RI values were above the limit of a standard refractometer). The stone was virtually clean, with only one small cleavage fracture near the culet. Viewed with a prism-type spectroscope, the sample showed faint but sharp lines at about 560 and 570 nm, and a narrow grey band at ~580–590 nm. It fluoresced strong whitish blue to short-wave UV radiation, and very weak orange to long-wave UV. These properties, and its hydrostatic SG of 5.94, are consistent with those expected for scheelite. The absorption spectrum is attributed to the presence of 'didymium', a mixture of the rare-earth elements praseodymium and neodymium, and similar spectra are known in scheelite from other occurrences (e.g. Gunawardene, 1986; Dedeyne and Quintens, 2007). EDXRF chemical analysis

Figure 24: This 4.28 ct scheelite from Khaplu, northern Pakistan, exhibits an unusually light colour for material from this locality. Photo by Dirk van der Marel.

confirmed the presence of Ca and W as major elements; no minor elements were detected.

The FTIR spectrum exactly matched the spectra of brownish yellow scheelite from Sri Lanka (Godakawela, Sabaragamuwa Province) and colourless scheelite from Mexico (Santa Cruz, Sonora State), both present in the Dr Edward J. Gübelin Gem Collection and documented in the GIA Gem Project (i.e. https://s3.amazonaws.com/gubelin/scheelite-34884.pdf and https://s3.amazonaws.com/gubelin/scheelite-34472.pdf). The Raman spectrum matched very well with the spectra of both yellow and colourless scheelite from Sonora, Mexico, that are present in the RRUFF database (http://rruff.info/scheelite), with well-defined peaks at approximately 911, 837, 796, 399, 332, 210, 114 and 82 cm^{-1}. The peaks at 911 and 796 cm^{-1} are due to the stretching of the WO_4^{2-} anion in the structure of scheelite, whereas those at 399 and 332 cm^{-1} are caused by the bending of this anion (Frost et al., 2004).

J. C. (Hanco) Zwaan

References

Dedeyne R. and Quintens I., 2007. *Tables of Gemstone Identification*. Glirico, Gent, Belgium, 307 pp.

Frost R.L., Duong L. and Weier M., 2004. Raman microscopy of selected tungstate minerals. *Spectrochimica Acta A*, **60**, 1853–1859, http://dx.doi.org/10.1016/j.saa.2003.10.002.

Gunawardene M., 1986. Colombage-Ara scheelite. *Gems & Gemology*, **22**(3), 166–169, http://dx.doi.org/10.5741/gems.22.3.166.

Spessartine from the Democratic Republic of Congo

In approximately 2009, some unusual yellow-brown crystals were purchased by gem dealer Dudley Blauwet from his East African supplier. His supplier obtained them in Kenya from someone who had reportedly brought them from the Democratic Republic of Congo (DRC). Because of their elongate habit, his supplier thought they were zircon. However, subsequent testing at the Gemological Institute of America laboratory in Carlsbad showed they were actually spessartine (D. Blauwet, pers. comm., 2014). Blauwet planned to sell the crystals to mineral collectors, but due to their small size he eventually decided to have them faceted. He had ~40 stones cut that ranged from 0.20 to 0.84 ct, and loaned four of the faceted samples (0.62–0.84 ct; Figure 25) to the American Gemological Laboratories for examination.

The most interesting characteristic of these spessartines is their unusual yellow-brown colour, quite different from the typical orangy yellow to yellow-orange that is shown by this garnet species. As expected for spessartine, the RI of all samples was over-the-limit of a standard refractometer. Their SG values ranged from 4.19 to 4.21, consistent with spessartine. Inclusions in all the stones consisted of small flake-like particles, partially healed fissures and goethite

Figure 25: These near–end-member spessartines (0.62–0.84 ct), reportedly from the Democratic Republic of Congo, display an unusual yellow-brown colour. Photo by Bilal Mahmood.

(identified by Raman spectroscopy). EDXRF analysis showed major amounts of Si, Al and Mn, and traces of Fe and Mg; this is consistent with nearly pure spessartine. Visible-range spectroscopy showed strong absorptions at 409, 430, 461 and 485 nm, all of which are due to Mn^{2+} (Manning, 1967). A broad absorption at 527 nm was also present, and is due to Fe^{2+} (Manning, 1967). These absorption features are all typical of spessartine, despite the unusual yellow-brown colour of these samples.

Spessartine is known from several African countries (i.e. Nigeria, Namibia, Madagascar, Tanzania and Kenya; Shigley et al., 2010), but this is the first time that this author is aware of it being reported from the DRC. According to Blauwet, his supplier has not encountered any additional production of this material.

Bryan Clark

References

Manning P.G., 1967. The optical absorption spectra of the garnets almandine-pyrope, pyrope and spessartine and some structural interpretations of mineralogical significance. *Canadian Mineralogist*, **9**(2), 237–251.

Shigley J.E., Laurs B.M., Janse A.J.A., Elen S. and Dirlam D.M., 2010. Gem localities of the 2000s. *Gems & Gemology*, **46**(3), 188–216, http://dx.doi.org/10.5741/GEMS.46.3.188.

SYNTHETICS AND SIMULANTS

First CVD Synthetic Diamond Discovered in a Parcel of Natural Melee-sized Diamonds

The GGTL Laboratories specialize in testing melee-sized diamonds, and virtually all parcels of yellow diamonds analysed in recent years have contained at least some HPHT-grown synthetics. Parcels of colourless diamonds tested in our laboratories have—thus far—been spared from such 'pollution' by synthetics. With the increasing availability of gem-quality CVD-grown synthetic diamonds in the past few years, the market has become concerned about finding them mixed into melee-sized parcels of colourless natural diamonds. Thus far, not a single melee-sized CVD synthetic diamond has been found at the GGTL Laboratories, even though we test large quantities of colourless melee diamonds.

Recently, however, our Liechtenstein laboratory received some parcels of colored diamond melee for testing. The stones, which had been sold through Hong Kong, included yellow, orange and pink diamonds, and as usual we found some HPHT-grown synthetics (5–10%) in the yellow parcels. Using the DFI fluorescence imaging system developed in our laboratories, we noticed one gem in a parcel of vivid yellow 1.4–1.7 mm melee that displayed unusual luminescence (Figure 26). When excited by the strong broadband long-wave UV source, it luminesced a relatively weak orange. Orange luminescence in diamonds showing a saturated yellow body colour is very rare. Through the luminescence spectrometer in use with the DFI system, the fluorescence of this

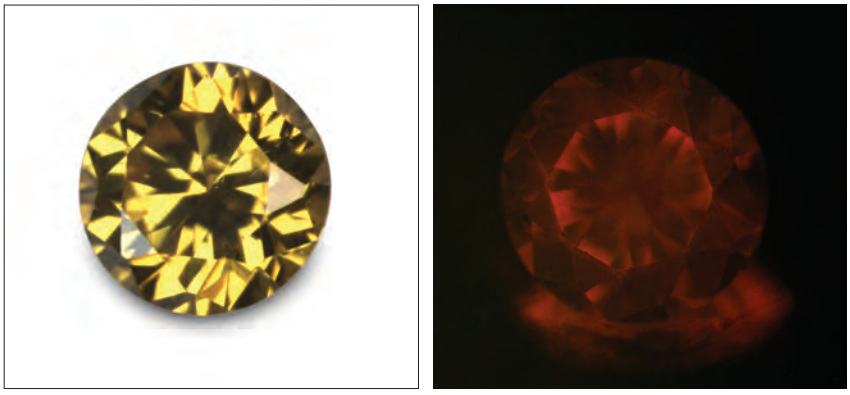

Figure 26: This 1.4-mm-diameter vivid yellow round brilliant (left) shows weak orange luminescence under strong broadband long-wave UV excitation (right). The gem proved to be a CVD-grown synthetic diamond. Photos by T. Hainschwang.

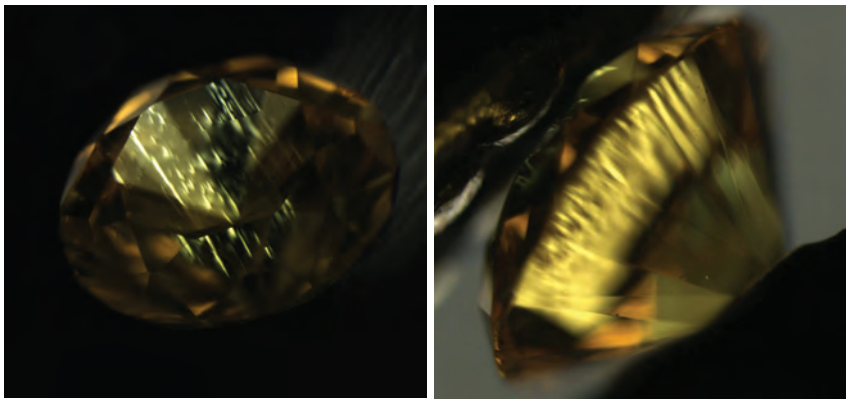

Figure 27: Viewed between crossed polarizers, in immersion, the 1.4-mm-diameter CVD synthetic diamond shows lamellar strain patterns associated with its planar growth structure. Photomicrographs by T. Hainschwang.

gem was immediately revealed to be related to NV centres, and the obvious presence of a silicon centre also was detected. Hence we strongly suspected it to be a CVD-grown synthetic.

Yellow CVD synthetic diamond is very uncommon, and has not been previously described as commercially available in the gem trade, with the exception of one 0.40 ct sample containing 4.5 ppm of C centres (Moe et al., 2014). HPHT-grown synthetic diamonds do not normally contain Si-centres, but the author has analysed one such sample that was produced in the Ukraine (unpublished data); in order to exclude the possibility that the present diamond was an HPHT-grown synthetic, all testing procedures were used to characterize it.

Viewed with crossed polarizing filters, the suspect stone clearly showed grey extinction along its lamellar growth structure (Figure 27). This type of growth pattern is characteristic of CVD-grown synthetic diamonds (e.g. Deljanin et al., 2003).

The infrared spectrum showed that the tiny gem was almost pure type Ib with a very low content of A aggregates (Figure 28). The C-centre content was determined to be approximately 175 ppm. The spectrum also showed several very

Figure 28: The infrared spectrum of the sample defines it as nearly pure type Ib, with tiny absorptions characteristic of CVD synthetic diamond.

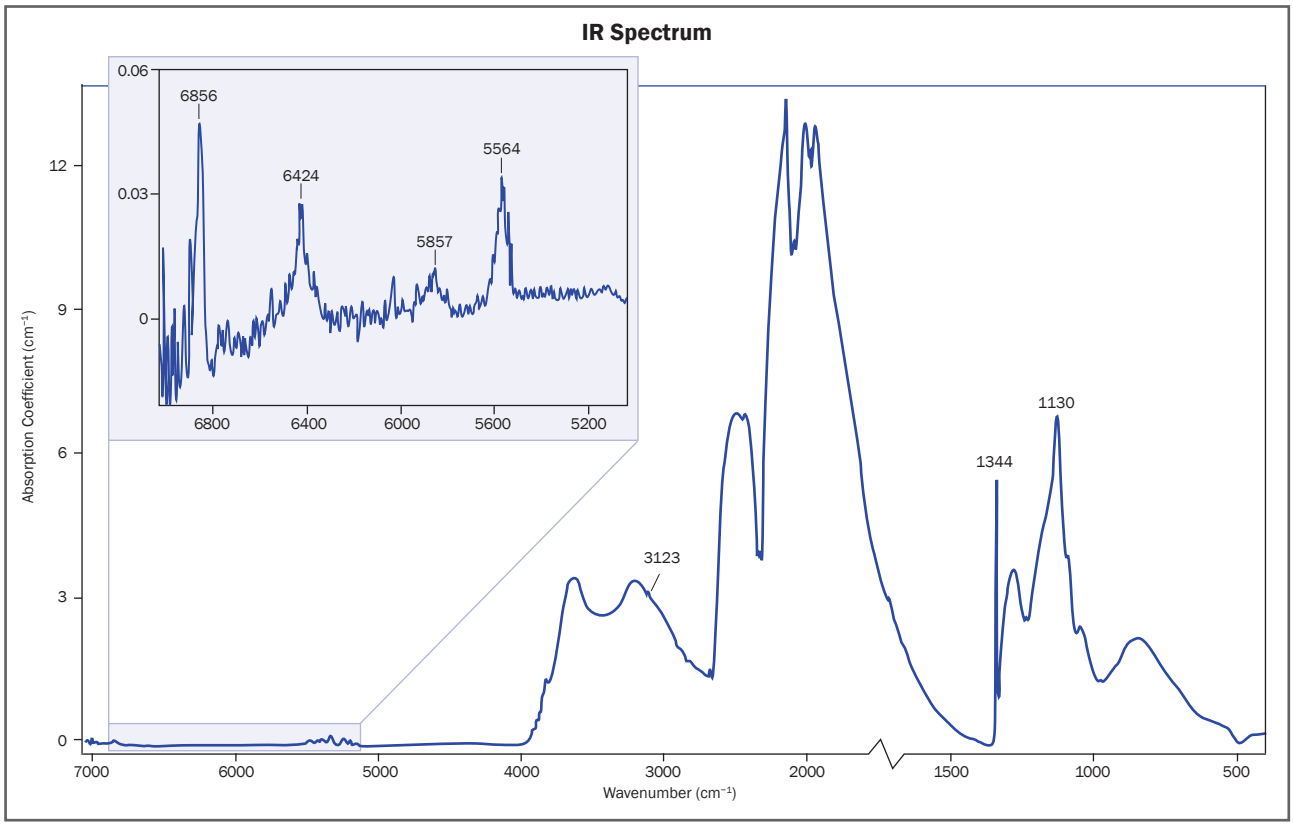

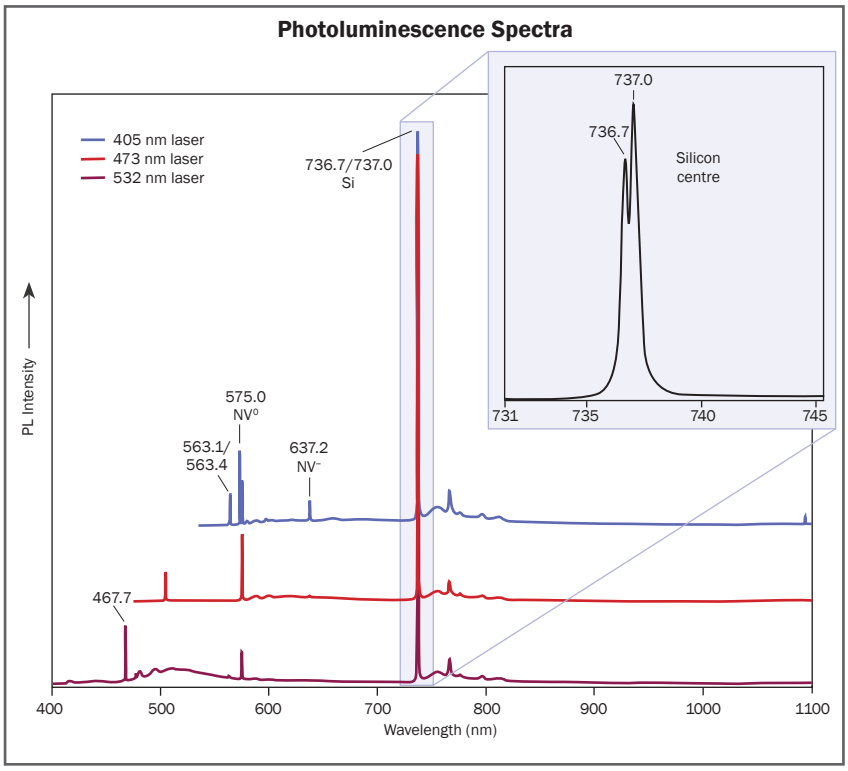

Figure 29: PL spectroscopy recorded using 405, 473 and 532 nm excitation shows dominant Si centre PL and several peaks that are unique to CVD synthetic diamond.

small absorption features that are characteristic of CVD synthetic diamond, such as a hydrogen-related peak at 3123 cm^{-1} and absorptions at 6856, 6424, 5857 and 5564 cm^{-1}.

Photoluminescence (PL) spectra were recorded with three different lasers (Figure 29) while the gem was immersed in liquid nitrogen. These spectra confirmed what the rest of the data had pointed toward: the vivid yellow gem was indeed a CVD synthetic diamond. The spectra were dominated by very strong Si-centre PL with its split zero-phonon lines at 736.7 and 737.0 nm and its vibronic structure extending to 820 nm. All other sharp PL features—with the exception of the NV^0 and NV^- centre emissions—are unique to CVD synthetic diamond: the sharp peak at 467.7 nm (Field, 1992) and the doublet at 563.1/563.4 nm (amongst many very weak sharp peaks) are additional emissions that prove the CVD synthetic origin of this gem.

This sample is the first CVD synthetic diamond known to this author that has been found in a parcel of melee-sized natural diamonds. Although the present case involves yellow melee, it will not be surprising to also find CVD synthetics in (near)-colourless diamond parcels in the future.

Thomas Hainschwang
thomas.hainschwang@ggtl-lab.org
GGTL Laboratories, Balzers, Liechtenstein

References

Deljanin B., Hainschwang T. and Fritsch E., 2003. Update on study of CVD diamonds. *Jewellery News Asia*, **231**, November, 134–139.

Field J.E., Ed., 1992. *The Properties of Natural and Synthetic Diamond*. Academic Press, London, 710 pp.

Moe K.S., Wang W. and D'Haenens-Johansson U., 2014. Lab Notes: Yellow CVD synthetic diamond. *Gems & Gemology*, **50**(2), 154–155.

Glass Imitation of Malachite

Malachite is a very common and popular ornamental material, with commercial amounts formerly mined especially from the Katanga Province of the Democratic Republic of Congo (DRC). Malachite from the Ural Mountains in Russia has been widely used in that country for

Figure 30: These silver earrings contain a glass imitation of malachite (9.5 mm in diameter). Photo by J. Hyršl.

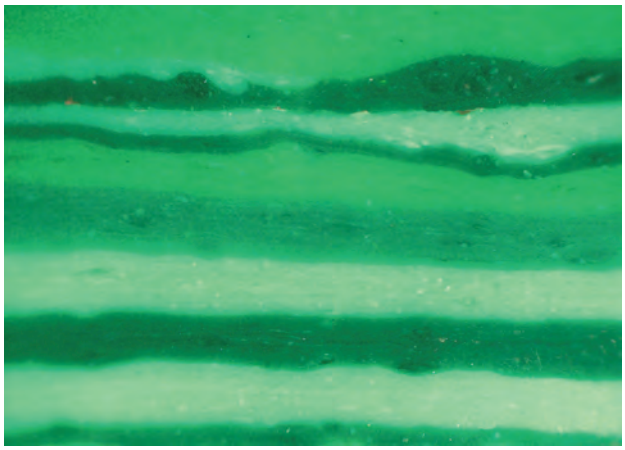

Figure 31: Viewed with the microscope, the glass imitation of malachite consists of irregular layers showing various amounts of green coloration. Photomicrograph by J. Hyršl; image width 4.0 mm.

decorative objects since the 19th century and is still popular there. After some of the historical sources of malachite were exhausted, synthetic malachite entered the market in the 1990s. This material was prepared in Moscow, but it proved too expensive in comparison with the natural stone.

This author recently examined some sterling silver earrings (probably manufactured in China) that appeared to be set with malachite (Figure 30). The gems showed typical parallel banding with light green, green and green-black bands that varied in width from 0.3 to 1.0 mm. The spot RI was 1.57 and the typical birefringence 'blink' exhibited by carbonates such as malachite was not seen. The cabochons were inert to short-wave UV radiation, but the light green bands fluoresced white to long-wave UV. These properties identify the material as a glass imitation. Microscopic observation showed an irregular thickness and inhomogeneous structure of the bands (Figure 31) that were probably caused by successive solidification of different-coloured layers of glass.

Natural malachite from the DRC is still quite cheap and abundant in the market, and it is surprising that such a time-consuming process was used to imitate such material.

Jaroslav Hyršl (hyrsl@hotmail.com)
Prague, Czech Republic

Dyed Quartzite and Chalcedony Beads Imitating Amazonite

Amazonite, the green-to-blue variety of microcline K-feldspar, is an attractive ornamental material that is commonly impregnated with various materials due to its platy structure and its susceptibility to damage along cleavage planes. Recently submitted to Stone Group Laboratories for identification was a suite of bead jewellery (earrings and a necklace) that reportedly featured amazonite. We presumed that the atypical appearance of this 'amazonite' (Figures 32 and 33) was the reason for its submission.

The beads in the earrings were a muted, uniformly coloured pastel greenish blue (e.g. Figure 32), and showed faint mottling and subtle banding with a granular texture. Their colour was too pale for typical amazonite, and they did not exhibit the iridescent platy structure commonly associated with this mineral. Raman analysis with a GemmoRaman-532 instrument readily identified them as quartz, and their granular texture indicated that the beads in the earrings were quartzite.

The beads in the necklace (Figure 33) varied broadly in both colour and pattern, but all of them tested as quartz with Raman spectroscopy. Most of the beads were of the chalcedony variety, although four of them had the granular texture of quartzite. Microscopic observation of the chalcedony beads revealed typical agate structures and banding, and a few would be best described as carnelian due to their reddish brown colour.

Figure 32: This 'amazonite' earring (16 mm in diameter) was found to consist of dyed quartzite. Photo by B. Williams.

Figure 33: The wide variation in colour and pattern seen in these 12 mm beads provided a strong indication that they were not amazonite. The beads proved to consist of chalcedony and quartzite, most of which had been dyed. Photo by B. Williams.

In some beads, faint dye concentrations could be seen along fissures and areas of greater porosity, but many of them showed no evidence of dyeing other than an unnatural colour for quartz. While it was not possible to confirm the type of dye used, traces of Cu were detected in the greenish blue beads by EDXRF spectroscopy; copper salts are commonly used as a blue dye.

Amazonite is readily available and affordable, so there is little reason for such imitations. These days it seems that anything can be imitated, even less expensive, plentiful materials.

Cara and Bear Williams

MISCELLANEOUS

Gem Notes from Myanmar

The jadeite mining area near Hpakan was closed to mining for nearly two years due to armed fighting between government forces and the Kachin Independent Army. Mining was allowed to resume at the end of September 2014 under a peace agreement. At present in the Hpakan region there are 808 private mining companies registered, with a total of 15,638 claims. Twenty-two percent of the companies are in partnership with the Myanmar government. These larger companies control 302 mining plots. Now 36 companies are preparing to start mining jadeite.

A jade and gems emporium was held 15 October 2014 in Naypyidaw for domestic gem merchants paying in local currency (kyats). There were nearly 7,000 rough jadeite lots shown, all classified as 'utility jade' (low-quality material), and some sold for higher prices than expected. In the gemstone section, 160 lots were displayed (51% ruby, 17% sapphire, 14% peridot and 12% other gems). The outcome of this sale has not yet been announced.

The information for this report was obtained from the *Weekly Eleven* newspaper (20 October and 3 November 2014).

U Tin Hlaing (p.tinhlaing@gmail.com)
Dept. of Geology (retired)
Panglong University, Myanmar

The Fire Within

"For in them you shall see the living fire of the ruby, the glorious purple of the amethyst, the sea-green of the emerald, all glittering together in an incredible mixture of light."

– Roman Elder Pliny, 1st Century AD

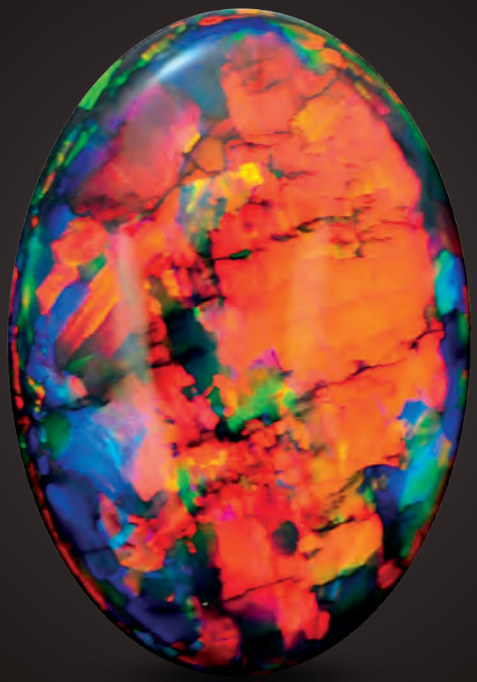

Black Opal 15.7 Carats

Suppliers of Australia's finest opals to the world's gem trade.

CODY OPAL

Level 1 - 119 Swanston Street Melbourne Australia

T. +61 3 9654 5533 E. INFO@CODYOPAL.COM

WWW.CODYOPAL.COM

INTERNATIONAL COLORED GEMSTONE ASSOCIATION MEMBER

JOG

The Rhodesian Star: An Exceptional Asteriated Diamond

Thomas Hainschwang, Franck Notari and Erik Vadaszi

The physical and optical properties of an exceptional asteriated diamond called *The Rhodesian Star* are described in detail. The stone shows a dramatic six-lobed star pattern formed by a dark grey cloud that strongly contrasts with the diamond's light greenish grey-yellow body colour. Analysis by various optical and spectroscopic methods identified the growth of the diamond as mixed-habit cuboid-octahedral, with the lobes forming the star pattern corresponding to cuboid growth sectors. These sectors are rich in hydrogen and nickel and are full of microscopic inclusions, possibly consisting of voids that are partially filled with graphite.

The Journal of Gemmology, 34(4), 2014, pp. 306–315, http://dx.doi.org/10.15506/JoG.2014.34.4.306

Introduction

'Asteriated' diamonds contain a star-shaped cloud of light-scattering inclusions, and they used to be quite rare (Wang and Mayerson, 2002; Darley et al., 2009). With the discovery of enormous diamond deposits in Zimbabwe in 2006 and the appearance of such stones in the international markets around 2011, these diamonds have become more common. In very rare cases, attractive, well-defined star-shaped patterns are seen in complete diamond octahedra without the need to cut them into slices to make the star pattern more visible. Such is the case for the diamond studied for this report (Figure 1), named *The Rhodesian Star* after the old nomenclature of Zimbabwe. It is extremely likely that the diamond was mined in that country, since rough diamonds of similar appearance and properties are virtually unknown from other localities.

Asteriated diamonds from historical sources (Brazil and India) were described by Rondeau et al. (2004) using samples dating from 1802 to 1844. They characterized such diamonds as nitrogen-rich, with mixed-habit cuboid-octahedral growth and enrichment of hydrogen and nickel in the cuboid sectors. The correlation between symmetrical clouds and high hydrogen content was also pointed out by Wang and Mayerson (2002). Virtually all asteriated diamonds have a near-colourless to light brown or brown-yellow body colour with a somewhat darker brown-to-grey star pattern. The pattern always consists of two stars with three-fold symmetry, hence a six-fold star can be seen in complete octahedra. When such diamonds are sliced to enhance the contrast between the cloud and the surrounding diamond, patterns with two, three, four or six lobes can be seen (e.g., Figure 2).

Until now only a very few attractive complete octahedra of asteriated diamonds have appeared in the market and been analysed by a laboratory. This study reports the physical and optical properties of an exceptional 11.38 ct asteriated diamond: The Rhodesian Star.

Figure 1: The Rhodesian Star, a spectacular 11.38 ct asteriated diamond, is positioned here to show the star pattern reflected through four of the polished octahedral faces. Photo by E. Vadaszi.

Background

When the diamond was purchased by one of the authors (EV) in early 2014, it had windows polished on the octahedral faces in order to make the star pattern more visible, since its surface had an otherwise sandblasted look. Such matte-surfaced diamonds are common from Zimbabwe, and they typically also have a thick translucent-to-opaque green to nearly black crust. The original weight of the diamond was indicated to be close to 14 ct, and the polishing of the windows reduced it to a little over 13 ct.

After purchase, the stone's eight octahedral faces were repolished to display the star pattern to the best extent possible. Since polishing precisely parallel to the octahedron is virtually impossible due to diamond's greatest hardness along this plane (Kraus and Slawson, 1939), the faces were polished slightly oblique to the original octahedral surfaces. The polishing process was a very noisy and rather long process that took five full days. The boundaries between the octahedral faces were left with their original sandblasted appearance, hence resembling the surface of a nicely bruted girdle.

The result of this work is a unique and spectacular asteriated diamond weighing 11.38 ct and measuring 13.57 × 13.52 × 13.51 mm, of light greenish grey-yellow colour. The dark grey star-shaped cloud is much sharper and shows a far higher contrast than any other asteriated diamond that these authors are aware of.

Materials and Methods

The diamond was analysed at the Liechtenstein branch of GGTL Laboratories. The inclusions and strain pattern were visualized using a Leica M165C trinocular microscope, equipped with a Leica DFC420 CCD camera with a resolution of 5 megapixels. The strain pattern was analysed with the stone immersed in alcohol between crossed polarizing filters.

The luminescence of the diamond was observed in 254 nm short-wave (SW) and 365 nm long-wave (LW) radiation from a 6 W UV

Figure 2: Asteriated diamonds are commonly sliced to best display their star patterns. These two diamond slices in the collection of the French National Museum of Natural History date from 1844 and originate from India. Reprinted with permission from Rondeau et al. (2004).

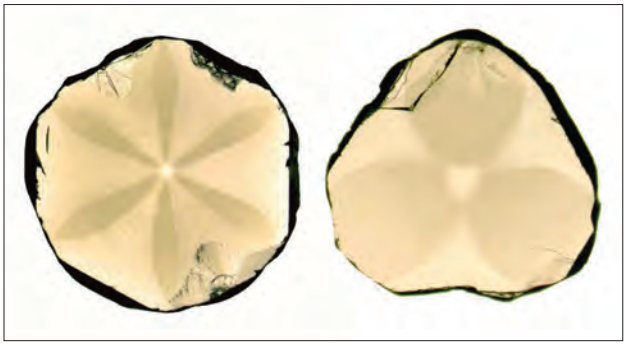

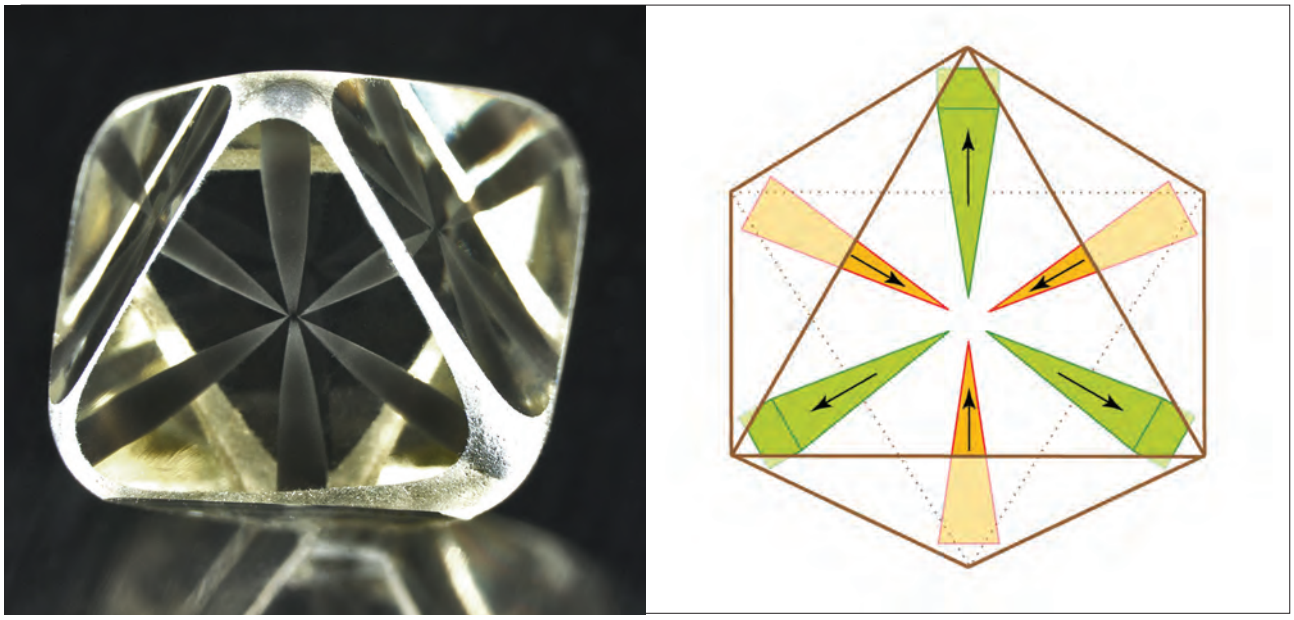

Figure 3: The star pattern shows exceptionally high contrast to the rest of the diamond (left, photo by T. Hainschwang). On the right is a graphical representation of the two sets of three-fold stars, which shows the pattern seen in The Rhodesian Star.

lamp (model UVP UVSL-26P). The luminescence was also observed in broadband UV using three different excitation bands (LW band 1: 300–410 nm; LW band 2: 355–375 nm; SW/LW band: 250–350 nm) from a GGTL DFI luminescence microscope using a suitably filtered 300 W full-spectrum xenon lamp. The luminescence images recorded with the GGTL DFI system were acquired with a Leica DFC450 C CCD camera with a resolution of 5 megapixels and the CCD sensor thermoelectrically cooled with a delta of −20°C compared to the surrounding temperature. Infrared spectra were recorded in transmission mode with a resolution of 4 cm^{-1} on a PerkinElmer Spectrum 100S Fourier-transform infrared spectrometer equipped with a thermoelectrically cooled DTGS detector, using a 5× beam condenser, over a range of 8500–400 cm^{-1}, with 100–500 scans.

Photoluminescence spectra were recorded on a GGTL system using 405, 473, 532 and 635 nm laser excitations, and a high-resolution echelle-type spectrograph by Catalina Scientific equipped with an Andor Neo sCMOS camera with a resolution of 5 megapixels, thermoelectrically cooled to −40°C. The system was set up to record spectra in the range of 350–1150 nm with an average resolution of 0.04 nm. All photoluminescence spectra were recorded with the diamond cooled to 77 K by direct immersion in liquid nitrogen.

Ultraviolet-visible–near infrared (UV-Vis-NIR) spectra were recorded on a GGTL D-C 3 spectrometer system using a combined xenon, tungsten-halogen and LED light source. A quadruple-channel spectrometer with a Czerny-Turner monochromator and a thermoelectrically cooled CCD detector was employed, with an average resolution of 0.3 nm. The spectrum was measured with the diamond placed in an integrating sphere of 15 cm diameter and cooled to about 77 K (−196°C).

Results and Discussion

Visual Observation and Microscopy

The asteriated pattern is caused by the combination of two stars, each showing the typical three-fold symmetry of diamond (Figure 3). The stars are oriented in different planes, so when they are viewed with magnification only one star is in focus at a time (Figure 4).

The tiny black inclusions forming the star patterns in some asteriated diamonds have been identified with Raman spectroscopy as highly crystalline graphite (Rondeau et al., 2004). The dark appearance and strong contrast of the lobes in The Rhodesian Star are due to a high density of such grey-to-black microscopic inclusions (Figure 5). The exact nature of these inclusions

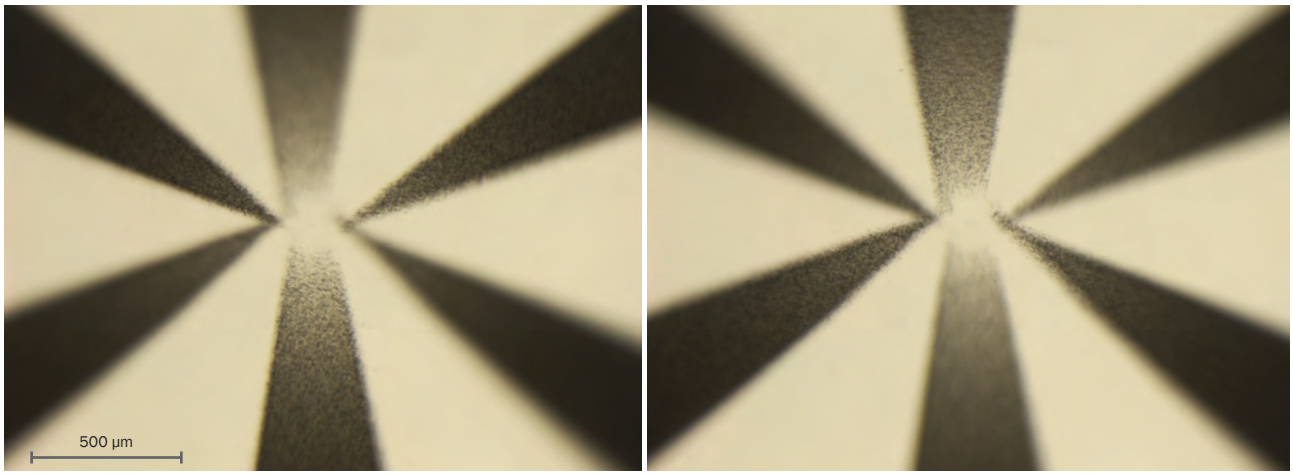

Figure 4: Each three-lobed star in the diamond originates from a separate plane, so only one star is in focus at a time when viewed with magnification. Photomicrographs by T. Hainschwang.

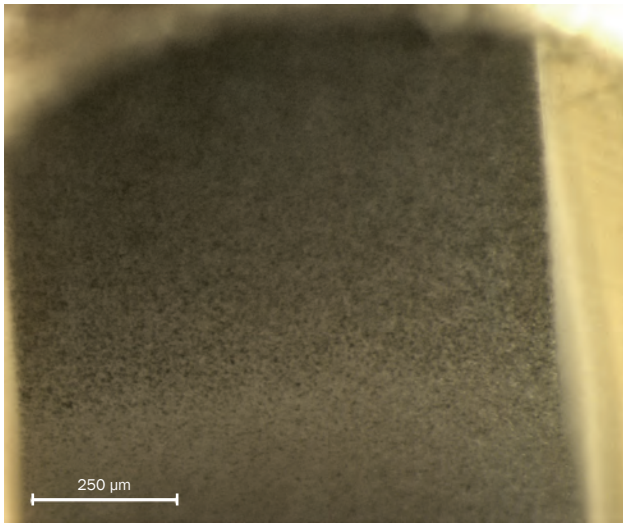

Figure 5: The dark appearance of the star pattern in the diamond is caused by microscopic particles that probably consist of voids that are partially or completely filled by graphite. Photomicrograph by T. Hainschwang.

was not determined due to time restraints when testing the diamond, but it is likely that they consist of voids that are partially or completely filled by graphite (cf. Klein-BenDavid et al., 2007).

Also observed in The Rhodesian Star were dark green radiation stains (Figure 6). Such stains are—as the name indicates—related to radiation and are characteristic for many natural rough diamonds (Nasdala et al., 2013). The stains on The Rhodesian Star are of natural origin. Similar stains may be observed in laboratory-irradiated diamonds treated by direct contact with radium salts, but such stains typically have a perfectly round shape, in contrast to the irregular shape of the stains in naturally irradiated diamonds (Hainschwang and Notari, 2014). The latter stains are caused by natural alpha radiation, and because of the low penetration depth of alpha particles, they are always limited to an area very near the surface. As determined by optical microscopy combined with the measurement capability of the Leica DFC450 C CCD camera, the depth of the stains in this diamond was found to be 5–10 µm. The presence of the pristine green radiation stains shows that the diamond has not been exposed to heat above 400–500°C, since such stains turn brown upon annealing (Nasdala et al., 2013).

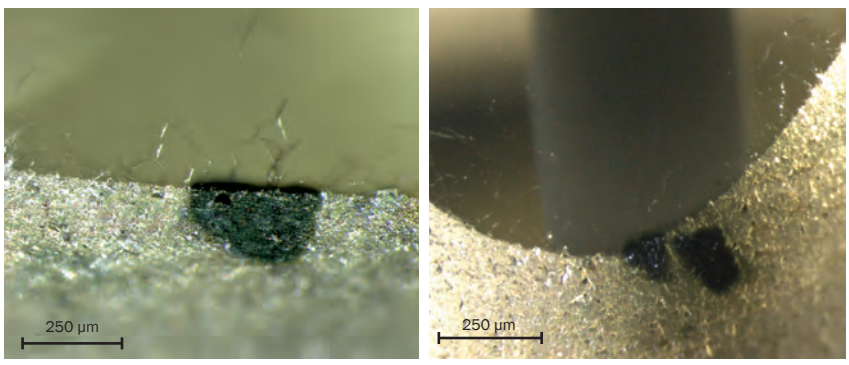

Figure 6: Several irregularly shaped dark green radiation stains on the surface of the diamond clearly show that it was exposed to natural alpha radiation and that it has not been heated to more than 400–500 °C during the polishing process. Photomicrographs by T. Hainschwang.

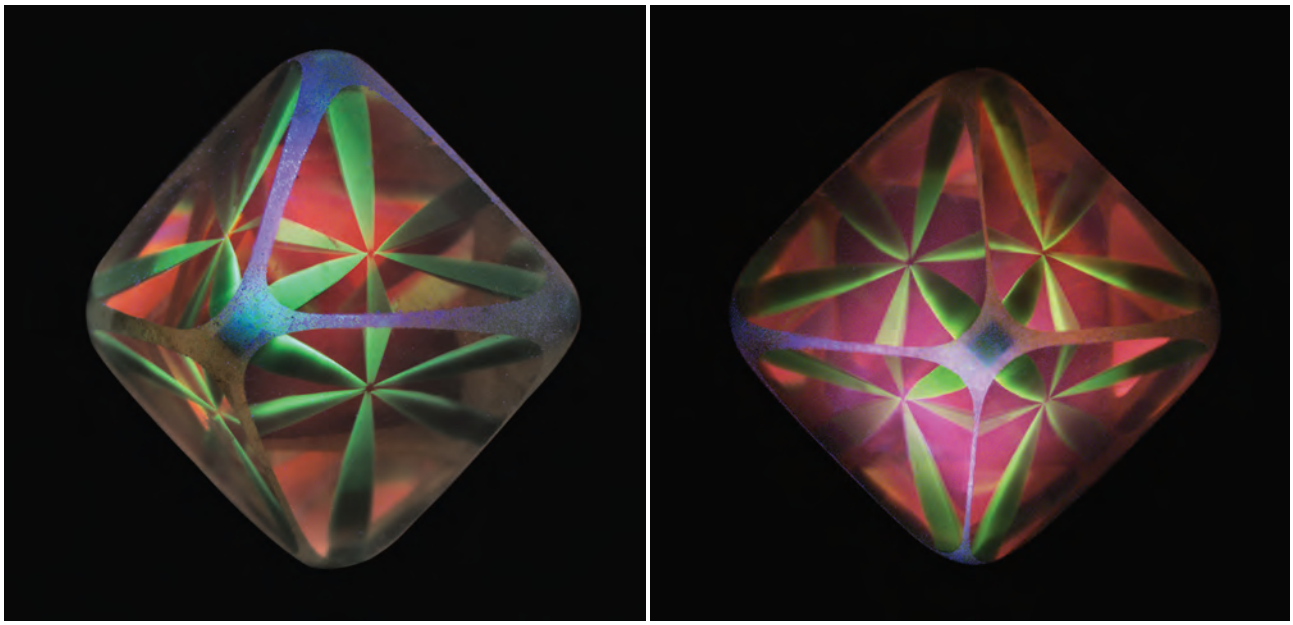

Figure 7: The Rhodesian Star displays beautiful luminescence patterns when exposed to the strong broadband UV excitation of the GGTL DFI fluorescence microscopy system (left = 300–410 nm and right = 355–375 nm excitation). Photos by T. Hainschwang.

While radiation stains are known in diamonds from many deposits, they are especially prominent in diamonds from Zimbabwe, which is the likely origin of this diamond.

Luminescence

Luminescence imaging is a technique where a material is typically excited by a UV source and its emission colours are observed.

The Rhodesian Star shows no apparent fluorescence under standard long- and short-wave UV lamps. However, when exposed to a high-power UV source such as the GGTL DFI fluorescence microscope, the stone exhibits a spectacular fluorescence pattern (see Figures 7– 9 and the cover of this issue). The star pattern glows green while the rest of the diamond luminesces pink-orange to purple-pink, depending on the specific UV excitation band used: 250–350 nm excitation causes pink-orange PL, 300–410 nm produces orangy pink PL, and 355–375 nm excites purple-pink PL.

UV excitation reveals that the lobes forming the star pattern have a square cross-section, which is particularly apparent at the corners of the octahedron (Figure 8). The square shape could lead to the conclusion that the lobes correspond to cube sectors such as those present in synthetic diamond. However the sectors almost certainly are of cuboid growth, a rather common form that exists

Figure 8: In this luminescence image (250–350 nm excitation), the square cross-section (and hence the cuboid nature) of a lobe of The Rhodesian Star is evident at the corner of the diamond octahedron. Photomicrograph by T. Hainschwang.

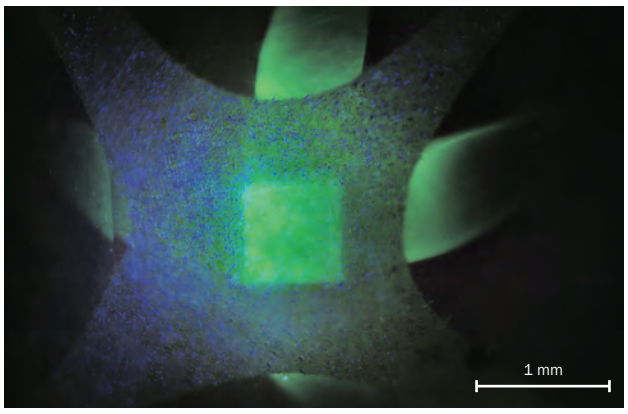

Figure 9: This close-up view of the luminescence of The Rhodesian Star under 250–350 nm excitation displays the green-luminescing lobes, which follow the cuboid directions of the diamond. Photomicrograph by T. Hainschwang.

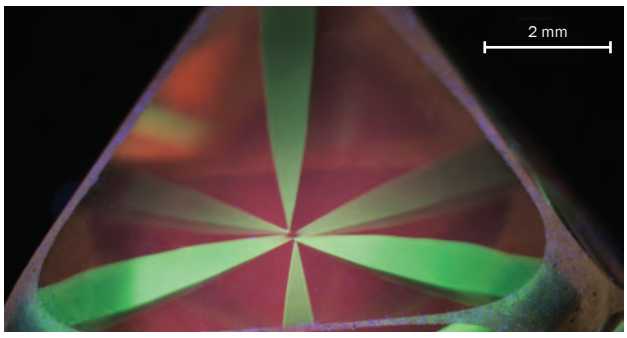

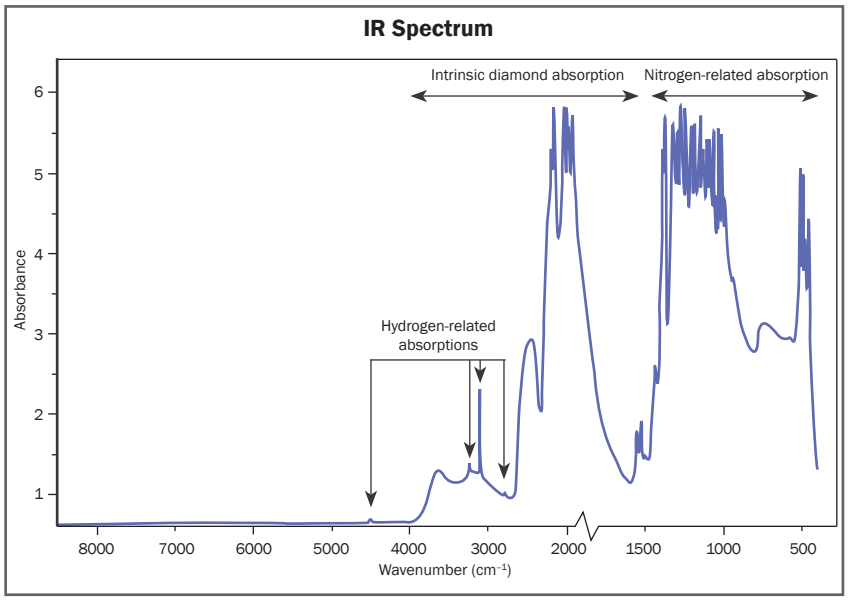

Figure 10: The infrared spectrum of The Rhodesian Star shows it is a type IaA>B diamond with very high nitrogen and moderate hydrogen content.

only in natural diamond. Cuboid sectors are known to be typically rich in hydrogen and nickel-related defects (Lang et al., 2004). These nickel-related defects are responsible for the green luminescence in these sectors (see PL Spectroscopy section for more details). A sketch of the two three-fold stars observed in this diamond, and the square cross-section of the lobes, is shown in Figure 3.

Infrared Spectroscopy

Infrared spectroscopy is a well-known method used to distinguish different diamond types based on the presence or absence of substitutional nitrogen and/or boron impurities and the aggregation state of the nitrogen. The presence of hydrogen also can be confirmed by this technique, and certain radiation-related defects can be detected.

The infrared spectrum of The Rhodesian Star characterizes the stone as a type IaA>B diamond (Figure 10); hence the A-aggregate form of nitrogen dominates the B-aggregate form of nitrogen. The stone contains very high concentrations of nitrogen and moderate amounts of hydrogen. The nitrogen content could not be properly determined; due to the thickness of the diamond and its enriched nitrogen content, the necessary nitrogen absorptions (482 cm^{-1} for A aggregates and 1010 cm^{-1} for B aggregates) could not be properly resolved. Infrared spectra recorded from the individual sectors show that by far most of the hydrogen is located within the 'star' cuboid sectors.

UV-Vis-NIR Spectroscopy

Performed at low temperature (–196°C, with the sample immersed in liquid nitrogen), UV-Vis-NIR spectroscopy is useful for detecting many important defect centres in diamond. Among these are the N3/N2 centres, which are responsible for the yellow coloration of many diamonds, and several radiation-related defects such as GR1, the 594 nm centre, etc.

The Rhodesian Star shows a standard cape spectrum, with distinct N3 and N2 absorptions at 415.2 and 478 nm, respectively. Several radiation-related features also can be seen, such as GR1 at 741.2 nm (caused by the neutral carbon vacancy), 3H at 503.5 nm and the 594 nm centre (Figure 11). These absorptions are rare in untreated natural diamond—with the exception of naturally irradiated green to greenish blue stones—although they have been found to be rather common in untreated diamonds from Zimbabwe (Breeding, 2011; Crepin et al., 2011). These rough stones often have a thick very dark green 'skin' from natural irradiation, and although the vast majority of the diamonds have a mixed brown/yellow body colour in their transparent core, they show minor traces of natural radiation damage in their spectra.

PL Spectroscopy

Laser-excited PL spectroscopy is a very sensitive method for detecting the defects responsible for the observed luminescence. The diamond sample is immersed in liquid nitrogen, and the

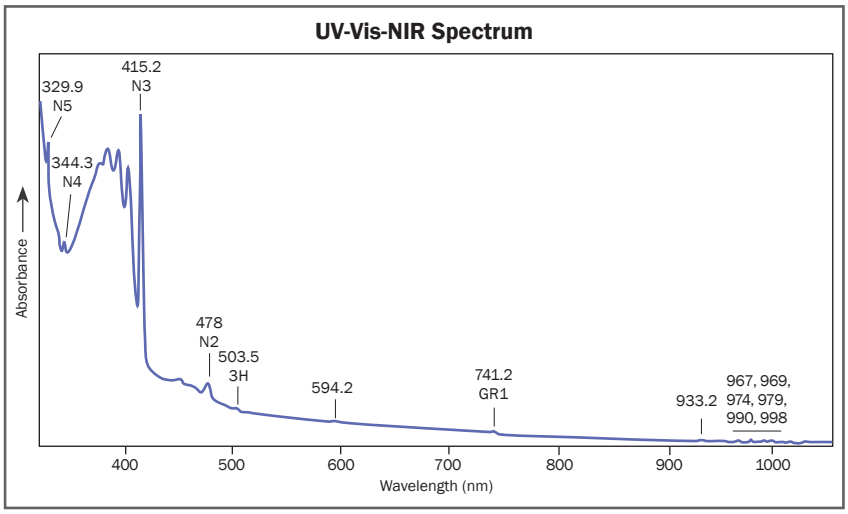

Figure 11: The UV-Vis-NIR spectrum of The Rhodesian Star indicates that its light greenish grey-yellow body colour originates from strong N3/N2 absorption combined with GR1 absorption. The overall slight green hue originates from surface-related green coloration caused by natural radiation exposure. The path length of the beam through the GR1-damaged surface is very short, so absorbance of the GR1 band is very low. Several other absorptions, such as the 594.2 nm peak, also indicate that the stone experienced exposure to radiation.

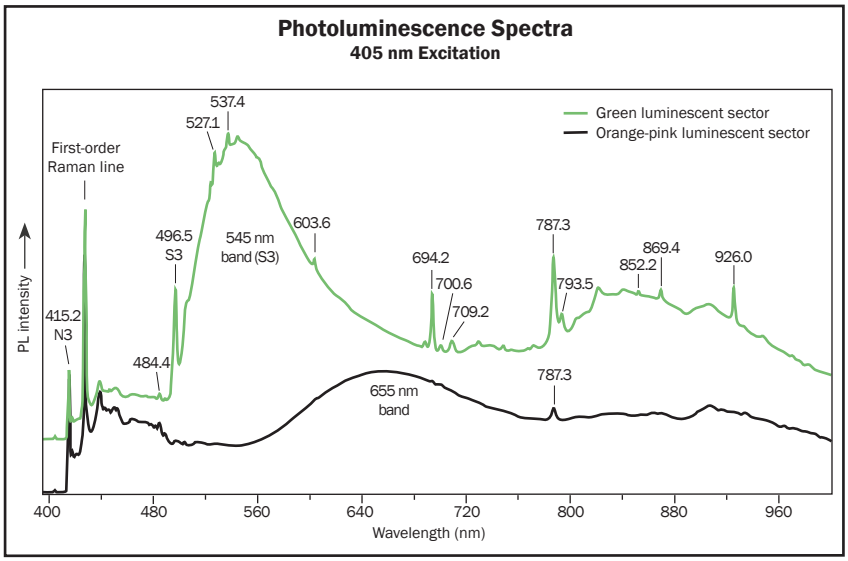

Figure 12: The PL spectra of the differently luminescing sectors of The Rhodesian Star obtained with 405 nm excitation show that the green PL of the lobes is due to strong nickel-related (S3) defect luminescence, while the orange-pink PL from the octahedral sectors originates from a broad emission band of unknown origin centred at 655 nm. The spectra clearly show that the cuboid sectors are rich in nickel while the octahedral sectors are not.

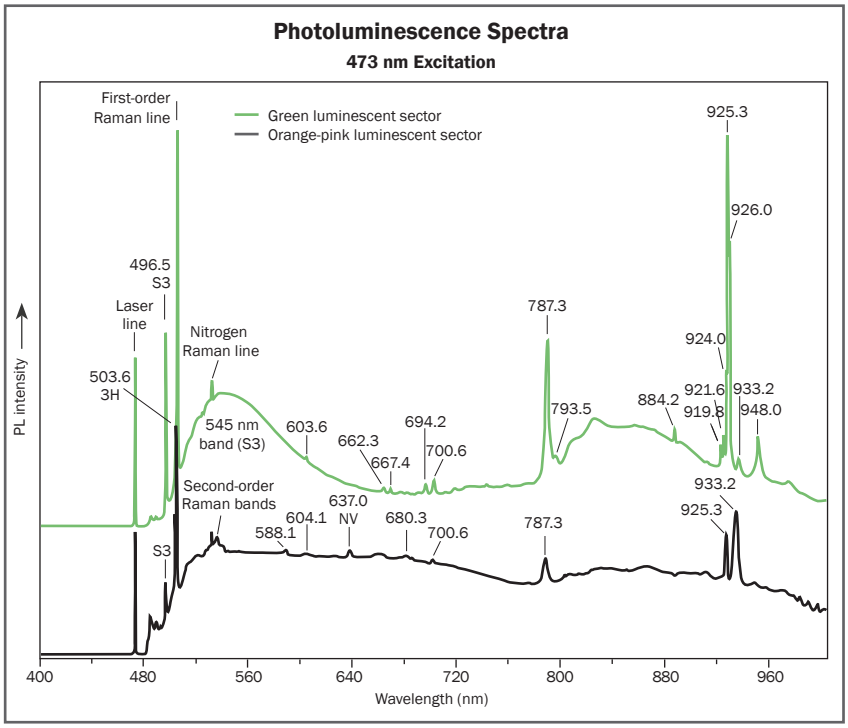

Figure 13: As with the 405 nm laser, PL spectroscopy of The Rhodesian Star obtained with 473 nm excitation shows that the green PL of the lobes originates from strong S3 defect luminescence. The extremely broadband emission seen in the octahedral sectors indicates a much different PL colour than was seen with 405 nm and strong UV excitation; the colour most closely resembles 'beige' or some sort of brown hue. The cuboid sectors are richer in nickel defects than the octahedral sectors. (The nitrogen line is produced by Raman scattering from the liquid nitrogen surrounding the specimen.)

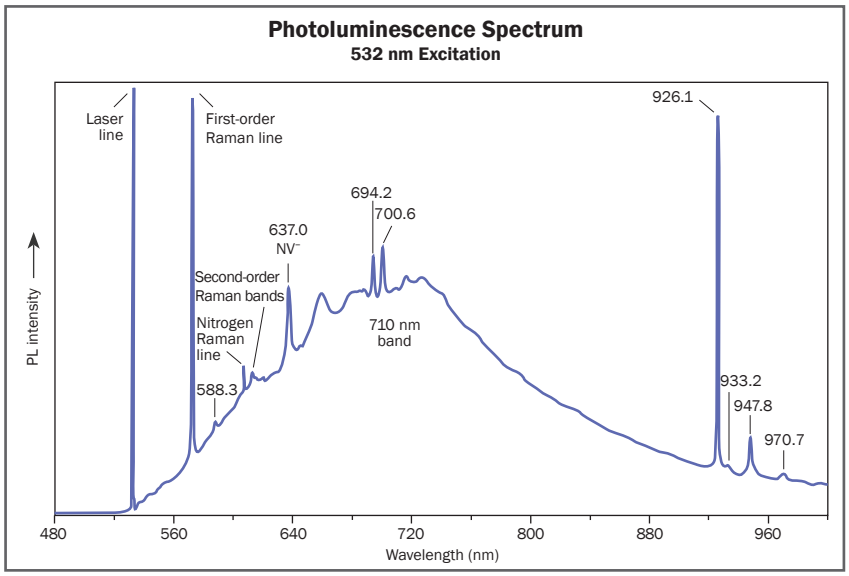

Figure 14: The PL spectrum of The Rhodesian Star obtained with 532 nm excitation is characterized by a broad band centred at 710 nm, along with distinct NV^- centre PL and several nickel-related emissions (possibly including those in the 900–950 nm range). Both growth sectors in the diamond were simultaneously excited by the laser when recording this spectrum. (The nitrogen line is produced by Raman scattering from the liquid nitrogen surrounding the specimen.)

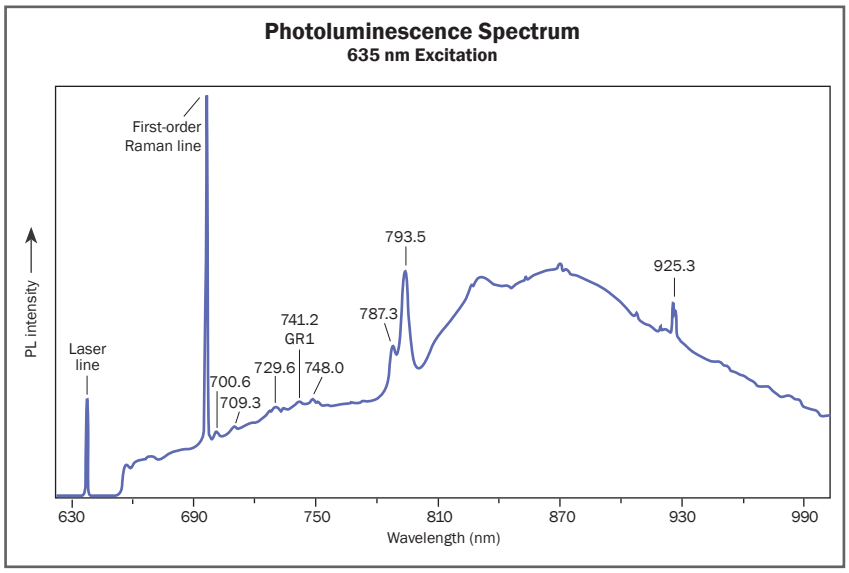

Figure 15: The PL spectrum of The Rhodesian Star obtained with 635 nm excitation is characterized by several nickel-related defects, with those at 787.3 and 793.5 nm being particularly intense. Both growth sectors in the diamond were simultaneously excited by the laser when recording this spectrum.

luminescence is produced using laser excitation of various wavelengths. The resulting luminescence is measured by a high-resolution spectrometer and plotted as a spectral curve.

The Rhodesian Star was tested with four different lasers (405, 473, 532 and 635 nm; Figures 12–15). Using 405 and 473 nm excitations, differences in PL luminescence between the octahedral and cuboid growth sectors could be depicted in the corresponding spectra. However, it was not possible to measure the green luminescence in the 'star sector' using the 532 or 635 nm excitations, because these wavelengths are longer than 500 nm and therefore do not excite the centre responsible for the green PL.

The green luminescence of the star-shaped cloud is caused by the S3 centre, which is a nickel-related defect that can be seen as a sharp line at 496.5 nm and a broad band centred at 545 nm (Kanda and Watanabe, 1999; Figure 12). This defect is characteristic of diamonds of mixed cuboid-octahedral growth, and is mainly present in the cuboid sectors of natural diamonds (Welbourn et al., 1989; Lang et al., 2004; Hainschwang, 2014). It is the predominant defect in so-called re-entrant cube mixed-habit cuboid-octahedral natural diamonds (Hainschwang et al., 2013). It is also characteristic of HPHT synthetic diamonds grown using a nickel-iron solvent, particularly after annealing, but may be found in as-grown synthetic diamonds produced using relatively high temperatures. However, in synthetic diamonds the defect is predominant in octahedral growth sectors (Kupriyanov et al., 1999).

The orange-red to orange-pink luminescence of the rest of the diamond is caused by an

unknown defect that is seen as a broad emission band centred at 655 nm (using 405 nm laser excitation; Figure 12).

Many of the other emission bands and lines detected with the four lasers can also be assigned to nickel-related defects (Zaitsev, 2001), such as those at 694.2, 700.6, 787.3 and 793.5 nm (again, see Figures 12–15). The causes of the PL features above 900 nm are unknown, although the 926.1 nm emission has been tentatively assigned to a nickel-related defect (Hainschwang et al., 2005). It is possible that the other lines from around 900 to 950 nm are nickel-related as well, with the exception of the 933.2 nm feature which is very probably nitrogen related. This line shows up in absorption and also in luminescence when the N3 and N2 absorptions are intense.

With the exception of a very weak GR1 feature at 741.2 nm (Figure 15) and an NV^- centre emission at 637.0 nm (Figure 14), no radiation-related features were detected by PL spectroscopy. The straightforward detection of many radiation-related features with absorption spectroscopy and the quasi-non-detectability of these defect centres by PL spectroscopy can be explained by the fact that they are present only in the upper few microns of the stone. Since the PL spectra were taken from either the lobes or from the bulk of the diamond—without the use of a microscope—the radiation-related PL from the surface was not well excited and thus not detected.

The very sensitive method of photoluminescence spectroscopy clearly shows that the sectors containing the star pattern originate from nickel-rich cuboid growth, while the rest of the diamond consists of normal octahedral growth that is poor in defects other than nitrogen.

Conclusions

The Rhodesian Star is a superb example of an asteriated diamond. Gemmological testing has demonstrated that the star pattern is the result of cuboid-octahedral growth and that the grey-to-black particles are restricted to the cuboid sectors only. Spectroscopy confirmed that hydrogen and nickel defects are confined to the cuboid sectors, as previously documented in such diamonds. The spectacular luminescence patterns seen when the diamond is exposed to a high-power UV source are the result of nickel-related defects (S3) in the cuboid sectors, which are responsible for the bright green PL. The orange-red to purple-pink luminescence of the octahedral portions of the crystal originate from a broadband emission from unknown defect(s). Although it is extremely rare to see such luminescence with the use of standard UV lamps, the purple to nearly red luminescence is actually quite common in natural diamonds when they are exposed to intense UV excitation from our GGTL DFI fluorescence microscope. While orange-to-red PL (excited by UV to violet light) is known from various types of emission centres, the only well-characterized defects known to produce this luminescence are the NV^- and NV^0 centres, although it is very rare for them to emit strong PL in untreated diamonds.

The properties of The Rhodesian Star—particularly its surface texture and appearance, and the spectral data such as the radiation-related defects—indicate that its origin is Zimbabwe, which is one of the best-known sources for asteriated diamonds.

References

Breeding C.M., 2011. Hydrogen-rich diamonds from Zimbabwe with natural radiation features. *Gems & Gemology*, **47**(2), 129–130.

Crepin N., Anthonis A. and Willems B., 2011. A case study of naturally irradiated diamonds from Zimbabwe. *Gems & Gemology*, **47**(2), 105.

Darley J., Emerson E. and Johnson P., 2009. Lab Notes: Diamond with flower-shaped cloud. *Gems & Gemology*, **45**(4), 290.

Hainschwang T., 2014. Diamants de Type Ib: Relations entre les Propriétés Physiques et Gemmologiques des Diamants Contenant de l'Azote Isolé. PhD thesis, University of Nantes, France (in French).

Hainschwang T. and Notari F., 2014. Green diamonds. Gem-A Conference, London, 1–2 November.

Hainschwang T., Katrusha A. and Vollstaedt H., 2005. HPHT treatment of different classes of type I brown diamonds. *Journal of Gemmology*, **29**(5/6), 261–273, http://dx.doi.org/10.15506/jog.2005.29.5.261.

Hainschwang T., Karampelas S., Fritsch E. and Notari F., 2013. Luminescence spectroscopy and microscopy applied to study gem materials: A case study of C centre containing diamonds. *Mineralogy and Petrology*, **107**(3), 393–413, http://dx.doi.org/10.1007/s00710-013-0273-7.

Kanda H. and Watanabe K., 1999. Distribution of nickel related luminescence centers in HPHT diamond. *Diamond and Related Materials*, **8**(8–9), 1463–1469 http://dx.doi.org/10.1016/s0925-9635(99)00070-9.

Klein-BenDavid O., Wirth R. and Navon O., 2007. Micrometer-scale cavities in fibrous and cloudy diamonds—A glance into diamond dissolution events. *Earth and Planetary Science Letters*, **264**(1–2), 89–103, http://dx.doi.org/10.1016/j.epsl.2007.09.004.

Kraus E.H. and Slawson C.B., 1939. Variation of hardness in the diamond. *American Mineralogist*, **24**, 661–676.

Kupriyanov I.N., Gusev V.A., Borzdov Yu.M., Kalinin A.A. and Pal'yanov Yu.N., 1999. Photoluminescence study of annealed nickel- and nitrogen-containing synthetic diamond. *Diamond and Related Materials*, **8**(7), 1301–1309, http://dx.doi.org/10.1016/s0925-9635(99)00122-3.

Lang A.R., Yelisseyev A.P., Pokhilenko N.P., Steeds J.W. and Wotherspoon A., 2004. Is dispersed nickel in natural diamonds associated with cuboid growth sectors in diamonds that exhibit a history of mixed-habit growth? *Journal of Crystal Growth*, **263**(1–4), 575–589, http://dx.doi.org/10.1016/j.jcrysgro.2003.11.116.

Nasdala L., Grambole D., Wildner M., Gigler A.M., Hainschwang T., Zaitsev A.M., Harris J.W., Milledge J., Schulze D.J., Hofmeister W. and Balmer W.A., 2013. Radio-colouration of diamond: A spectroscopic study. *Contributions to Mineralogy and Petrology*, **165**(5), 843–861, http://dx.doi.org/10.1007/s00410-012-0838-1.

Rondeau B., Fritsch E., Guiraud M., Chalain J.-P., Notari F., 2004. Three historical "asteriated" hydrogen-rich diamonds: Growth history and sector-dependent impurity incorporation. *Diamond and Related Materials*, **13**(9), 1658–1673, http://dx.doi.org/10.1016/j.diamond.2004.02.002.

Wang W. and Mayerson W., 2002. Symmetrical clouds in diamond—The hydrogen connection. *Journal of Gemmology*, **28**(3), 143–152, http://dx.doi.org/10.15506/jog.2002.28.3.143.

Welbourn C.M., Rooney M.-L.T. and Evans D.J.F., 1989. A study of diamonds of cube and cube-related shape from the Jwaneng mine. *Journal of Crystal Growth*, **94**(1), 229–252, http://dx.doi.org/10.1016/0022-0248(89)90622-2.

Zaitsev A.M., 2001. *Optical Properties of Diamond: A Data Handbook*. Springer, Berlin, Germany, http://dx.doi.org/10.1007/978-3-662-04548-0.

The Authors

Dr Thomas Hainschwang FGA is director and research scientist at GGTL Laboratories, Gnetsch 42, LI–9496, Balzers, Liechtenstein. E-mail: thomas.hainschwang@ggtl-lab.org

Franck Notari is manager and researcher at GGTL Laboratories, 4bis route des Jeunes, CH-1227 Les Acacias, Geneva, Switzerland.

Erik Vadaszi is a gem merchant residing in Idar-Oberstein, Germany.

Objective Diamond Clarity Grading

Michael D. Cowing

The diamond clarity grading scale used worldwide today was introduced by the Gemological Institute of America (GIA) in 1953. To help address varying interpretations and inconsistencies in clarity grading between laboratories (and even within some labs), this article introduces an objective system for diamond clarity grading. The determination of the clarity grade is influenced by up to five factors: size, number, contrast (colour and relief), position and nature of the inclusions. The proposed system assesses these factors (with emphasis on the first four) by using an objective metric that emulates the intuitive analysis done by experienced diamond graders. Using high-quality photographs of more than 100 randomly selected diamond examples, this article demonstrates a high degree of agreement between clarity grades obtained using this system and those determined by GIA and the American Gem Society Laboratories (AGSL). The system's objective methodology may offer a means for improving inter- and intra-laboratory grading consistency.

The Journal of Gemmology, 34(4), 2014, pp. 316–332, http://dx.doi.org/10.15506/JoG.2014.34.4.316

Introduction

Diamond grading by gem laboratories, gemmologists, and valuers/appraisers consists of an evaluation of the four diamond characteristics of cut, colour, clarity and carat weight. These '4 Cs' are the criteria upon which cut and polished diamonds (e.g. Figure 1) are valued and marketed.

Clarity grading is a judgement of the degree to which a diamond is free of inclusions and imperfections when viewed with the 10× magnification of a jeweller's loupe or gemmological microscope. In April 1953, GIA under then-president Richard T. Liddicoat introduced systems for both the colour and clarity grading of diamonds (Shuster, 2003). GIA's clarity grading scale expanded upon terms and definitions that had evolved through trade usage over more than a century. For example, Wade (1916) described diamond imperfection with terms such as 'v. v. s., or very very slight', 'slightly imperfect' and 'imperfect'. GIA's expansion of clarity grading terminology was necessary, as Liddicoat noted, because "There weren't a large enough number of grades to fit the market….We had to have more" (Shuster, 2003).

GIA's clarity grading scale, like its diamond grading system, has become the model for laboratories throughout the world. The terminology and definitions of this scale are universally used to communicate to the gem trade and consumers the purity aspect of diamond quality.

Today, non-GIA laboratories commonly employ clarity scales and terminology that largely retain the nomenclature and definitions of the original GIA system, although these systems have evolved and their implementations vary to

Figure 1: Faceted diamonds such as these are graded according to the '4 Cs' of cut, colour, clarity and carat weight. The round brilliants shown here have clarity grades ranging from VS_1 to SI_1 and weigh 1.12–1.83 ct. Photo by M. Cowing.

differing extents from GIA and from one another. This evolution has resulted in inconsistent grading from lab to lab and even within labs. Standardized clarity grading remains an elusive goal that, due to its subjective nature, many believe is unattainable.

This article introduces a new method of clarity grading that challenges this belief. It is comprised of objective metrics that are used to model the techniques of expert graders whose proficiency results from extensive experience and practice. Photographic examples that use GIA-graded diamonds demonstrate the accuracy and consistency of this system. First, a review of the GIA definitions of each clarity grade will show the subjective nature of existing methodology. Then the new objective system will be introduced and illustrated by various examples from several clarity categories.

The Diamond Clarity Grading Scale

GIA's clarity grading scale consists of 11 grades (Figure 2a): Flawless (Fl), Internally Flawless (IF), two grades of Very Very Slightly Included (VVS_1, VVS_2), two grades of Very Slightly Included (VS_1, VS_2), two grades of Slightly Included (SI_1, SI_2), and three grades of Included (formerly Imperfect; I_1, I_2, I_3).

Diamond imperfections are classified as either external surface features called blemishes or internal features called inclusions (which may also extend to the surface). Blemishes include features such as small extra crown facets, surface graining and certain naturals. They affect determinations between the top two clarity grades of Fl and IF. Below IF, inclusions are the principal determiners of a diamond's clarity grade. Surface scratches, which have depth, are graded as inclusions. In practice, no distinction is made between a shallow feather and a deep scratch. What counts most is inclusion noticeability, which is strongly weighted toward the face-up view (P. Yantzer, pers. comm., 2014). Although inclusions are three-dimensional in nature, it is their two-dimensional appearance mainly observed face-up that is assessed for noticeability.

A diamond's clarity characteristics are plotted using darkfield illumination (side lighting against a dark background), but the final judgement of clarity is made with the diamond held face-up using overhead (above-diamond) lighting. The latter arrangement reveals the noticeability of inclusions as seen under typical viewing circumstances.

The following clarity grade definitions (GIA, 1994; GIA, 2004, 2006) assume a skilled grader working with 10× fully corrected magnification (loupe or microscope) and effective illumination (diffused horizontal lighting with a loupe or darkfield illumination with a microscope):

- Flawless (Fl): No inclusions or blemishes of any kind.
- Internally Flawless (IF): No inclusions and only insignificant blemishes.

a

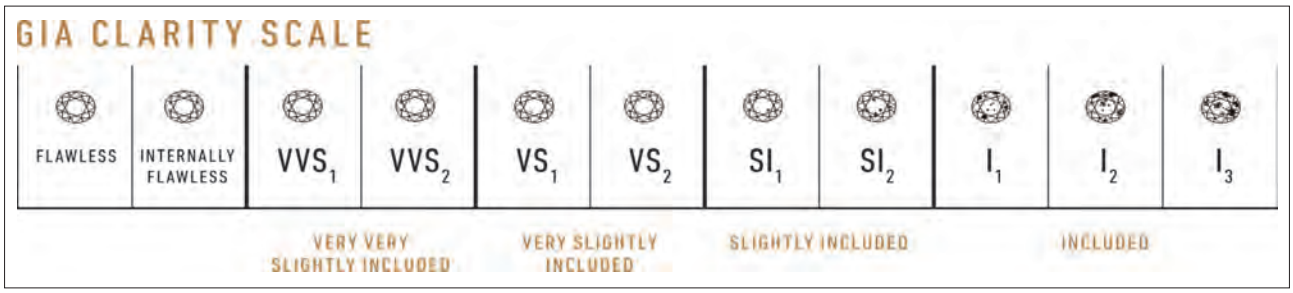

b

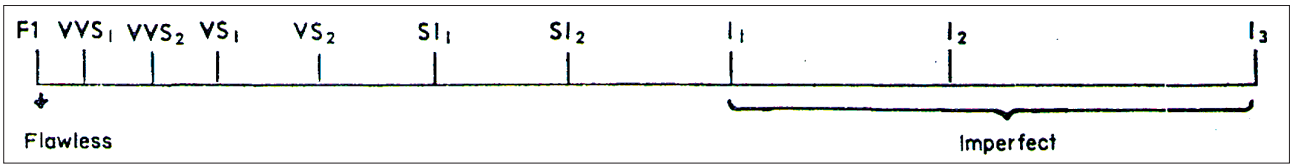

c

Figure 2: (a) GIA's clarity grading scale consists of 11 grades, ranging from Flawless to Included (formerly Imperfect). (b) This early representation of GIA's clarity scale (GIA, 1969) shows an increase in spacing from higher to lower grades. (c) This diagram shows the actual increase in spacing (and in inclusion dimensions) of a portion of the grading scale, corresponding to a doubling in dimensions of grade-setting inclusions from one grade to the next lower grade.

- Very Very Slightly Included: Minute inclusions that range from extremely difficult (VVS_1) to very difficult (VVS_2) to see.
- Very Slightly Included: Minor inclusions that range from difficult (VS_1) to somewhat easy (VS_2) to see.
- Slightly Included: Noticeable inclusions that are easy (SI_1) or very easy (SI_2) to see with 10× magnification, but usually are not easily noticeable to the unaided eye.
- Included (formerly Imperfect): Obvious inclusions under 10× magnification that are easily eye-visible face-up (I_1, I_2 and I_3); for I_3, they severely affect transparency and brightness, and may threaten durability.

Attaining Accuracy and Consistency in a Subjective Clarity Grading System

The subjective definitions of the clarity grades make it challenging to attain accuracy and consistency with this system. This is particularly the case for the beginning grader, as it is difficult to comprehend what an experienced observer sees as 'extremely difficult', 'very difficult', 'difficult' or 'somewhat easy' to locate under 10× magnification. In addition, GIA's diamond grading course notes that "It is important to remember...that it is impossible to develop a precise description of any clarity grade except flawless….Clarity grading is like appraising a painting...: It is the overall picture that sets the clarity grade. Clarity grading is as much an art as an objective science; becoming really proficient at it takes time, experience, and practice" (GIA, 1994, p. 2).

Observations like these may seem daunting. However, GIA does offer this encouragement: "...most people learn to 'sense' the grade immediately. With a little practice, you will know by a sort of educated gut instinct what grade category a stone falls into, almost at first glance" (GIA, 1994, p. 15).

Developing a 'sense' for the clarity grade is subjective and open to variability in interpretation from grader to grader and from lab to lab. How

is it possible that experienced graders can most often agree on a diamond's clarity grade, at least within a particular lab's system? The not very satisfying answer given in diamond courses is that consistency is only gained over time, through observation of diamonds of all clarities, sizes and shapes with their myriad inclusion variations.

Inclusion Characteristics that Impact Diamond Clarity Grades

Determination of the overall impact that inclusions have on the clarity grade is influenced by up to five factors: *size, number, contrast* (colour and relief), *position* and *nature*. "The nature of a clarity characteristic is based on two general distinctions. Whether it is internal or external is one: Below IF, the clarity grade is almost always set by inclusions; blemishes generally have little or no effect on it. The second is whether a particular characteristic poses any risk to the stone. Most do not" (GIA, 1994, p. 12). Below IF, this most often leaves the combined judgement of the first four of these factors as the determiner of the clarity grade.

The clarity grade of most diamonds is correctly established by assessing the single largest inclusion or a small number of similar major inclusions. Such factors are referred to as the 'grade-makers'. The four main clarity factors (size, number, contrast and position), judged together for the largest grade-maker inclusion(s), most often determine a diamond's clarity grade.

A salient feature among the four clarity factors is *size* which, along with the degree of *contrast* between the inclusion and the surrounding diamond, determines the visibility of a given inclusion. The larger the inclusion and the greater its contrast, the more it stands out and the lower the grade. *Number* comes into consideration when the largest 'grade-maker' inclusions are more numerous than one. Three or four similar grade-maker inclusions are likely to lower the clarity one grade more than would a single similar feature. Multiple grade-maker–size inclusions are effectively handled in most cases by grading them the same as an equivalent inclusion with similar total area. Lastly, consideration is given to the *position* of the grade-maker inclusions within the diamond. Viewed face-up, those under the table (in what is called the 'heart' of the diamond) are most noticeable and are graded most severely. Inclusions touching or near the girdle are least noticeable and are often graded more leniently. Features that are deep enough in the 'heart' often reflect in multiple positions, which may result in a lower grade. Early GIA instruction was to penalize by one grade an inclusion that had a lot of reflections (P. Yantzer, pers. comm., 2014).

To arrive at a clarity grade, the new objective system evaluates the four clarity characteristics together, combining them in a manner that emulates the practice of experienced graders. This is done by utilizing aspects of human perception concerning the noticeability of inclusions. An analysis of early efforts at objective clarity grading (discussed below) leads to two key observations:

1. The grade-defining property of inclusion noticeability is directly related to inclusion area. If inclusion 'grade-makers' have the same area and only differ in their length and width, they are perceived to have similar noticeability and most often will receive the same grade.
2. The increase in inclusion size from one grade to the next is not constant, but approximately follows a doubling of the inclusion's dimensions. That rough dimension doubling, which is a quadrupling in area, is surprisingly consistent from grade to grade across the entire clarity scale.

From Figure 2b it is clear that the range or distances on the GIA clarity grading scale between the lower grades is significantly larger than the distances between the higher grades. However, based on the inclusion size factor indicated in the second key observation mentioned above, the actual increase in distance from grade to grade is even more pronounced, as shown partially in Figure 2c. Surprisingly, an approximate doubling in dimensions of grade-setting inclusions occurs from grade to grade across the entire scale. Because of this doubling in dimension (and therefore an increase in area by about a factor of four), each decrease in clarity grade corresponds to a large multiplicative escalation in inclusion size and noticeability. Figure 3 provides an example of

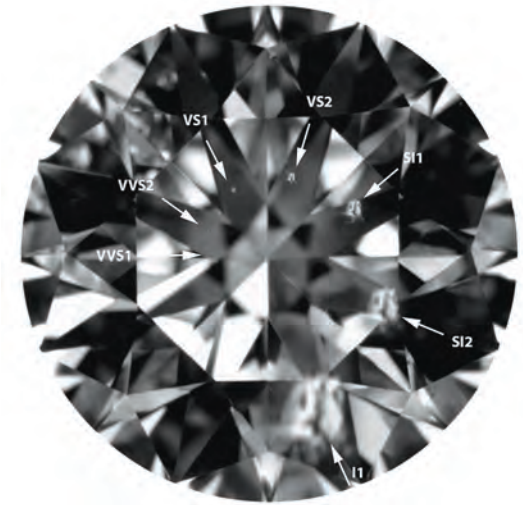

Figure 3: Illustrating the relative increase in inclusion size from grade to grade are these seven inclusions that have been digitally inserted in a 1.11 ct diamond (6.66–6.63 × 4.11 mm). The inclusions are sized according to clarity grades that range from VVS_1 to I_1.

Figure 4: This 1.11 ct diamond (6.66–6.63 × 4.11 mm) contains four SI_1-size inclusions that have different dimensions, but the same area and contrast, and thus similar noticeability. Each has an area determined to be approximately 35,000 µm².

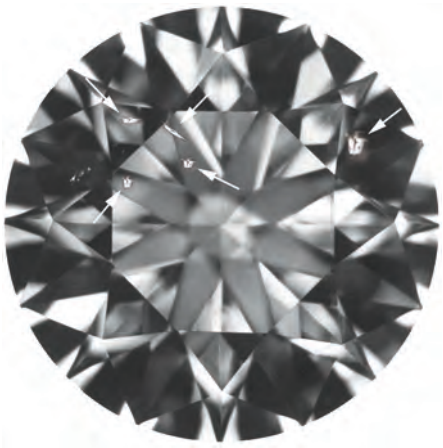

Figure 5: This 0.70 ct diamond (5.74–5.71 × 3.52 mm) contains four VS_2-size inclusions between the 10 and 11 o'clock positions near the table edge. All of these inclusions have the same area and noticeability, despite their varying dimensions.

Figure 6: The same 0.70 ct diamond as in Figure 5 is shown here containing four VS_1-size inclusions at 5 o'clock inside the table. Each one has one-quarter the area of the VS_2-size inclusion seen at 10 o'clock. Taken together, the VS_1 inclusions would receive one lower grade of VS_2.

this increase in inclusion size from clarities of VVS_1 to I_1.* To provide visual support for the two key observations listed above, carefully sized inclusions also have been inserted into the darkfield diamond images in Figures 4–6.

In Figure 4, four SI_1-size inclusions in a 1.11 ct diamond have different dimensions but nearly identical area and contrast, and therefore each one has similar noticeability. Individually, each inclusion would be graded identically as SI_1 because each has the same area (roughly 35,000 µm²) and the same contrast (relief).

In Figure 5, the four inclusions between the 10 and 11 o'clock positions in the 0.70 ct diamond are the 'crystals' in Figure 4 reduced to half their dimensions and a quarter of their area (8,800 µm²). This reduces their noticeability and improves the clarity by one grade to VS_2 when

* Unless otherwise noted, all of the diamond images from Figure 3 onward were taken by Jonathan Weingarten and are scaled to show 10× magnification. The original colour photographs were converted by the author to black-and-white images after it was determined that the colours resulting from diamond's high dispersion distracted from finding and judging the noticeability of inclusions.

Figure 7: This 1.11 ct SI_2-graded diamond (6.66–6.63 × 4.11 mm) contains a white crystal and a string of five smaller dark-appearing inclusions, for a combined clarity grade of high SI_2.

Figure 8: Contrast the stone in Figure 7 with this 1.05 ct diamond (6.57–6.59 × 4.03 mm), which received the same SI_2 clarity grade despite having a much larger reflecting crystal inclusion.

they are considered individually. Again, despite their differing dimensions, all four inclusions are individually graded the same because each has the same area and amount of contrast. All four together have the same area as the single SI_1 inclusion seen at the 2 o'clock position in Figure 5. Thus, with similar overall area and impact on noticeability, four VS_2-size grade-maker inclusions evaluated together most often receive the same clarity grade as a single SI_1 grade-maker.

Reducing those four crystals by another factor of two in dimension (and factor of four in area) results in the group of four tiny crystals that are seen at the 5 o'clock position in the 0.70 ct diamond in Figure 6. Individually each of these inclusions is graded VS_1. Evaluated together as a group, they have similar total area and noticeability as the VS_2 inclusion at the 10 o'clock position in Figure 6. Therefore collectively these inclusions would receive one clarity grade lower (VS_2) than when they are considered individually.

An additional example is provided by this diamond's original string of three VS_1-size crystals under the crown main facet at 10 o'clock in both Figures 5 and 6. Considered together, GIA graded these inclusions VS_2.

Since for each successive grade a particular inclusion type increases in dimension by about a factor of two, the range of inclusion dimensions *within* each successive grade also increases by the same factor. For example, an inclusion in a low-borderline SI_2 can be almost twice the dimensions (and about four times the area) of a high borderline SI_2 of similar nature. Compare the large differences in size and noticeability between the identically GIA-graded (SI_2) ~1 ct diamonds in Figures 7 and 8. The SI_2 in Figure 7 should bring a large premium over the SI_2 in Figure 8, but price guides and the market in general currently value them the same. Shouldn't a clarity grading system account for what should be a significant value difference between these two widely different clarity appearances? The current scale lacks sufficient definition for the market in the grades of SI_2 and below. These two identically graded SI_2 diamonds bring to mind Liddicoat's statement "There weren't a large enough number of grades to fit the market.... We had to have more."

With more lower-clarity diamonds entering the market, the relatively large range of SI_2 and the much greater range of I_1 created market demand for an intermediate grade for stones containing inclusions with a combined area that is close to I_1 but that have too good an appearance to be lumped together with typical I_1 diamonds. That need prompted the introduction of an SI_3 grade in 1992, initially by Tom Tashey, then owner of EGL Los Angeles (T. Tashey, pers. comm., 2014). However, attempts to meet this market need have largely been frustrated by misuse. The lack

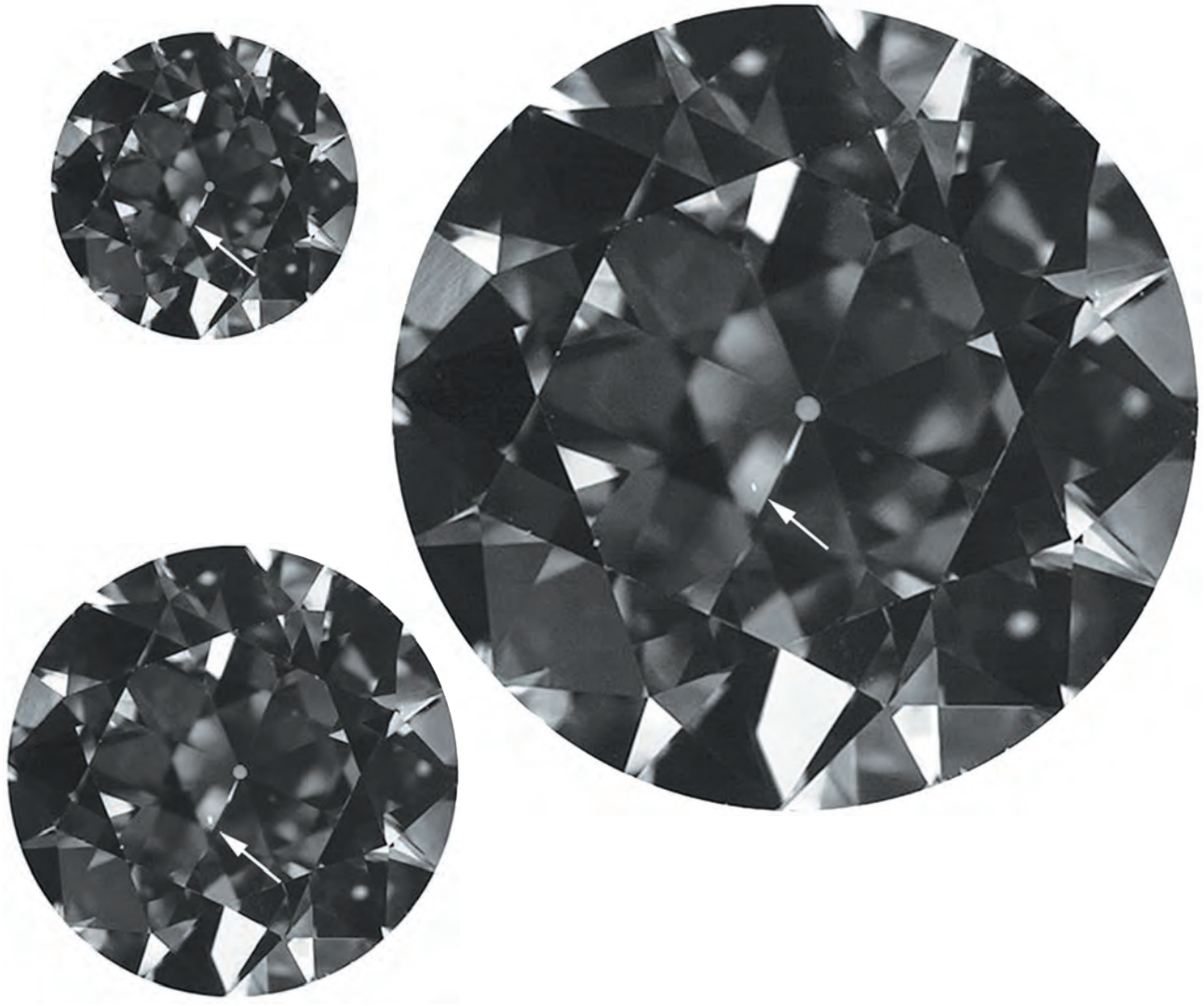

Figure 9: An identical VS_2-size crystal inclusion is shown in these diamond images that have been rescaled to the equivalent of ⅓, 1 and 6 ct. The inclusion has similar noticeability in all three images, and would result in the same grade over this large range of diamond sizes.

of objective grading standards has led to wide discrepancies and an increase in inclusion sizes that are assigned SI_3 grades. In fact, diamonds graded SI_3 often extend well into the GIA I_1 grade. (Note that although many in the diamond trade and some laboratories have adopted the SI_3 designation, it is not recognized by GIA.)

The Relationship of Inclusion Size to Diamond Size

Thus far absolute inclusion size has been addressed, but not inclusion dimension relative to diamond size. In very small diamonds, inclusions that occupy a significant percentage of the diamond's dimensions may be graded more severely. As well, an inclusion in a large diamond may be less noticeable and for that reason may be graded less severely. In general, the system presented here has been found to be accurate independent of diamond size over roughly the range of round diamond diameters from 4.5 mm (⅓ ct) to 11.8 mm (6 ct). This is particularly the case for clarities ranging from VVS_1 to VS_2, as well as most SI_1 diamonds. To illustrate this, the image of a VS_2-size inclusion in a 1.00 ct diamond was copied and pasted into the same location in two images of the same diamond scaled to ⅓ ct and 6 ct (Figure 9). The inclusion in all three diamonds is seen to be of the same category: a 'minor inclusion that is somewhat easy to see under 10× magnification', corresponding to VS_2 over this range of sizes.

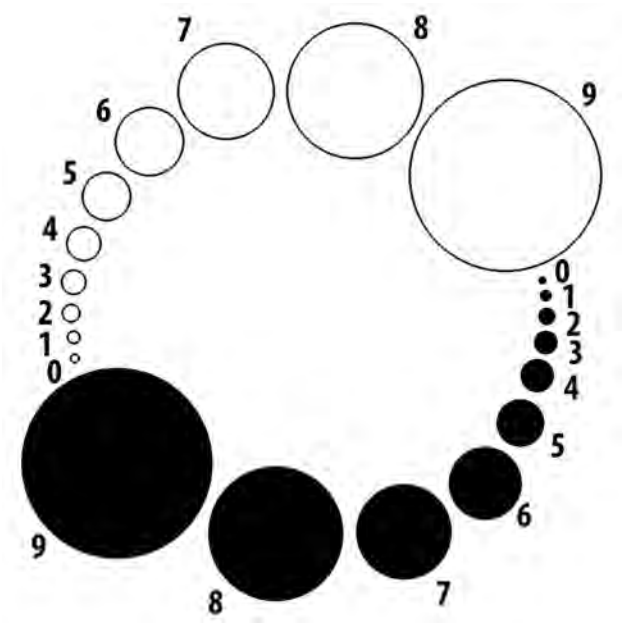

Figure 10: The Porton graticule consists of circle diameters increasing by the factor $\sqrt{2}$. Drawing by M. Cowing.

Previous Objective Clarity Grading Systems

In the 1970s, there were two notable attempts to reduce the subjectivity of diamond clarity grading through objective measurements of inclusion size combined with refinements in the factors of inclusion contrast, number, and location within the stone.

Contributions by Roy Huddlestone and DGL, London

Huddlestone introduced at the Diamond Grading Laboratories (DGL) the use of a Porton graticule to measure diamond inclusions. As mentioned by Bruton (1978), this graticule, a version of which is shown in Figure 10, consists of circles numbered 0 to 9 that increase in diameter by the factor $\sqrt{2}$ (a doubling in area). By fitting an inclusion's length and width to the nearest Porton circles that just enclose each dimension, a measure of inclusion size in Porton numbers is obtained. This transformation from dimensions to circle numbers is a useful and ultimately instructive process. An approximate representation of an inclusion's area (multiplication of length by width) is obtained by simply adding the corresponding circle numbers for its length and width. (Addition in the 'Porton domain' equates to multiplication of length times width, yielding a measure of an inclusion's area.) If the inclusion is rectangular, the area measurement is exact. Irregular or circular features have slightly less area than the product of length and width, but with a little ingenuity they are adequately characterized by this technique. For instance, a tapering inclusion's area is accurately approximated by adding the Porton circle number for its length to that for its average width.

In DGL's system, the total area score, which was obtained in this manner for each significant inclusion, was converted to a 'primary point count' (Burr et al., 1981) that was then adjusted for 'brightness' (the equivalent of contrast or relief) and 'its position in the stone' to arrive at a final point count establishing the clarity grade.

Contributions by Kazumi Okuda

Okuda incorporated his version of the circle graticule into his diamond grading microscope. Having been introduced to DGL's system by Roy Huddlestone (R. Huddlestone, pers. comm., 2014), he used a circle graticule to measure inclusion area in a manner similar to DGL. An important difference is that Okuda's circles increased in diameter not by the factor $\sqrt{2}$ but by a factor of 2. Table I shows Okuda's conversion from micrometre measurement to his circle numbers. As seen in an excerpt of the instruction manual (Figure 11), a representation of inclusion area is obtained by adding the circle numbers that just enclose the inclusion's length and width.

Okuda's most important contribution to objective clarity grading was his clarity conversion table (Figure 12), which converts the area score to a clarity grade. For cases in which no adjustment is needed for contrast or position, such as a grade-

Table I: Okuda's conversion from micrometres to circle number.

Size (μm)	Circle number
10	1
20	2
40	3
80	4
160	5
320	6
640	7
1,280	8
2,560	9
5,120	10

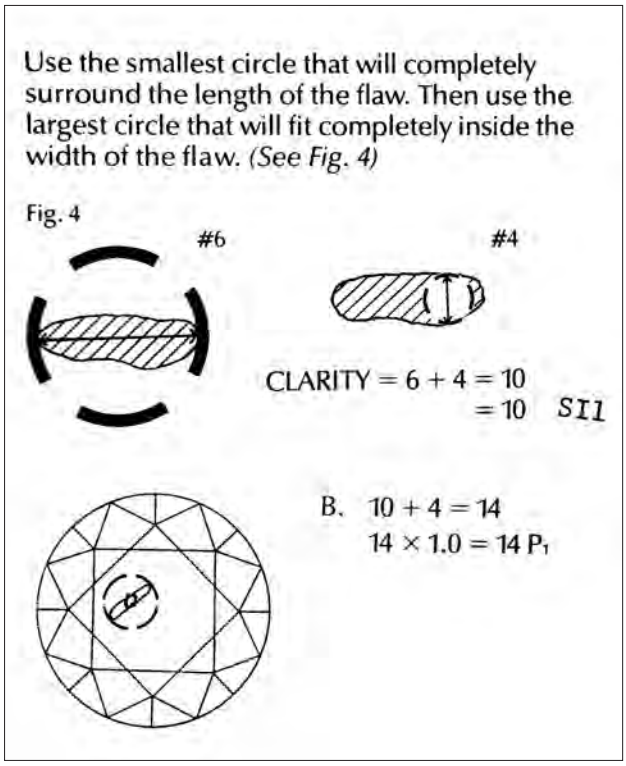

Figure 11: This excerpt from Okuda (1978) illustrates how a measure of inclusion area is obtained by the addition of circle numbers corresponding to their length and width.

Figure 12: The Okuda clarity conversion table shown here converts the area score obtained from the sum of the circle numbers for length and width to a clarity grade. From Okuda (1978).

CLARITY No.		CLARITY
(A)	(B)	
0	1	FL
2	3	VVS_1
4	5	VVS_2
6	7	VS_1
8	9	VS_2
10	11	SI_1
12	13	SI_2
14	15	P_1
16	17	P_2
18	19	P_3
20		Rejection

maker crystal or feather inclusions of medium contrast located under the diamond's table, the clarity grade is obtained directly from the conversion table using the area score obtained from the sum of the circle numbers for length and width. However, Okuda's grading system had two shortcomings:

1. It lacked an adjustment for variations in inclusion contrast.
2. Although there was an adjustment for position, it was applied to the area score as a multiplicative factor. As will be seen, this adjustment must be applied additively in the circle number domain in order to mirror GIA grading practice correctly in a uniform fashion throughout the clarity scale.

The New Clarity Grading System

The first step in the new clarity grading system is to measure the inclusion dimensions using 32× to 45× microscope magnification, employing either a vernier caliper or a reticule capable of approximately ±10 µm accuracy. The author recommends today's version of the 6-inch Mitutoyo Digimatic digital calipers that he has employed for over 30 years. The ±10 µm accuracy suffices for typical inclusion sizes of VS_1 and larger. VVS_1- and VVS_2-size inclusions are more easily and accurately measured (using the same digital calipers) from an enlarged photograph.

With insights from the transformation from inclusion dimensions to Porton circle numbers and Okuda's clarity table, the author has developed a new continuous grading scale consisting of a graph with a curve increasing with a $\sqrt{2}$ relationship; it will be included in the author's upcoming ebook (Cowing, in press). The graph is used to provide a transformation of inclusion dimensions to the exponential domain. The sum of the transformed length and width provides an inclusion area score like that obtained using the discrete circles of the Porton graticule. However, the advantage of using this graph over the discrete circles is its continuous nature. It does not require the nonlinear interpolation necessary when measuring an inclusion's length or width that falls between circle sizes.

Table II. Adjustment guidelines due to inclusion contrast.

Scale	1	2	3	4	5
Description	Low-contrast inclusion difficult to observe with overhead lighting; a 'cloud' is a good example	Inclusion with contrast in between a cloud and typical crystals and feathers	Typical contrast of a clear or white crystal or feather as seen with overhead lighting	A more solid white or darker than usual crystal or feather between typical and high contrast	High contrast with overhead lighting, either black on a light background or a bright reflector on a dark background
Adjustment to clarity grade	−2e to −4e (one to two grades higher)	−1e to −2e (one-half to one grade higher)	No adjustment	+0.5e to +1e (one-quarter to one-half grade lower)	+1e to +2e (one-half to one grade lower)

Adjustments to the Area Score due to Inclusion Number, Contrast and Position

After finding the starting clarity grade from the combined total inclusion area score of the grade-maker inclusions, adjustments are made according to inclusion number, contrast and position.

Number: Instances where there are a number of similar grade-maker–size inclusions are effectively handled by summing them to the approximate dimensions of a similar inclusion having the same total area. This commonly results in an adjustment of one grade lower when there are multiple (i.e. about four) similar grade-maker–size inclusions (four times the area of one of them). Note that near-borderline inclusion sizes may drop into the next lower grade with as few as two grade-maker–size inclusions.

Contrast: As taught by GIA, inclusion contrast, which is referred to as 'colour and relief', "can affect visibility as much as size….*Relief* is the contrast between the inclusion and the [surrounding field of the] stone; the greater the relief, the more it will affect the clarity grade" (GIA, 1994, p. 12).

To address the influence of contrast or relief on the clarity grade, the new system employs a simple 1-to-5 scale along with their corresponding adjustments (Table II). Any adjustment is applied additively in the exponential domain. A one-grade-lower clarity adjustment corresponds to an addition of +2e (the 'e' notation refers to an exponential scale).

Needing no adjustment is a medium-contrast crystal or white feather, which would be designated a 3 on the contrast scale. A very high contrast inclusion is 5 on the scale, and most often requires an adjustment of one grade downward (i.e. a +2e adjustment). For example, a black crystal that obviously stands out against the surrounding diamond with overhead lighting would receive a +2e adjustment to the clarity grade. In the other direction, a very low contrast inclusion that barely stands out, such as a cloud, is designated a 1 on the contrast scale and adjusts the initial clarity grade upward by 1–2 grades (a –2e to –4e change). Inclusions requiring intermediate adjustments (i.e. designated 2 or 4 on the contrast scale) may not change the clarity grade if the diamond falls near the middle of a particular grade. However, a borderline grade will probably change.

Position: Adjustments for position are based on observation of GIA practice and are described in Table III. No adjustment is needed for the easiest-to-locate inclusions under the table or just outside

Table III. Adjustment guidelines due to inclusion position.

Position	Inside table or just outside it	VS_2 size or smaller, touching or very near girdle	VS_2 size or smaller, near girdle	SI_1 size, near or touching girdle	SI_2 or larger, anywhere in diamond
Adjustment to clarity grade	No adjustment	−1e to −2e (one-half to one grade higher)	−0.5e to −1e (one-quarter to one-half grade higher)	−0.5e to −1e (one-quarter to one-half grade higher in a large diamond)	No adjustment

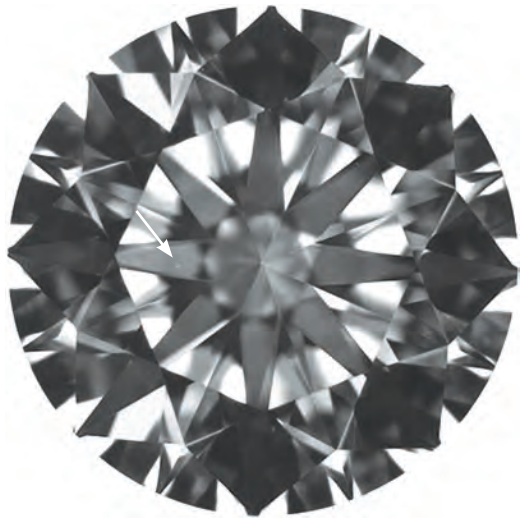

Figure 13: This 1.20 ct VS_1-graded diamond (6.83–6.85 × 4.17 mm) contains a crystal inclusion measuring 90 × 42 µm (under the table at 9 o'clock), which corresponds to a clarity grade of VS_1 using the new system.

it. An adjustment is made for as much as a one grade upward (–1e to –2e) for VS_2 and smaller inclusions that touch the girdle or are just inside it. A position adjustment of one-quarter to one-half grade upward may apply to inclusions outside the table but not very near the girdle. This would only change the clarity grade in borderline cases. Larger inclusions (SI_2 and greater) are unlikely to be adjusted for position because of their obvious nature anywhere in the diamond from girdle to table.

Final Grading Call Considerations

It is important to point out that these inclusion measurements and judgements are all made from a face-up two-dimensional perspective. However, if a grade-maker inclusion extends deeper into the stone than the dimensions of its face-up measurement (so that it appears significantly larger when viewed from the side), consideration must be given to lowering the grade obtained by face-up observation. In most instances, such an adjustment is not more than one grade lower than the face-up call.

It is also important to note that the final clarity grade is made by observation of the overall inclusion visibility in the face-up position under overhead lighting (not darkfield illumination). This is usually accomplished in the laboratory by viewing the diamond with a 10× loupe under the small 7-inch fluorescent-tube light attached to the microscope; diamond traders more commonly use a fluorescent desk lamp.

Objective Clarity Grading Example

Figure 13 provides an example of a single grade-maker crystal inclusion of medium contrast (3 on the contrast scale) located under the table:

1. Measure inclusion length and width (in microns): 90 × 42 µm.
2. Convert length and width from microns to the exponential domain (see Table I): 4.2e + 3.1e.
3. Sum the exponent numbers to obtain the inclusion area score: 7.3e.
4. Make adjustments for contrast and position: In this case there are none, since the inclusion has typical contrast (3) and its position is under the table.
5. Look up the total adjusted clarity grade for 7.3e (see, e.g., Figure 12): VS_1.

Comparison with Clarity Grades Determined by Gem Laboratories

To evaluate numerous laboratory-graded diamonds in conjunction with this study, it was expedient to experiment with grading of inclusions using high-quality photographs. Without the actual diamonds in hand, the question was: Can inclusions, their sizes and their contrast/relief be measured and adequately judged from diamond photographs? With good photographs where the grade-maker inclusions are in focus, the answer is yes. An initial experiment involved grading the diamonds photographed in Roskin (1994). From the darkfield diamond images in that book, a vernier caliper was used to measure the dimensions of each diamond's grade-maker inclusions along with the stone's dimensions. The actual inclusion dimensions were then obtained by scaling according to the ratio of actual diamond diameter divided by the diamond image diameter. Objective grading using inclusion measurements from the images resulted in near-perfect agreement with the stated clarity grades of all the diamonds pictured in the book.

The majority of images in the author's database, and all of those used in this article, were obtained

Figure 14: This 0.92 ct VVS_1-graded diamond (6.22–6.23 × 3.85 mm) contains a VVS_2-size pinpoint. The position of this inclusion near the girdle at 6 o'clock calls for a half-grade adjustment, making the clarity grade a low VVS_1.

from the website for the diamond and jewellery retailer Good Old Gold (www.goodoldgold.com), which lists the company's diamond inventory, commonly with corresponding grading reports from GIA or AGSL. Also available are darkfield images pointing out the grade-maker inclusions, and for some diamonds there are images taken with overhead lighting. Owner Jonathan Weingarten graciously granted the author access to this ready-made database. The inclusion dimensions and other noticeability factors were measured and judged from the available darkfield and overhead lighting images in a manner similar to that employed for 'grading' Roskin's (1994) diamond images. The clarity grades obtained with the new objective system were compared to laboratory-determined grades for more than 100 randomly selected diamonds in Good Old Gold's inventory, over a range of sizes from ⅓ to 6 ct and clarities from VVS_1 to I_2. The grades obtained with the new system accurately reflected laboratory grading in over 90% of the examples. 'Solid' clarity grades (those in the middle half of a grade range) almost always matched those determined by the laboratory. In fact, the author has been employing this objective system's methodology since the early 1980s, and has found throughout this time period a close agreement with the clarity grading calls of both GIA and AGSL. The author continues to augment the current database with GIA-graded diamonds he has examined and photographed (both with darkfield and overhead lighting) and then graded with this new system.

The following examples were selected to show the application of the new system to GIA-graded diamonds with a range of clarities.

VVS_1 Example

The VVS_1 clarity grade is defined by the presence of minute inclusions that are extremely difficult to see with 10× magnification. The question of when an inclusion becomes visible to the experienced observer at 10× magnification is important, as it defines the boundary between Fl or IF and VVS_1. According to Bruton (1978), a possible example of such an inclusion is a white pinpoint of approximately 5 µm that appears bright with very high contrast against a dark background. However, if the pinpoint has medium contrast, then the threshold of 10× visibility doubles to 10 µm. This inclusion area of 10 × 10 µm corresponds to a clarity score of 1e + 1e = 2e, which is the boundary between IF (0e–1.999e) and VVS_1 (2.0e–3.999e).

The 0.92 ct diamond in Figure 14 has a single pinpoint at 6 o'clock near the girdle under a crown half. The inclusion has a diameter of 24 µm for a clarity score of 2.3e + 2.3e = 4.6e, corresponding to an initial grade of VVS_2. The pinpoint's position outside the table near the girdle calls for a half-grade adjustment of 4.6e – 1e = 3.6e, for a final clarity grade of a low VVS_1.

VVS_2 Example

The VVS_2 clarity grade is defined by the presence of minute inclusions that are very difficult to see with 10× magnification. Earlier it was stated that a number of grade-maker–size inclusions are effectively handled by grading them as an equivalent inclusion with similar total area. The presence of about four similar grade-maker inclusions is likely to lower the clarity one grade more than would a single similar feature by itself. An evaluation of the 1.55 ct VVS_2-graded diamond in Figure 15a provides a practical example illustrating both principles. The stone contains five pinpoints (see plot in Figure 15b), but the largest and only one visible at 10× magnification measures 23 × 21 µm = 2.1 + 2.1e = 4.2e, which corresponds to a high borderline VVS_2. Two of the additional pinpoints (visible in

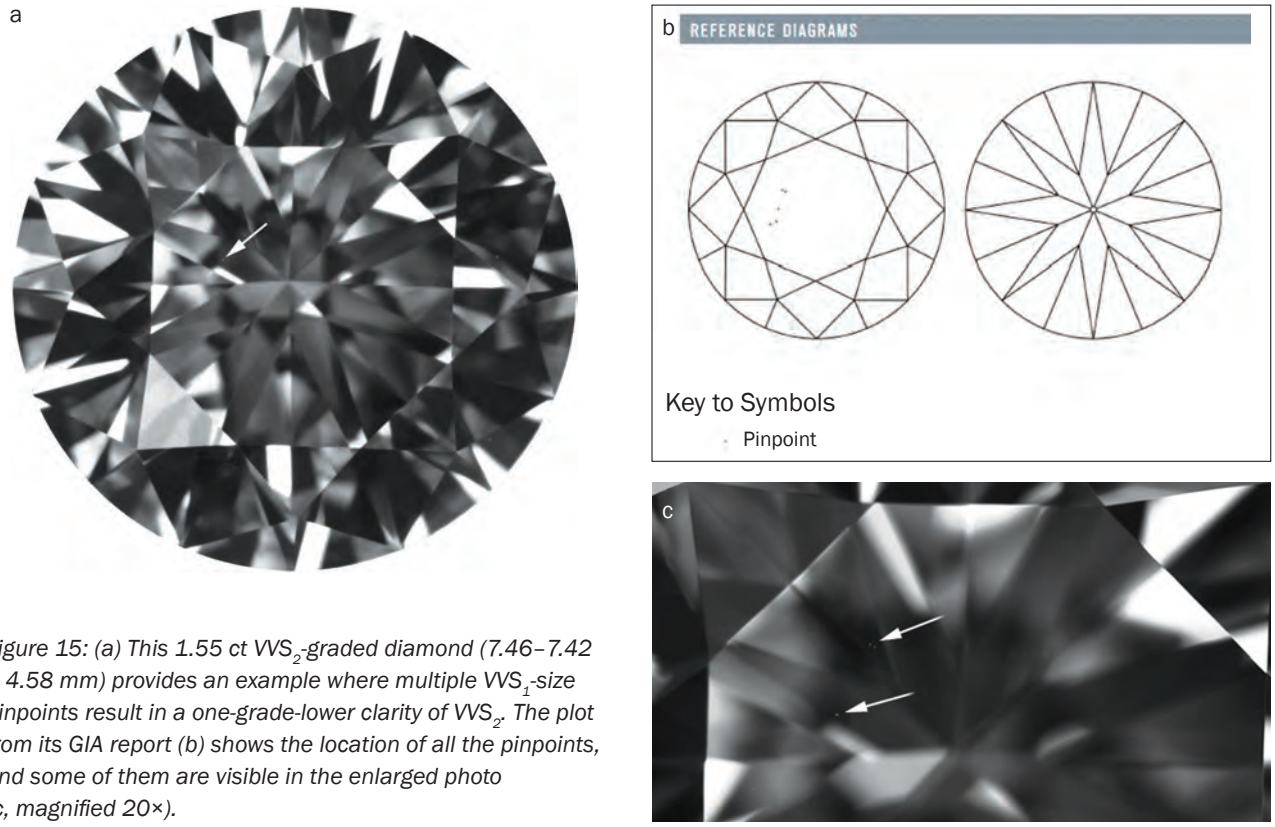

Figure 15: (a) This 1.55 ct VVS_2-graded diamond (7.46–7.42 × 4.58 mm) provides an example where multiple VVS_1-size pinpoints result in a one-grade-lower clarity of VVS_2. The plot from its GIA report (b) shows the location of all the pinpoints, and some of them are visible in the enlarged photo (c, magnified 20×).

Figure 15c) are each 18 × 18 µm = 1.9 + 1.9e = 3.8e (low VVS_1 pinpoints individually) and the other two are even smaller. An inclusion having the combined total area of all five pinpoints would be approximately 70 × 20 µm = 3.8e + 2.0e = 5.8e, which would have a final clarity grade of low VVS_2.

There is an additional way to arrive at the clarity grade for this example. The three pinpoints mentioned above are low-VVS_1 in size, and along with the two additional tiny VVS_1 pinpoints that are not visible in the photos, the group has the equivalent noticeability of four low-VVS_1 grademakers, bringing the call down one grade from a low VVS_1 to a low VVS_2.

VS_2 Examples

The VS_2 clarity grade is defined by the presence of minor inclusions that are somewhat easy to see with 10× magnification. The 0.90 ct VS_2-

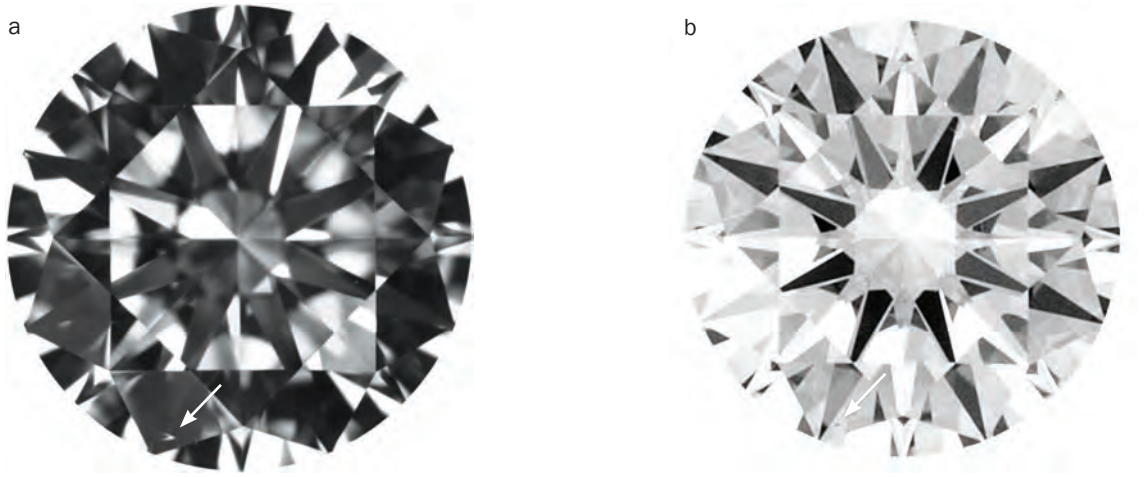

Figure 16: A 0.90 ct VS_2-graded diamond (6.26–6.24 × 3.76 mm) containing an arrowhead-shaped feather located at 7 o'clock is shown with darkfield illumination (a) and overhead lighting (b). This example illustrates how inclusions typically appear less distinct with overhead lighting (where the final clarity grade call is made) than with darkfield.

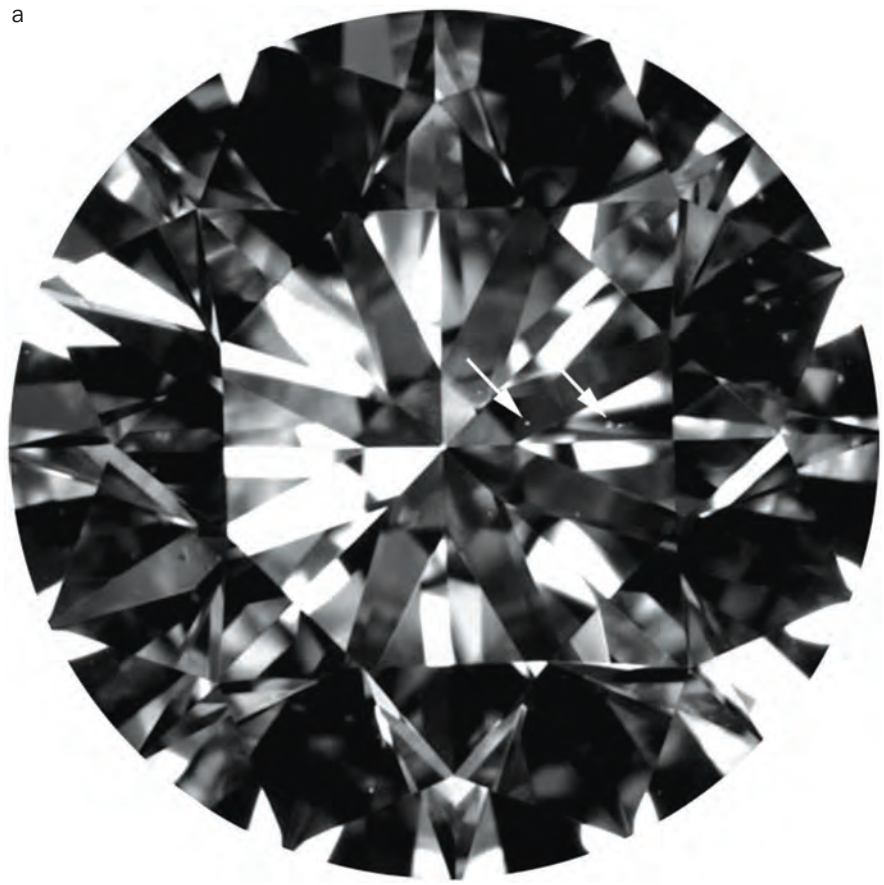

Figure 17: (a) This large VS_2-graded diamond (5.70 ct, 11.48–11.53 × 7.13 mm) contains a string of five tiny crystals that taken together have the combined area of a VS_2. The plot from its GIA report (b) shows the location of all the inclusions, most of which are visible in the enlarged photo (c, magnified 20×).

graded round brilliant in Figure 16 contains an arrowhead-shaped feather of medium contrast (3) located under a crown main facet at 7 o'clock. The two images of Figure 16 illustrate the fact that with overhead illumination (where the final clarity grade call is made), inclusions of medium contrast are typically less distinct than they are with darkfield. This is because darkfield illumination is designed to illuminate inclusions by making them appear bright against a dark background. The feather has approximate dimensions of 162 × 65 µm = 5.2e + 3.8e = 9e, which corresponds to an initial call of a solid VS_2. An adjustment is needed due to the feather's location near the girdle; about –0.7e is appropriate, making the final score 8.3e, and the clarity grade a high VS_2.

The 5.70 ct VS_2-graded round brilliant in Figure 17 contains a string of five tiny crystals under the table around 3 o'clock. Together they add up to an equivalent inclusion size of 167 × 83 µm that translates to 5.2e + 4.1e = 9.3e, for a clarity grade of VS_2.

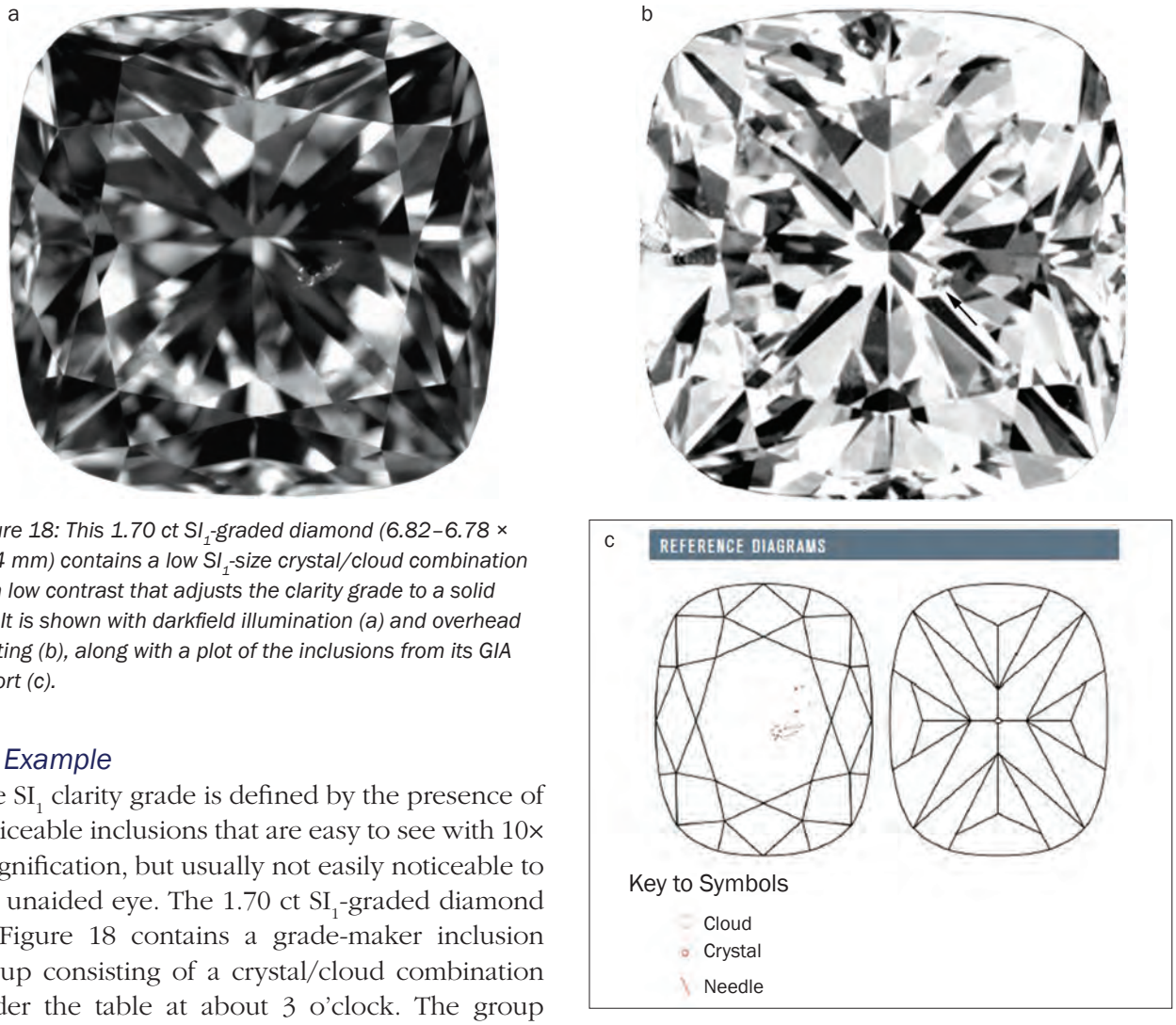

Figure 18: This 1.70 ct SI_1-graded diamond (6.82–6.78 × 4.74 mm) contains a low SI_1-size crystal/cloud combination with low contrast that adjusts the clarity grade to a solid SI_1. It is shown with darkfield illumination (a) and overhead lighting (b), along with a plot of the inclusions from its GIA report (c).

SI_1 Example

The SI_1 clarity grade is defined by the presence of noticeable inclusions that are easy to see with 10× magnification, but usually not easily noticeable to the unaided eye. The 1.70 ct SI_1-graded diamond in Figure 18 contains a grade-maker inclusion group consisting of a crystal/cloud combination under the table at about 3 o'clock. The group of inclusions is of low contrast (2) and has a combined area equivalent to 649 × 130 µm, which translates to 7.1e + 4.6e = 11.7e. After a half-grade adjustment (–1e) for the low contrast of the inclusions, the score is 10.7e, which corresponds to a clarity grade of SI_1.

SI_2 Example

The SI_2 clarity grade is defined by the presence of noticeable inclusions that are very easy to see with 10× magnification, but typically not easily noticeable to the unaided eye. The 0.74 ct SI_2-graded diamond in Figure 19 contains a grade-maker cluster of low-contrast (2) feathers extending deep under the table. Summing the area of each feather yields an approximate inclusion area of 685 × 372 µm = 7e + 6.2e = 13.2e, corresponding to a middle SI_2. An adjustment of one-half grade upward (–1e) for the low inclusion contrast yields a clarity score of 12.2e. However, this diamond provides an unusual case of having features that are not apparent with darkfield illumination but are noticeable with overhead lighting (numerous feather reflections located outside the table). It is challenging to speculate from the photo how apparent these reflections were to the grader. They appear to warrant an adjustment of one-half to one full grade downward (+1e to +2e), yielding a score of 13.2e to 14.2e, corresponding to a low SI_2 bordering on a high I_1. The SI_2 clarity grade received at the laboratory was probably due to the fact that these additional features are reflections that were not very noticeable.

I_1 Example

The I clarity grades are defined by the presence of obvious inclusions with 10× magnification that are eye-visible face-up. The 1.01 ct I_1-graded cushion brilliant cut in Figure 20 contains a large grade-maker inclusion under the table edge at 7 o'clock that shows moderately high relief (4) with overhead illumination. The approximate

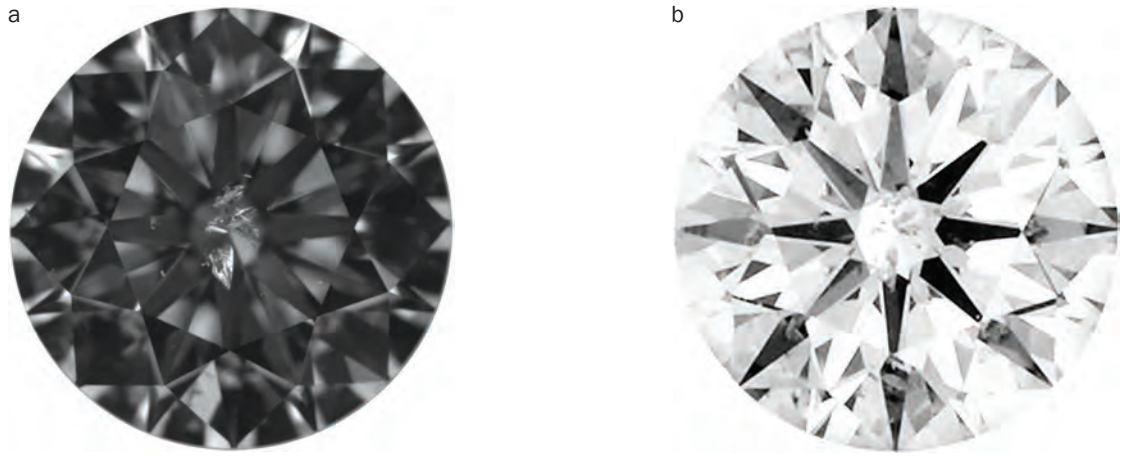

Figure 19: Shown with darkfield illumination (a) and overhead lighting (b), this 0.74 ct SI_2-graded diamond (5.80–5.82 × 3.60 mm) has a grade-maker cluster of feathers with a combined area that sums to SI_2 size. An adjustment for their low contrast is more than offset by the fact that they reflect outside the table. With overhead illumination the reflections outside the table are apparent, leading to a low-borderline SI_2 clarity grade.

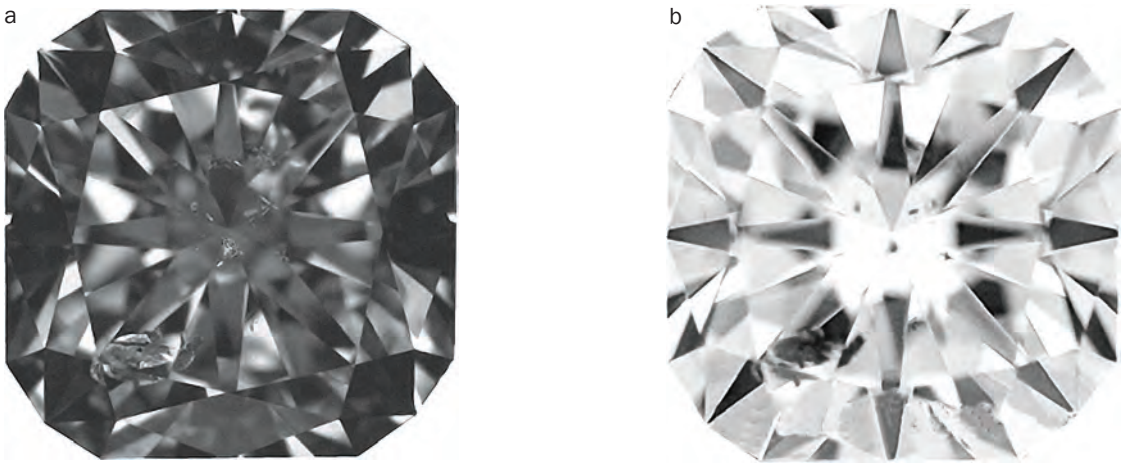

Figure 20: Shown with darkfield illumination (a) and overhead lighting (b), this 1.01 ct I_1-graded diamond (5.85–5.89 × 3.85 mm) contains a large I_1-size inclusion. The high contrast seen with overhead lighting adjusts the grade downward to a low I_1.

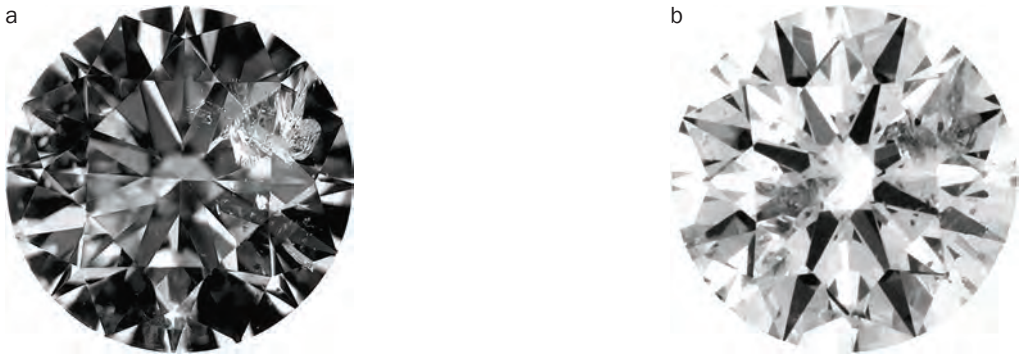

Figure 21: This 0.35 ct I_2-graded diamond (4.55–4.54 × 2.78 mm) contains a large I_1-size fracture that is best seen with darkfield illumination (a). Viewed with overhead lighting (b), a reflection of the fracture causes a doubling of its apparent area, which combined with the relatively small size of the diamond leads to a solid I_2 clarity grade.

dimensions are 1026 × 545 µm = 7.7e + 6.8e = 14.5e, for a clarity grade of high-medium I_1. After adjusting one-half grade downward (+1e) for the moderately high contrast, the final score is 15.5e, corresponding to a low I_1.

I_2 Example

The 0.35 ct I_2-graded round brilliant in Figure 21 contains a large fracture that is best seen and measured using darkfield illumination. It is 1165 × 757 µm = 7.8e + 7.3e = 15.1e, for an initial

clarity grade of middle I_1. When the stone is examined with overhead lighting, the reflection of this fracture requires an adjustment of one-half to one grade downward (+1e to +2e), for a score of 16.1e to 17.1e, corresponding to a high-to-middle I_2. In addition, since the inclusion's appearance constitutes a significant percentage of this rather small diamond, the +2e adjustment is appropriate for a final grade of a solid I_2.

Conclusions

This article introduces a new objective form of clarity grading based on metrics that model the techniques of experienced graders. The system emulates the analysis performed by these graders, who assess the combined factors of inclusion characteristics (size, number, contrast, position and nature) to arrive at the clarity grade.

A small sampling of grading examples are discussed here that compare the results obtained from this new system to photographs of GIA-graded diamonds. They were selected from more than 100 recently documented photographic examples that support the success of this system in matching clarity grades obtained by gem laboratories.

A particularly notable outcome of this study is the approximate but consistent four times increase in inclusion area from grade to grade across the entire GIA clarity scale. This multiplicative relationship resulted from the natural evolution and expansion of the clarity grades and terms used in the diamond trade well before GIA's formalization of the grading scale. It speaks to human perception of the relative noticeability of diamond inclusions.

With the success of this objective system in matching GIA grading, its accuracy and consistency suggests the possibility of its use for improving inter- and intra-laboratory grading consistency.

References

Bruton E., 1978. *Diamonds*. N.A.G. Press Ltd., London, p. 517.

Burr K.F., Brightman R.F., Chandler R. and Huddlestone R.V., 1981. The D.G.L. Clarity Grading System for Polished Diamonds. Diamond Grading Laboratories Ltd., London, 81 pp.

Cowing M.D., in press. *Grading Diamond Clarity Objectively*. To be self-published.

GIA, 1969. Diamond Grading Assignment 20. Gemological Institute of America, cover page.

GIA, 1994. Diamond Grading Assignment 4. Gemological Institute of America.

GIA, 2004, 2006. Diamond Grading Lab Manual. Gemological Institute of America, pp. 109–120.

Okuda K., 1978. Okuda Diamond Grading Microscope Reference Manual. Okuda Jewelry Technical Institute Co. Ltd., New York, New York, USA, 16 pp.

Roskin G., 1994. *Photo Masters for Diamond Grading*. Gemworld International Inc., Northbrook, Illinois, USA, 94 pp.

Shuster W.G., 2003. *Legacy of Leadership*. Gemological Institute of America, Carlsbad, California, USA, p. 121.

Wade F.B., 1916. *Diamonds—A Study of the Factors that Govern Their Value*. G. P. Putnam's Sons, New York, New York, USA, 150 pp.

The Author

Michael D. Cowing, FGA
AGA Certified Gem Laboratory
1035 St. Stephens Church Rd.
Crownsville, Maryland 21032 USA
Email: michaelgem@gmail.com

Acknowledgements

The author is grateful to Jonathan Weingarten of Good Old Gold (Massapequa Park, New York, USA) for supplying the raw diamond photographs in this article. He is grateful to the following individuals for discussions and review:

- Peter Yantzer, executive director of the AGSL in Las Vegas, Nevada, USA, and former director of GIA's diamond grading laboratory in Santa Monica, California, USA, concerning aspects of GIA and AGSL clarity grading.
- Phil Yantzer, vice president of laboratory services at GIA in Carlsbad, concerning aspects of GIA clarity grading.
- Gary Roskin, former GIA assistant lab director in Santa Monica, concerning aspects of GIA clarity grading.
- Roy Huddlestone, former director of DGL in London, concerning aspects of DGL's clarity grading system.
- Thomas Tashey, owner of Professional Gem Sciences Laboratory in Chicago, Illinois, USA, concerning aspects of GIA clarity grading and the SI_3 grade.

RareSource

YOUR DIRECT SOURCE FROM THE MINE®

Edward Boehm and the passionate team at RareSource search the globe to bring our clients the finest gemstones

WWW.RARESOURCE.COM


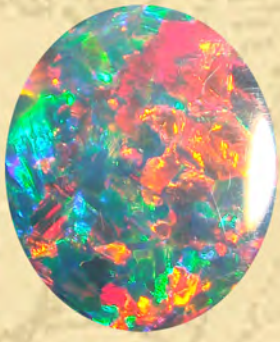


Specializing in Natural, Untreated & Rare Gems

+1-423-752-3191

P.O. Box 4009
Chattanooga, TN 37405
USA

info@raresource.com

A Comparison of *R*-line Photoluminescence of Emeralds from Different Origins

D. Brian Thompson, Joshua D. Kidd, Mikko Åström, Alberto Scarani and Christopher P. Smith

A fundamental task for gemmologists is determining whether an emerald is natural or synthetic. Within the laser-excited photoluminescence spectrum of emerald, the peak positions and relative intensities of two emissions in the 680–685 nm range, known as *R* lines, can help identify if a sample is natural, and can also provide information about its geological origin. In particular, the R_1 line of synthetic emerald is positioned at the shortest wavelength, while for natural emeralds with a non-schist origin this line is found at the same or longer wavelengths, and for schist-type emeralds the line peaks at an even longer wavelength. This measurement can supplement origin results obtained from established methods, such as inclusion microscopy, spectroscopy (e.g. ultraviolet-visible–near infrared [UV-Vis-NIR], Fourier-transform infrared [FTIR] and Raman) and trace-element analysis by laser ablation–inductively coupled plasma–mass spectrometry (LA-ICP-MS).

The Journal of Gemmology, 34(4), 2014, pp. 334–343, http://dx.doi.org/10.15506/JoG.2014.34.4.334

Introduction

Emerald, the green to bluish green variety of beryl [$Be_3Al_2(SiO_3)_6$], is a beautiful and important gemstone (e.g. Figure 1). Pure beryl does not absorb visible light and therefore appears colourless. The green colour of emerald results from trace amounts of Cr and/or V; Fe may add a yellowish or bluish tinge. A Cr^{3+} ion substituting for Al^{3+} at its crystal site is surrounded by an octahedral arrangement of six oxygen ions. Then six silicon and three beryllium ions, the next-nearest neighbours with which the chromium shares the oxygens, result in a trigonal distortion of this crystal site (Wood, 1965). Crystal field theory explains how the three electrons in a Cr^{3+} ion's *d* orbital, when placed in beryl's octahedral oxygen field, absorb light across the red-orange and blue-violet wavelength ranges, so that emerald only transmits light in the green range (Wood et al., 1963; Wood, 1965; Mitra, 1996; Avram and Brik, 2013).

Chromium is the only emerald chromophore that exhibits photoluminescence (PL); vanadium does not cause PL in emerald. According to

Figure 1: Some of the emeralds studied for this report are shown here. Top row, from left to right: 0.76 ct from Davdar, China; and 0.71 and 0.66 ct from Colombia. Bottom row, from left to right: 1.14 ct synthetic Tairus 'Platinum'; 2.34 ct synthetic Chatham; and 0.37 and 0.23 ct from Kafubu, Zambia. Composite photo by Bilal Mahmood, American Gemological Laboratories.

crystal field theory, there are two possible paths by which Cr^{3+} in an octahedral ligand field may photoluminesce: one path leads to broadband luminescence and the other leads to a pair of narrow luminescence lines (Avram and Brik, 2013). Laser-excited PL spectra demonstrate that emerald displays both types of luminescence (e.g. Figure 2). The broadband structure, peaking at around 710–720 nm, results from a Stokes-shifted reversal of the electron transition that produces emerald's red-orange absorption band (Lai, 1987). Superimposed upon this structure are two narrow lines appearing between 680 and 685 nm that arise from electronic decay of a doublet metastable state (Wood, 1965); these are known as the *R* lines. The longer-wavelength line is denoted R_1 and the shorter-wavelength line is R_2 (Carceller-Pastor et al., 2013).

Moroz et al. (2000) collected Raman and PL spectra from one synthetic and nine natural emeralds of various geological origins. They found that the peak positions of the *R* lines in the PL spectra of schist-origin emeralds showed moderate shifts toward longer wavelengths, as compared to emeralds of non-schist origin and synthetic emeralds. The authors suggested these wavelength shifts may be caused by impurity metal ions substituting at octahedral aluminium sites. *Schist-origin* emeralds have a metamorphic or metasomatic origin in biotite or phlogopite schist; this is the most common emerald deposit type worldwide. *Non-schist origin* describes a few emerald deposits of varying geology. Colombian deposits, where emeralds are hosted by sedimentary black shale, are the primary examples (Groat et al., 2008; Giuliani et al., 2012). Also in this category are Nigerian emeralds, which are hosted by cavities in albitized granite (Groat et al., 2008; Giuliani et al., 2012).

This article provides a preliminary examination of the efficacy of using *R*-line peak shift in emerald PL spectra as an aid for identifying their

Figure 2: Laser-excited PL spectra (E⊥c) of three representative samples are shown: (a) a schist-origin emerald from the Ural Mountains, Russia (no. 9 in Table I); (b) a non-schist-origin emerald from Colombia (no. 19); and (c) a Chatham synthetic emerald (no. 24).

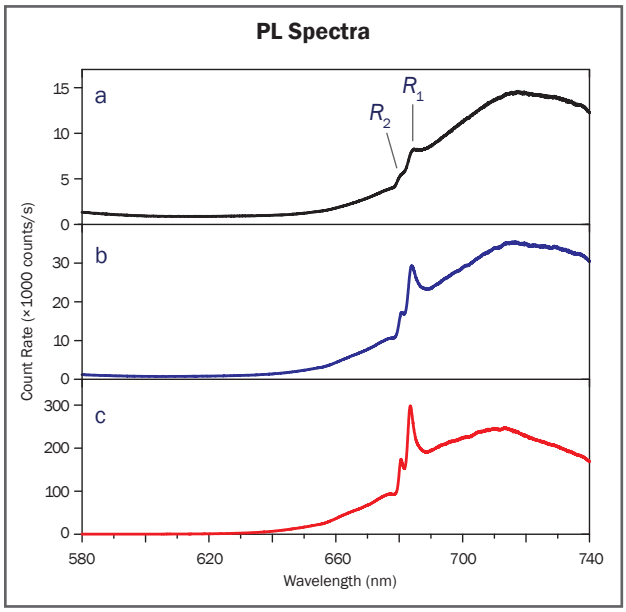

Table I: Emerald samples used in this study and their R *line measurements.*

Sample	Origin	Weight (ct)	Shape	R_2 peak position (nm)	R_1/R_2 peak height ratio	R_1 peak position (nm)	R_1-line FWHM (nm)	R_1/ broadband peak height ratio
Schist Origin								
1	Nova Era, Brazil	0.75	Pear cut	680.73	3.00	684.09	3.39	0.24
2	Nova Era, Brazil	0.58	Pear cut	680.73	2.27	683.95	2.99	0.35
3	Belmont, Brazil	0.31	Emerald cut	680.39	3.42	684.36	3.44	0.03
4	Bahia, Brazil	0.59	Pear cut	680.44	3.29	684.22	3.61	0.12
5	Davdar, China	0.76	Emerald cut	680.51	3.75	684.21	3.53	0.11
6	Mozambique	1.44	Hexagonal prism	680.73	3.10	683.93	3.22	0.30
7	Mozambique	0.96	Hexagonal prism	680.73	3.75	684.16	3.35	0.31
8	Ural Mountains, Russia	0.60	Pear cabochon	680.65	2.73	683.95	3.04	0.15
9	Ural Mountains, Russia	0.42	Oval cabochon	680.44	3.27	684.16	3.57	0.11
10	Lake Manyara, Tanzania	1.13	Hexagonal prism	680.75	3.34	684.04	3.13	0.37
11	Lake Manyara, Tanzania	0.78	Hexagonal prism	680.75	3.54	684.14	3.35	0.26
12	Kafubu, Zambia	0.37	Oval cut	680.48	3.19	684.25	3.61	0.14
13	Kafubu, Zambia	0.23	Oval cut	680.50	3.49	684.26	3.57	0.13
14	Sandawana, Zimbabwe	0.42	Emerald cut	680.31	3.65	684.25	3.66	0.05
15	Sandawana, Zimbabwe	0.46	Teardrop cut	680.23	2.66	684.09	3.76	0.05
Non-schist Origin								
16	Colombia	0.98	Pear cut	680.69	2.74	683.85	2.73	0.51
17	Colombia	0.71	Emerald cut	680.69	2.78	683.75	2.46	0.58
18	Colombia	0.83	Pear cut	680.73	3.16	683.87	2.77	0.48
19	Colombia	0.66	Emerald cut	680.64	3.09	683.85	2.82	0.34
20	Colombia	0.72	Pear cut	680.64	2.63	683.80	2.86	0.31
21	Nigeria	3.78	Hexagonal prism	680.66	2.67	683.58	2.20	0.91
22	Nigeria	4.70	Hexagonal prism	680.64	2.56	683.56	2.28	0.78
23	Nigeria	2.38	Hexagonal prism	680.64	2.80	683.58	2.20	0.83
Synthetic*								
24	Chatham	2.34	Emerald cut	680.59	2.60	683.51	2.29	0.63
25	Chatham	1.19	Emerald cut	680.57	2.60	683.55	2.37	0.58
26	Tairus 'Biron'	1.12	Pear cut	680.67	2.80	683.61	2.15	0.61
27	Tairus 'Biron'	1.07	Emerald cut	680.70	2.60	683.64	2.28	0.52
28	Tairus 'Platinum'	1.25	Emerald cut	680.66	2.60	683.55	2.28	0.61
29	Tairus 'Platinum'	1.14	Emerald cut	680.68	2.30	683.58	2.24	0.67
30	Tairus 'Colombian colour'	1.14	Emerald cut	680.72	2.60	683.65	2.05	0.55
31	A.G. 'Agee'	0.42	Emerald cut	680.70	2.60	683.63	2.23	0.57
32	Malossi	2.07	Emerald cut	680.77	2.40	683.53	2.33	0.38

*The Chatham synthetic emeralds were flux-grown; all the other synthetic emeralds were created by hydrothermal methods.

geological origin. We also investigate the influence of sample type and optic axis orientation on this peak shift, and suggest a mechanism to account for the variations in *R*-line positions.

Materials and Methods

PL spectra were collected at room temperature from 32 rough and cut samples (Table I): 23 natural emeralds from 11 different localities were provided by American Gemological Laboratories, and nine synthetic emeralds were acquired directly from their manufacturers or marketers.

A continuous wave diode-pumped solid-state (DPSS) laser emitting about 100 mW at 532 nm (Laserglow LRS0532) was used as an excitation source.[1] A 500 µm diameter optical fibre with a 25° field-of-view collimating lens aligned perpendicular to the laser beam was used to collect the PL emission from the emeralds. A gem clip was used to position the sample at the intersection of the laser beam and fibre's field of view, such that the beam overlapped the emerald edge closest to the optical fibre. This sampling geometry was chosen to minimize PL emission travelling through non-illuminated emerald before entering the fibre.

The PL emission collected by the fibre entered a CCD-type spectrometer (Ocean Optics USB4000) that dispersed light over the wavelength range 580–740 nm. Discrete-line emissions from Ar and Ne spectral lamps were used to calibrate the spectrometer's wavelength scale. Across the *R*-line wavelength range, the spectrometer had full-width at half-maximum (FWHM) resolution of 0.20 nm, and the width of each spectrometer channel was 0.045 nm. To construct each sample's PL spectrum, 100 accumulated scans were averaged, where typically each scan's integration time was one second. (For a Tairus 'Colombian colour' synthetic emerald with very little Cr, each scan's integration time was 10 seconds.) In a similar manner, with the light source shuttered, a 'dark' spectrum was recorded and the final PL pattern

[1] PL spectra of three samples were also collected using each of the three emission wavelengths of an argon-ion laser: 514, 488 and 454 nm. Regardless of the wavelength of the excitation, we observed no change in *R*-line peak wavelength positions or relative heights.

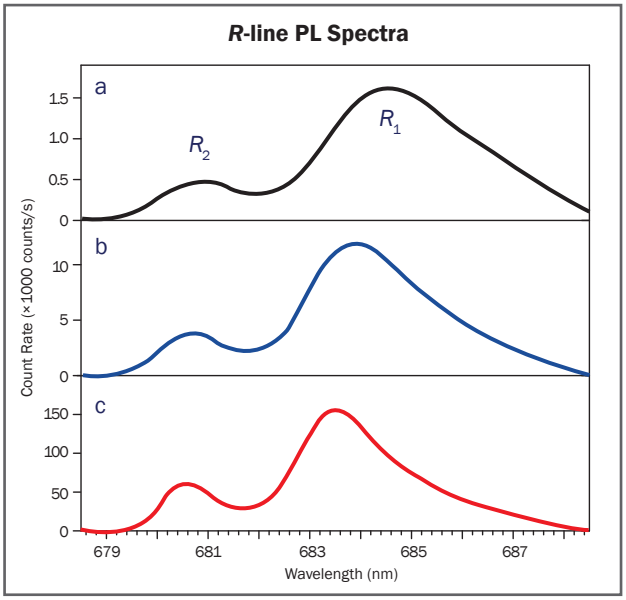

Figure 3: These R-line PL spectra result from performing a baseline subtraction of the spectra in Figure 2(a,b,c).

was created by subtracting this background from the sample spectrum.

Emerald's PL spectrum (e.g. Figure 2) exhibits local minima on either side of the *R* lines. To isolate the *R*-line contribution in each PL spectrum, a baseline was subtracted from the data, and the line's endpoints at 678.5 and 688.5 nm were selected to be close to where these local minima occur. The resulting spectra (e.g. Figure 3) are referred to as *R*-line spectra.

Emerald is optically uniaxial, resulting in differences in PL emission when the excitation laser beam's polarization is perpendicular to the emerald's c-axis (E⊥c) vs. that occurring when the beam is polarized parallel to the c-axis (E||c); both R_1 and R_2 peak positions change, as does the R_1/R_2 peak height ratio (Moroz et al., 2000). To collect orientation-dependent PL spectra from a sample lacking crystal faces, a consistent method is needed for determining E⊥c and E||c. To develop this technique, we first collected a series of spectra from several emerald crystals showing prism faces, beginning with E||c and rotating in 10° intervals to E⊥c. A comparison between spectra (e.g. Figure 4) revealed that the R_1/R_2 peak height ratio was consistently greatest for E⊥c and lowest for E||c. So for all emerald samples listed in Table I, the orientation relative to the laser beam was rotated until the R_1/R_2 peak height ratio reached a maximum value to collect E⊥c spectra; subsequently the sample was rotated until the R_1/

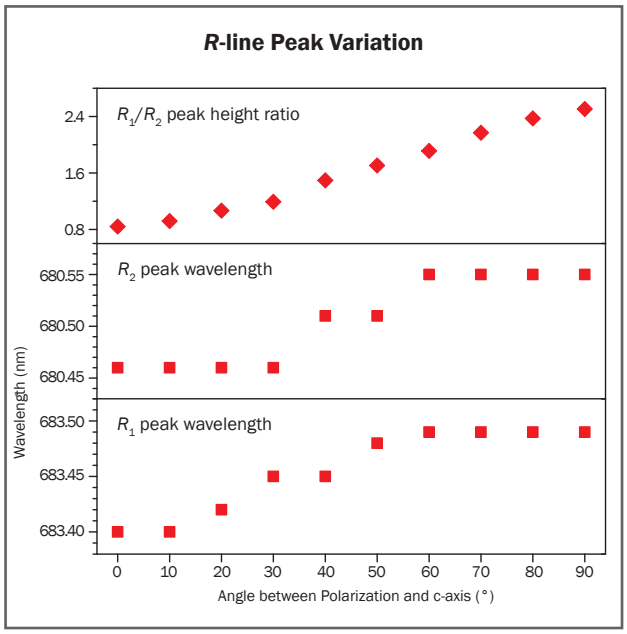

Figure 4: These plots show the angular variation of peak parameters extracted from R-line spectra of a Chatham synthetic emerald crystal with prism faces. The horizontal scale ranges from 0° (E||c) to 90° (E⊥c).

R_2 peak height ratio reached a minimum to collect E||c spectra. Using this method, we found that seven faceted emeralds had their c-axis parallel to the gem's table, six had their c-axis tilted about 45° from perpendicular to the gem's table, and the rest of the cut stones had their c-axis lying within 20° of perpendicular to the gem's table.

After spectral collection and baseline subtraction to create *R*-line spectra, peak-finding software (O'Haver, 2014) was used to extract R_1 and R_2 peak wavelengths and their corresponding relative emission strength, which were used to determine the R_1/R_2 peak height ratio. The R_1 and R_2 peak wavelengths reported in Table I are averages of values extracted from multiple spectral measurements; the uncertainty in peak position was ±0.02 nm or less. For most emeralds, we achieved this uncertainty with a minimum of four separate spectral measurements. However, some samples, such as the Tairus 'Colombian colour' synthetic emerald, required up to 16 measurements to achieve this uncertainty.

Results and Discussion

This study only examines the E⊥c spectra of each emerald, because the E||c spectra were found to show no origin dependence (see end of this section).

While the emeralds were exposed to the laser beam, red PL emission (Figure 5) was visible from all but one sample—the 'Colombian colour' synthetic emerald grown by Tairus. The green colour of this sample occurs without any significant influence of Cr (Schmetzer et al., 2006). Even so, the Cr concentration was high enough to be detected by PL spectroscopy.

Most natural emeralds also exhibit a yellow PL emission, either at spots on the surface or across the entire surface, due to oil or resin coatings used to improve emerald clarity (Johnson et al., 1999). In our samples, this emission appeared in the PL spectra of two natural emeralds (Figure 2a,b) as the non-zero signal between 580 and 620 nm. We saw no evidence of this additional emission disturbing the *R* line structure.

PL Spectral Features

The count rates at the peak of the broadband structure in the PL spectra (Figure 2) are dependent on Cr concentration. For example, the PL spectrum of a Chatham synthetic emerald (Figure 2c), with a reported Cr_2O_3 concentration of 0.35 wt.% (Huong, 2008), had a broadband peak count rate of 250,000 counts/s. In contrast, a Tairus 'Biron' synthetic emerald, with an estimated Cr_2O_3 concentration of 0.25 wt.% (Kane and Liddicoat, 1985; Huong, 2008),

Figure 5: Red PL emission of an emerald is seen here through a colour filter that removes the green excitation light. Photo by Shannon Wells, University of North Alabama.

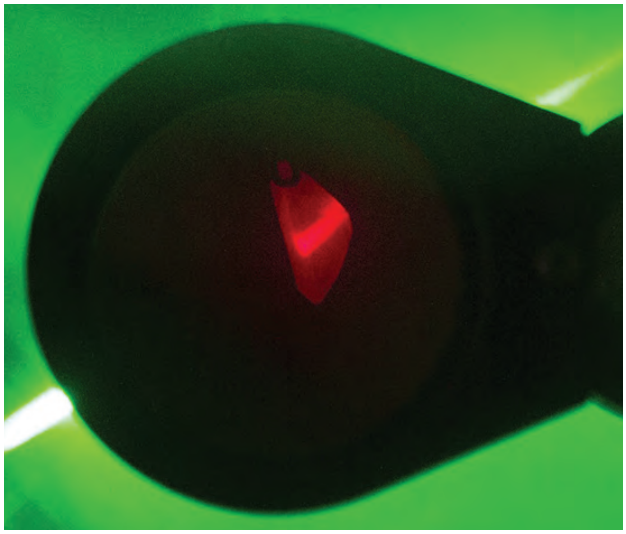

exhibited a peak count rate of 70,000 counts/s. At the other extreme, a peak count rate of only 100 counts/s was observed from the Tairus 'Colombian colour' synthetic emerald with a reported Cr_2O_3 concentration of 0.04 wt.% (Schmetzer et al., 2006). However, due to possible variations from one emerald to another in the luminescence collection volume (defined by the overlap of light beam, emerald and optic fibre field of view), these count rates provide only a qualitative measure of chromium concentration. In addition, some impurities such as iron may quench luminescence. Nevertheless, the broadband peak count rates in the PL spectra of both schist-origin and non-schist-origin emeralds (Figure 2a,b) suggest that they have comparable Cr concentrations.

The *R*-line spectra of the schist-origin, non-schist-origin and synthetic emeralds (e.g. Figure 3) showed two *R* lines with widths and peak separation an order of magnitude larger than the spectrometer's resolution. Besides the two peaks, no other fine structure appeared in any of the spectra collected.

The R_2 line in each spectrum had a Gaussian (bell-shaped) profile, and it peaked at a similar—but not the same—wavelength in each sample. Figure 6 shows a plot of the R_2 peak positions of all the emerald samples (see also Table I). Most of the peak positions occurred within a 0.25 nm-wide range, with the schist-origin emeralds exhibiting somewhat more variation.

The R_1 line in each spectrum had an asymmetric profile with an extended tail along the long-wavelength side. The relative height of each R_1 line was commonly between 2.5 and 3.5 times that of the corresponding R_2 line. Figure 7 presents the R_1/R_2 peak height ratios of all the emerald samples (see also Table I). Although samples from each particular origin exhibited a characteristic range of *R*-line peak height ratios, those from different sources showed significant overlap in some cases.

However, the peak positions of the schist-origin, non-schist-origin and synthetic emeralds' R_1 lines showed clearer trends: those of the synthetic emeralds peaked at the shortest wavelengths, while the R_1 lines of some non-schist emeralds were shifted to longer wavelengths, and those of schist-origin emeralds were present at even longer wavelengths (Figure 8 and Table I). The R_1 line of the schist-origin emeralds was positioned at wavelengths above 683.9 nm, while those of the non-schist-origin and synthetic emeralds peaked at wavelengths below that value. In fact, the R_1 line of all the tested synthetic emeralds peaked at wavelengths below 683.7 nm.

In addition, as R_1-line peak positions were shifted to longer wavelengths, their line-width also increased (as seen in Figure 3) and their height tended to decrease relative to the peak height of the broadband structure (as seen in Figure 2).

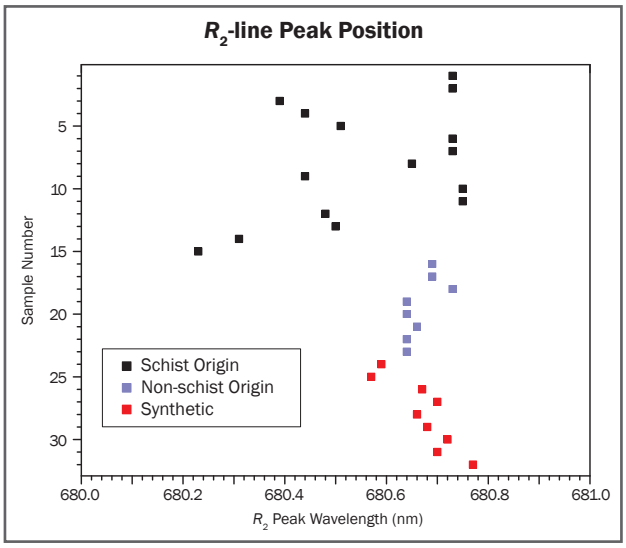

Figure 6: The R_2 *peak positions of the emerald samples showed considerable overlap. The width of the points matches the uncertainty in peak position.*

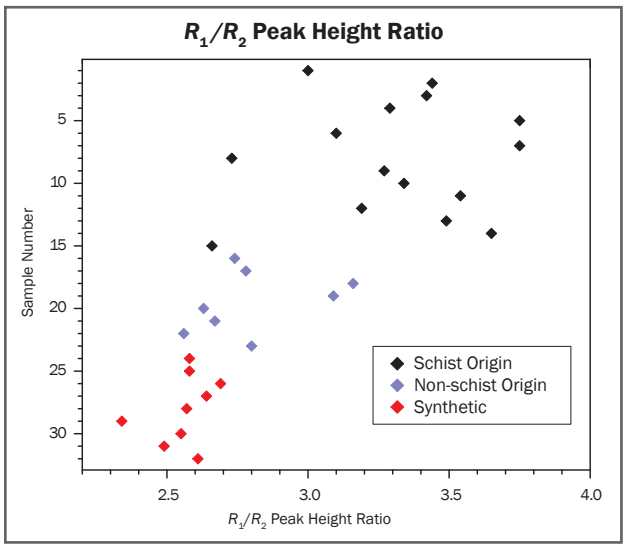

Figure 7: R*-line peak height ratios showed some overlap, and were not distinctive enough to separate emerald origin.*

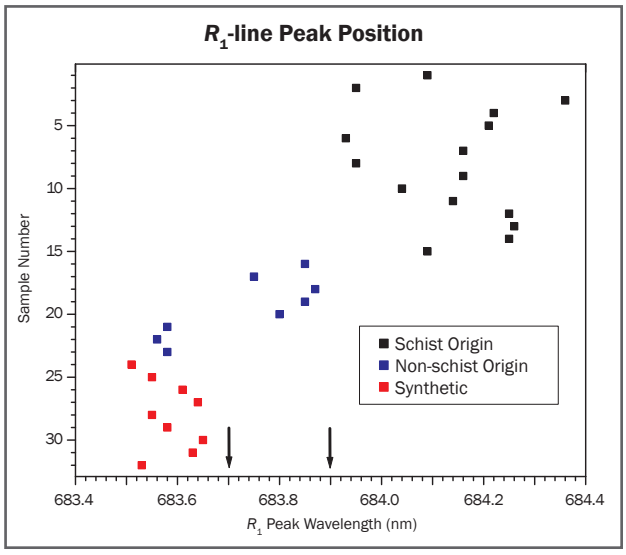

Figure 8: The R_1 peak positions are shown for the analysed samples. The arrows indicate wavelengths mentioned in the text: no R_1 lines of schist-origin emeralds were found to peak at wavelengths shorter than 683.9 nm, and no R_1 lines of synthetic emeralds were measured at wavelengths longer than 683.7 nm.

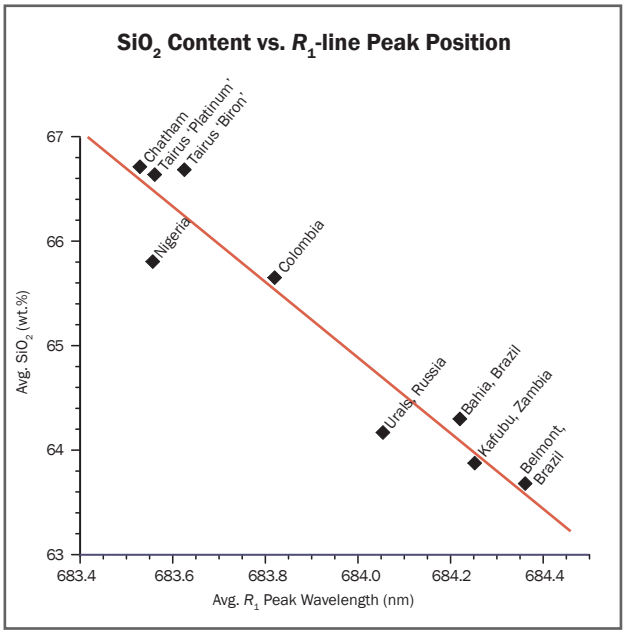

Figure 9: This plot shows average SiO_2 concentrations vs. average R_1 peak position of different emerald samples with the same origins. The SiO_2 values are taken from Huong (2008) and the R_1 peak positions are averages from our measurements. The trend line predicts an R_1 wavelength of 683.41 nm for an ideal beryl with 67 wt.% SiO_2.

The R_1-line FWHM values and R_1/broadband peak height ratios of all samples are listed in Table I, but they are not considered further in the present study.

Cause of PL Spectral Variations

Of the three quantities extracted from the *R*-line spectra and plotted (R_1 peak position, R_2 peak position and R_1/R_2 peak height ratio), the R_1 peak position displayed the strongest variation according to emerald origin. In considering possible reasons for this, we looked for correlation with other emerald properties. Stockton (1984) provided some initial clues for this. Stockton outlined a method for identifying whether or not an emerald is natural based upon measurement of its SiO_2 concentration (where ideal beryl contains 67 wt.% SiO_2). In particular, Stockton found that synthetic emeralds always exceeded 65.7 wt.% SiO_2. A SiO_2 concentration below 65.6 wt.% indicated that an emerald is of natural origin, whereas >65.7 wt.% SiO_2 would require further analysis.

Huong (2008) provided the chemical composition of 36 natural and synthetic emeralds from a variety of sources, and her results for SiO_2 concentration exhibited an origin-specific pattern similar to that of our R_1 peak positions. For synthetic emeralds, the SiO_2 concentration generally approached the value of ideal beryl, whereas non-schist-origin emeralds had lower SiO_2, and schist-origin emeralds had even lower SiO_2 values.

To further investigate these origin-specific patterns, we plotted SiO_2 concentration vs. R_1 peak position (Figure 9). Specifically, we used the average SiO_2 wt.% value of emeralds from various sources (as extracted from Huong's [2008] measurements), and plotted it against the average R_1 peak wavelength measured by us for emeralds from the same origins. The trend line fit to the data has a coefficient of determination $r^2 = 0.91$, with the largest variation arising from the Nigerian data point. Although the data points come from different sets of samples, this fit demonstrates a strong correlation between an emerald's R_1 peak position and its SiO_2 concentration. Thus we propose that an accumulation of vacancy defects or substitutional defects at silicon crystal sites may be responsible for shifts of R_1 peaks to longer wavelengths. The trend line has a slope 3.61 wt.%/nm, and predicts a peak wavelength of 683.41 nm at the 67 wt.% SiO_2 value for ideal beryl.

Stockton (1984) also outlined a method for identifying whether or not an emerald is natural or synthetic based upon its Al_2O_3 concentration.

However the spatial separation between a chromium site and the closest aluminium ion sites is likely too large for an aluminium point defect to exert much influence on *R* values (Lai, 1987). Even so, from Huong's (2008) measurements, Al_2O_3 concentration does show some origin dependence. A plot of this data in a fashion similar to Figure 9 showed much more scatter in the data points. The best-fit trend line had $r^2 = 0.69$, and six of the nine data points showed comparably large variations. Therefore, we consider any correlation between an emerald's R_1 peak position and its Al_2O_3 concentration to be more coincidence than causality.

Having proposed an accumulation of vacancies at silicon crystal sites as the most likely cause of the R_1 line shift, we briefly speculate upon what cations might substitute at these sites. Among trace elements detected by Huong (2000), an isovalent substitution of Ti^{4+} or Mn^{4+} seems most likely. However, her data found that these elemental impurities occur in very low concentrations in emerald; Ti concentration had little origin dependence, and Mn concentration of individual emeralds was not reported. The next most likely choice is an aliovalent substitution of Al^{3+} or Fe^{3+} with charge compensation by alkali ions located at interstitial sites within open channels parallel to the c-axis (Goldman et al., 1978). Indeed, Huong's (2000) data on alkali atom concentration displayed an origin-dependent pattern that parallels the R_1 line shift: namely, synthetics had little to no alkali concentrations, non-schist emeralds had low concentrations, and schist-origin emeralds had high concentrations of alkali impurities.

Recognizing a connection between the R_1 peak position and chromium's next-nearest neighbour silicon ions, we considered whether a similar connection exists between the R_2 line and chromium's other next-nearest neighbours, beryllium ions. Unfortunately we found almost no origin dependence either in our results for R_2 peak positions or in Huong's (2008) reported BeO concentrations. Of course, the fact that both exhibit no origin dependence may be an indication that they are connected.

As mentioned previously, E||c laser-induced PL spectra were also collected for all samples. The average R_1/R_2 peak height ratio in these spectra was 1.45. Along with this decrease in relative height of the R_1 peak compared to E⊥c spectra, these spectra exhibited a significant decrease in the origin-dependent shifts of R_1 peak positions. In particular, peak positions of Colombian emeralds overlapped those of schist-origin emeralds, and there was almost no separation between those and the peak positions of the synthetic and Nigerian emeralds. The spread of R_2 peak positions was also reduced in the E||c spectra and showed no origin dependence.

Implications for Origin Determination

Analysis of gemstone inclusions combined with UV-Vis-NIR, Raman and FTIR spectroscopy and LA-ICP-MS trace-element analysis are the primary methods used to establish an opinion of an emerald's origin. Laser-excited PL spectroscopy can provide an additional tool, and many gemmological laboratories already have suitable instrumentation; an extended-range Raman spectrometer operating at suitable excitation wavelength, when correctly calibrated, is capable of producing similar results.

For example, Colombian emeralds host characteristic three-phase inclusions (Gübelin and Koivula, 2008) that were once thought diagnostic of origin. However, similar inclusions have been observed in emeralds from deposits in Davdar, China (Marshall et al., 2012). The R_1 line of our schist-origin Davdar emerald peaked above 683.90 nm (Figure 8), while those of non-schist-origin Colombian emeralds peaked below that value. This result suggests that R_1 peak position can be used to distinguish between Davdar, China, and Colombian emeralds.

Of course, emeralds from all known deposits were not included in this preliminary study. For example, the characteristic three-phase inclusions also have been observed in emeralds from Panjshir, Afghanistan (Bowersox et al., 1991). Emeralds from this region have been documented in various geological environments, including hydrothermal veins, shear zones, and phlogopite schist reaction zones along the contact between leucogranite and serpentinite (Bowersox, 1985; Bowersox et al., 1991; Groat et al., 2008). Such wide variations suggest that R_1 peak measurements of emeralds from different deposits in Panjshir will show systematic mine-specific variations.

Figure 10: Attractive gem-quality emeralds are sourced from several world localities, and gemmological labs are often asked to identify their origin and separate them from synthetics. R-line PL spectroscopy can help address these challenges. This rough-and-cut pair of emeralds from Colombia show the saturated green colour that is prized for stones from this locality. The crystal, known as El Itoco*, weighs 94.4 g. Composite photo by Bilal Mahmood, American Gemological Laboratories.*

Our results also may be useful for assessing the geological origin of emeralds from new deposits or those of unknown deposit type. The characteristic three-phase inclusions mentioned above also have been found in emeralds from Musakashi, Zambia, which have an uncertain geological origin (Zwaan et al., 2005; Saeseaw et al., 2014). Zwaan et al. (2005) found their Musakashi emerald samples had an average SiO_2 concentration of 66.47 wt.%. Our trend-line fit (Figure 9) predicts that Musakashi emeralds are non-schist origin, with an R_1 line that peaks around 683.55 nm.

As a final example, the R_1 lines of all the synthetic emeralds analysed for this report (Figure 8) peaked at wavelengths below 683.70 nm. Therefore an R_1 line peaking at a wavelength above this value suggests the emerald is natural. Our Nigerian emeralds had R_1 lines that peaked below 683.70 nm, and the R_1 line of emeralds from Musakashi, Zambia, also are predicted to peak below that value. Therefore if an R_1 line peaks below 683.70 nm, further tests are required to determine whether or not the emerald is of natural origin.

Conclusions

Emerald is a beautiful gem material (Figure 10) that is available from several localities and has been synthesized by various manufacturers. From E⊥c laser-excited PL spectra collected from several emerald samples (schist origin, non-schist origin, and synthetic), we isolated the *R*-line contributions (680–685 nm range). We found that locating the peak wavelength position of the R_1 line can help identify natural vs. synthetic origin and also indicate whether a natural emerald comes from a schist or non-schist deposit type. From the literature, measurements of emeralds' SiO_2 concentrations display similar origin dependence. Thus, we suggest that an accumulation of point defects at silicon ion crystal sites may be responsible for shifts of R_1 peaks to longer wavelengths. The correlation between R_1 peak position and SiO_2 concentration has implications for determining an emerald's origin even when only one of these values is known. It is hoped that this preliminary study will encourage further research on more samples from each locality, as well as on emeralds from additional sources.

References

Avram N.M. and Brik M.G., 2013. *Optical Properties of 3d-Ions in Crystals: Spectroscopy and Crystal Field Analysis*. Springer, Heidelberg, Germany, http://dx.doi.org/10.1007/978-3-642-30838-3.

Bowersox G.W., 1985. A status report on gemstones from Afghanistan. *Gems & Gemology,* **21**(4), 192–204, http://dx.doi.org/10.5741/gems.21.4.192.

Bowersox G., Snee L.W., Foord E.E. and Seal R.R., 1991. Emeralds of the Panjshir Valley, Afghanistan. *Gems & Gemology*, **27**(1), 26–39, http://dx.doi.org/10.5741/gems.27.1.26.

Carceller-Pastor I., Hutchinson W.D. and Riesen H., 2013. Temperature dependence of the chromium(III) R_1 linewidth in emerald. *Chemical Physics Letters*, **564**, 33–36, http://dx.doi.org/10.1016/j.cplett.2013.02.009.

Giuliani G., Ohnenstetter D., Fallick A.E., Groat L.A. and Feneyrol J., 2012. Geographic origin of gems linked to their geological history. *InColor*, **19**, 16–27.

Goldman S.D., Rossman G.R. and Parkin K.M., 1978. Channel constituents in beryl. *Physics and Chemistry of Minerals*, **3**(3), 225–235, http://dx.doi.org/10.1007/bf00633572.

Groat L.A., Giuliani G., Marshall D.D. and Turner D., 2008. Emerald deposits and occurrences: A review.

Ore Geology Reviews, **34** (1–2), 87–112, http://dx.doi.org/10.1016/j.oregeorev.2007.09.003.

Gübelin E.J. and Koivula J.I., 2008. *Photoatlas of Inclusions in Gemstones*, Vol. 3. Opinio Publishers, Basel, Switzerland.

Huong L.T.T., 2008. Microscopic, Chemical, and Spectroscopic Investigations on Emeralds of Various Origins. PhD dissertation, University of Mainz, Germany.

Johnson M.L., Elen S. and Muhlmeister S., 1999. On the identification of various emerald filling substances. *Gems & Gemology*, **35**(2), 82–107, http://dx.doi.org/10.5741/gems.35.2.82.

Kane R.E. and Liddicoat R.T., 1985. The Biron hydrothermal synthetic emerald. *Gems & Gemology*, **21**(3), 156–170, http://dx.doi.org/10.5741/gems.21.3.156.

Lai S.T., 1987. Highly efficient emerald laser. *Journal of the Optical Society of America B: Optical Physics*, **4**(8), 1286–1290, http://dx.doi.org/10.1364/JOSAB.4.001286.

Marshall D., Pardieu V., Loughrey L., Jones P. and Xue G., 2012. Conditions for emerald formation at Davdar, China: Fluid inclusion, trace element and stable isotope studies. *Mineralogical Magazine*, **76**(1), 213–226, http://dx.doi.org/10.1180/minmag.2012.076.1.213.

Mitra S., 1996. *Fundamentals of Optical, Spectroscopic and X-ray Mineralogy*. New Age International, New Delhi, India.

Moroz I., Roth M., Boudeulle M. and Panczer G., 2000. Raman microspectroscopy and fluorescence of emeralds from various deposits. *Journal of Raman Spectroscopy*, **31**(6), 485–490, http://dx.doi.org/10.1002/1097-4555(200006)31:6<485::aid-jrs561>3.0.co;2-m.

O'Haver T., 2014. Peak Finding and Measurement. Computer software, University of Maryland at College Park, USA, http://terpconnect.umd.edu/~toh/spectrum/PeakFindingandMeasurement.htm.

Saeseaw S., Pardieu V. and Sangsawong, S., 2014. Three-phase inclusions in emerald and their impact on origin determination. *Gems & Gemology*, **50**(2), 114–132, http://dx.doi.org/10.5741/gems.50.2.114.

Schmetzer K., Schwarz D., Bernhardt H.J. and Häger T., 2006. A new type of Tairus hydrothermally-grown synthetic emerald, coloured by vanadium and copper. *Journal of Gemmology*, **30**(1/2), 59–74, http://dx.doi.org/10.15506/jog.2006.30.1.59.

Stockton C.M., 1984. The chemical distinction of natural from synthetic emeralds. *Gems & Gemology*, **20**(3), 141–145, http://dx.doi.org/10.5741/gems.20.3.141.

Wood D.L., 1965. Absorption, fluorescence, and Zeeman effect in emerald. *Journal of Chemical Physics*, **42**(10), 3404–3410, http://dx.doi.org/10.1063/1.1695742.

Wood D.L., Ferguson J., Knox K. and Dillon J.F., 1963. Crystal-field spectra of $d^{3,7}$ ions. III. Spectrum of Cr^{3+} in various octahedral crystal fields. *Journal of Chemical Physics*, **39**(10), 890–898, http://dx.doi.org/10.1063/1.1734388.

Zwaan J.C., Seifert A.V., Vrána S., Laurs B.M., Anckar B., Simmons W.B., Falster A.U., Lustenhouwer W.J., Muhlmeister S., Koivula J.I. and Garcia-Guillerminet H., 2005. Emeralds from the Kafubu area, Zambia. *Gems & Gemology*, **41**(2), 116–148, http://dx.doi.org/10.5741/gems.41.2.116.

The Authors

Dr D. Brian Thompson and Joshua D. Kidd
Department of Physics and Earth Science
University of North Alabama
Florence, Alabama 35632 USA
Email: dbthompson@una.edu

Mikko Åström and Alberto Scarani
M&A Gemological Instruments
Alhotie 14, 04430 Järvenpää, Finland

Christopher P. Smith FGA
American Gemological Laboratories
580 5th Avenue, Suite 706
New York, New York 10036 USA

Acknowledgements

The authors thank Tom Chatham (Chatham Created Gems & Diamonds, San Marcos, California, USA) for providing a flux-grown synthetic emerald crystal with hexagonal prismatic habit, which was used along with schist-origin and non-schist-origin hexagonal prisms to develop the c-axis alignment technique. The authors also appreciate guidance and arrangements for obtaining additional specimens for the ongoing research from Kenneth Scarratt (GIA Laboratory, Bangkok, Thailand) and John Emmett (Crystal Chemistry, Washington, USA).

Green and Pink Tourmaline from Rwanda

Ulrich Henn and Fabian Schmitz

Green and pink tourmaline is found in granitic pegmatites of the Karagwe-Ankole Belt in south-western Rwanda. The tourmalines studied for this report show typical gemmological properties and consist of elbaite with some rossmanite content. The green colour is caused by Fe^{2+} and the pink by Mn^{3+}, as is common for gem tourmaline.

The Journal of Gemmology, 34(4), 2014, pp. 344–349, http://dx.doi.org/10.15506/JoG.2014.34.4.344

Introduction

The most important sources of gem-quality tourmaline in Africa are Nigeria, Mozambique, Namibia, Tanzania and Zambia, as well as Madagascar. During the past several years, some additional countries have joined these producers, such as Malawi (Henn et al., 1990) and the Democratic Republic of Congo (DRC; Laurs et al., 2004; Henn, 2010). Tourmaline-bearing pegmatites in Rwanda have been known for a long time, but gem-quality material has been described only recently (Henn, 2013). The occurrences are located in the Rusizi District of south-western Rwanda. Geologically this area belongs to the Karagwe-Ankole Belt. Numerous granitic pegmatites are worked by artisanal miners in small shallow pits for cassiterite, wolframite and columbite-tantalite (Ngaruye, 2011). Gem tourmaline is produced as a by-product and, although some attractive stones have been faceted (e.g. Figure 1), the majority of the rough contains abundant inclusions and is only suitable for cabochons (e.g. Figure 2). Rwanda is also a source of gem-quality topaz and blue sapphire (Krzemnicki et al., 1996; Milisenda, 2003).

Geology

Rwanda consists of metasedimentary Meso-proterozoic basement rocks on a Palaeoproterozoic shield (Figure 3). About 1 billion years ago the Rhodinian amalgamation influenced the geology in this area (Fernandez-Alonso et al., 2012). During this orogeny, granitic pegmatites

Figure 1: These faceted tourmalines from Rwanda weigh 25.65 ct (left) and 1.26 ct (right). Note the typical fluid inclusions in the pink stone. DGemG Collection; photos by K. Schollenbruch, DGemG.

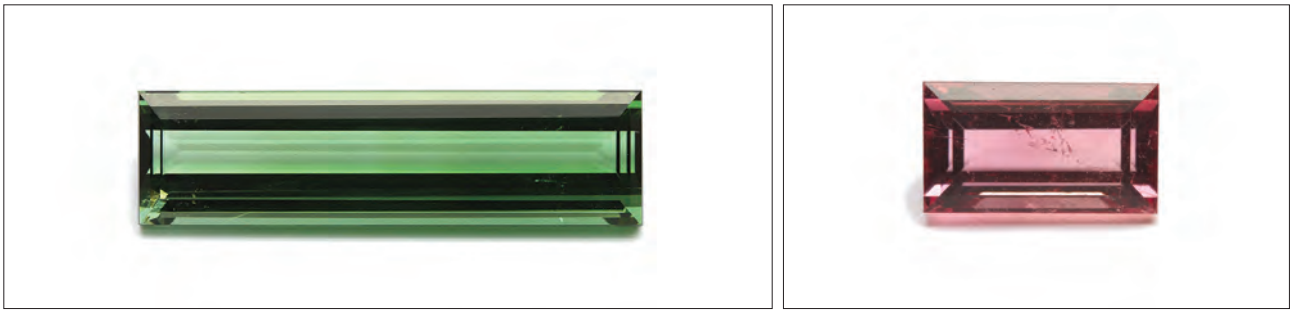

Figure 2: These cabochons were cut from Rwandan tourmaline. The stone on the right weighs 6.40 ct. Photo by K. Schollenbruch, DGemG.

(associated with so-called G4 granites or Kigali granites; Dewaele et al., 2010) with youngest ages of 986 million years intruded the metasediments. These miarolitic pegmatites are the source of the tourmaline found in Rwanda.

In the final stages of crystallization of the pegmatitic melt, the temperature decreased and incompatible elements accumulated to the point that a low-density melt with a high content of fluxing elements exsolved as a second phase. This melt fraction then separated and accumulated, forming the gem-bearing miarolitic cavities (cf. Simmons et al., 2012).

An important occurrence of gem (and non-gem) tourmaline is the M'buye mine in south-eastern Rwanda, near the border with Burundi. Geologically related tourmaline deposits are known from the area around Manono in south-east DRC. In addition, gem-quality green and blue-green tourmaline has been mined in eastern DRC, in North Kivu Province (Virunga area) during the past 15 years (Henn, 2010). In this context it is interesting to note that the well-known tourmaline deposits of Tanzania, Mozambique and Zambia are hosted by pegmatites related to younger granites of the Pan-African orogeny (see, e.g., Keller, 1992; Milisenda et al., 2000).

Materials and Methods

The Rwanda tourmalines examined for this report consist of five faceted stones (e.g. Figure 1), six cabochons (e.g. Figure 2) and 10 crystal sections (e.g. Figure 4). The tourmaline was supplied (as rough material) as an official gift by Rwanda government officials and business representatives

Figure 3: This simplified geological map of central-eastern Africa shows the main units of the Congo and Tanzania Cratons with the Kibara Belt (KIB) and Karagwe-Ankole Belt (KAB). Within these two belts, gem-quality tourmaline has been mined in south-west Rwanda and in south-east and eastern DRC. After Dewaele et al. (2013).

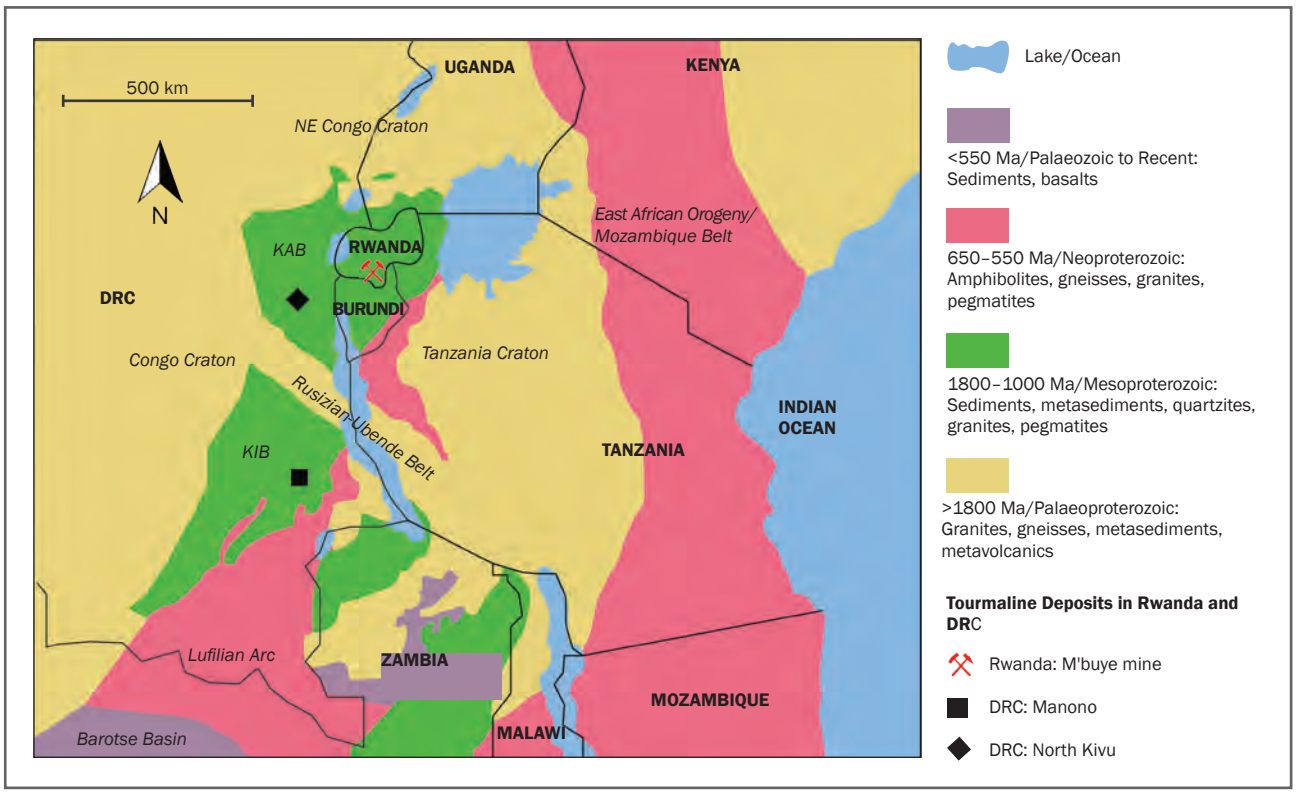

Figure 4: Tourmaline from Rwanda shows typical striations on the prism faces and is commonly colour-zoned in pink and green. The largest crystal in the left image is 22.53 mm long, and the diameter of the bottom crystal section in the right photo is 17.32 mm. Photos by K. Schollenbruch, DGemG.

to the German partner state of Rhineland-Palatinate. In the context of this partnership, the rough material was forwarded to lapidary firms in Idar-Oberstein for cutting and quality assessment.

A small face parallel to the c-axis was polished on the crystals and cabochons. On all samples, refractive indices were measured using a standard gemmological refractometer and specific gravity was determined with a hydrostatic balance. Inclusions were investigated with a gemmological immersion microscope. Visible absorption spectra of five green and five pink samples were measured in the 400–800 nm range with a PerkinElmer Lambda 12 spectrophotometer equipped with a polarization unit. The same samples were also tested for their Fe and Mn contents using a Thermo Scientific ARL QUANT'X energy-dispersive X-ray fluorescence (EDXRF) spectrometer. Complete chemical analyses of two representative samples (one green and one pink; 10 analyses each) were carried out using an electron microprobe at the Institute of Mineralogy and Petrography, University of Hamburg, Germany.

Results and Discussion

Physical and Gemmological Properties

The tourmaline crystals exhibited typical striations on their prism faces. The green samples ranged from yellowish green to light-to-dark green and into pinkish and bluish green. The pink tourmalines showed pinkish red, pink-violet, pure pink and faint 'rose' to brownish 'rose' coloration. Some of the crystals were strongly colour zoned in directions parallel or perpendicular to the c-axis. Examples included faint 'rose' (core) and faint blue (rim) as well as pink (core) and bluish green (rim) combinations.

The most common inclusions consisted of partially healed fractures and hollow tubes (Figure 5), which are characteristic of tourmaline. The partially healed fractures formed thin-planar or irregular fluid-filled areas that were interconnected through vein-like tubes. The hollow tubes were oriented parallel to the c-axis. The following properties were recorded from our samples: RI = 1.619–1.621 (n_e) and 1.639–1.641 (n_o), birefringence = 0.020 and SG = 3.04–3.07. These data fall within the known range for tourmaline.

Visible Absorption Spectroscopy

Figure 5: The most common internal features in tourmaline from Rwanda consist of fluid inclusions and hollow tubes. Photomicrograph by U. Henn; immersion, magnified 40×.

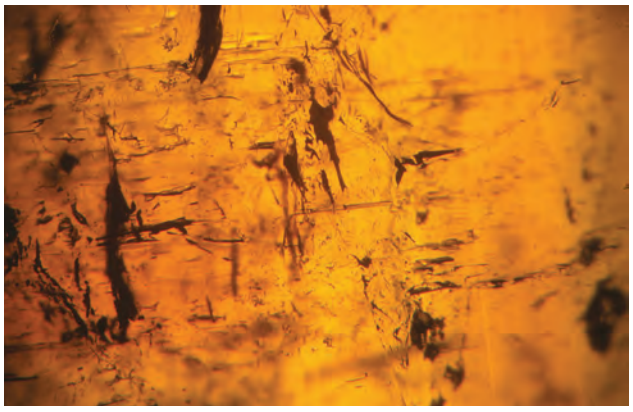

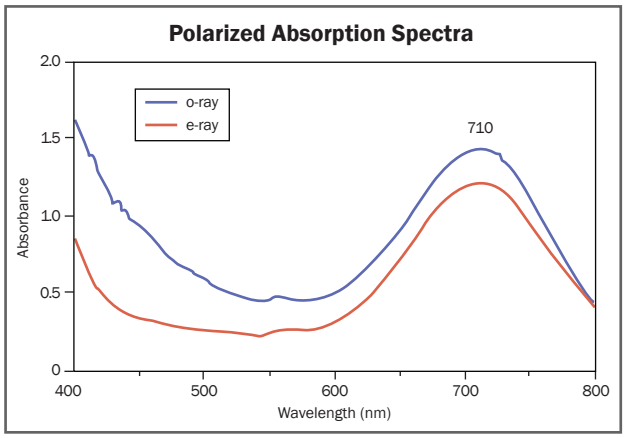

Figure 6: These representative polarized absorption spectra of a green Rwanda tourmaline (beam path length 7.1 mm) show a strongly pleochroic band (o>e) with a maximum at 710 nm that is caused by Fe^{2+}.

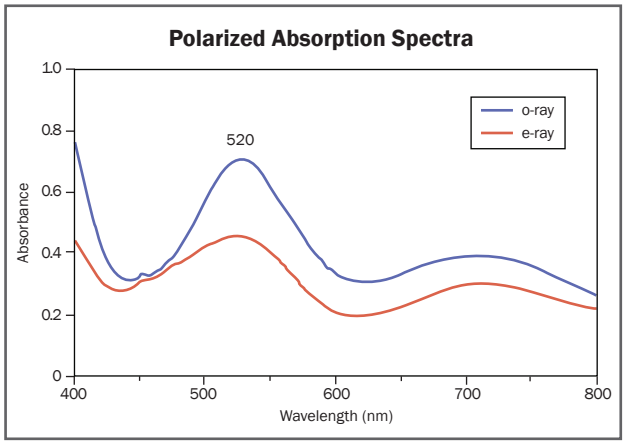

Figure 7: Polarized absorption spectra of pink Rwanda tourmaline (beam path length 3.8 mm) show a strongly pleochroic band (o>e) with a maximum at 520 nm that is caused by Mn^{3+}.

The absorption spectra of the green tourmalines showed a broad band with a maximum at 710 nm (Figure 6). This band was strongly pleochroic, and the spectrum taken with the beam polarized perpendicular to the c-axis (o-ray) showed stronger absorption than the spectrum with the beam polarized parallel to the c-axis (e-ray). The resulting pleochroism was intense green (o-ray) to moderate green (e-ray). According to Smith (1978), the 710 nm band is assigned to Fe^{2+} *d-d* transition and the additional weak absorptions at 560 and 495 nm are due to Fe^{3+}.

The absorption spectra of the pink tourmalines were dominated by an intense pleochroic band (o>e) in the green spectral range with a maximum at 520 nm (Figure 7). According to Manning (1969, 1973), this band is caused by spin-allowed *d-d* electron transitions of Mn^{3+} in octahedral coordination. The pleochroism was pink (o-ray) to light pink (e-ray). In addition, Mn^{3+} was also responsible for a small peak at 460 nm and a broad but weak absorption in the red region of the spectrum.

Chemical Properties

The tourmalines that were analysed by EDXRF contained 0.73–2.17 wt.% FeO (green samples) and 0.14–0.38 wt.% MnO (pink stones). Complete chemical analyses (by electron microprobe) of a representative green tourmaline and pink tourmaline are provided in Table I. The data plot in the elbaite field of alkali tourmalines, with moderate rossmanite and very low liddicoatite components (Figure 8). The green sample contained higher Fe concentration, consistent with its coloration, while the pink tourmaline had Mn as its main chromophoric element. The analyses are representative of the following formulas (Li, B and O/OH calculated stoichiometrically):

Green: $(Na_{0.62}Ca_{0.05}\square_{0.33})(Li_{1.39}Fe_{0.25}Mn_{0.09}Al_{1.28})$
$Al_6B_{3.00}(Si_{5.98}Al_{0.02})O_{27}(OH_{3.55}F_{0.45})$

Pink: $(Na_{0.51}Ca_{0.05}\square_{0.44})(Li_{1.25}Fe_{0.004}Mn_{0.03}Al_{1.72})$
$Al_6B_{3.00}(Si_{5.93}Al_{0.07})O_{27}(OH_{3.69}F_{0.31})$

Figure 8: Both of the Rwanda tourmaline samples analysed by electron microprobe for this report consist of elbaite with a significant rossmanite component, as shown in this compositional diagram (after Selway et al., 1998).

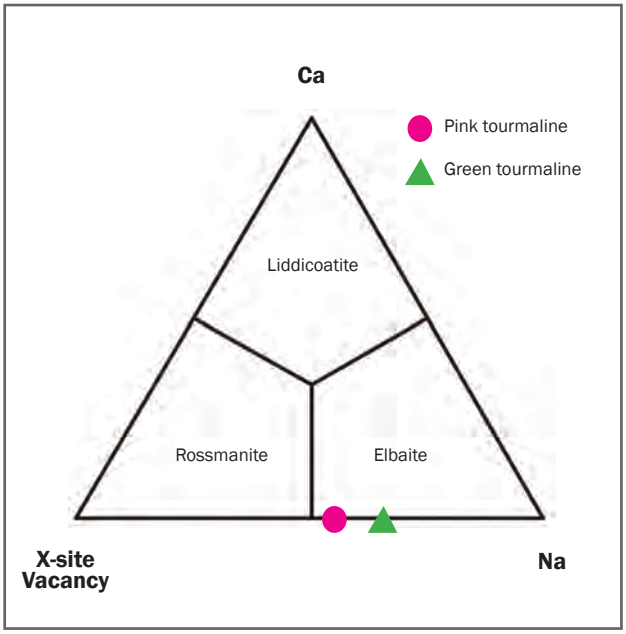

Table I: Chemical composition of green and pink tourmalines from Rwanda.

Sample	Green	Pink
Oxides (wt.%)		
SiO_2	38.27	38.34
TiO_2	0.01	0.01
B_2O_3 calc	11.12	11.24
Al_2O_3	39.66	42.75
FeO	1.89	0.03
MnO	0.66	0.20
CaO	0.29	0.28
Li_2O calc	2.21	2.01
Na_2O	2.06	1.70
K_2O	0.01	0.01
H_2O calc	3.40	3.58
F	0.92	0.63
Subtotal	100.51	100.78
−O=F	0.39	0.27
Total	**100.12**	**100.51**
Ions*		
Si	5.977	5.928
Ti	0.001	0.001
B	2.999	2.999
Al	7.301	7.791
Fe^{2+}	0.247	0.004
Mn	0.087	0.026
Ca	0.049	0.046
Li	1.387	1.250
Na	0.624	0.510
K	0.002	0.002
H	3.546	3.692
F	0.454	0.308
X-site vacancy	0.326	0.442
Ca/Ca+Na	0.072	0.080

*The amounts of elements not determinable by electron microprobe (B, Li, and H) were calculated according to stoichiometry as B=3, Li=3−Y and OH+F=4 (see Simmons et al., 2011).

Conclusion

The studied tourmalines from Rwanda show very similar physical and chemical properties to those from DRC, and also exhibit comparable inclusion characteristics (see Henn, 2010). This can be explained by the similar geological settings of the pegmatites of the Karagwe-Ankole Belt and the Kibara Belt, which extends from DRC to Zambia. These rocks contain metasediments that were intruded by granitic rocks and associated tourmaline-mineralized pegmatites. It seems likely that additional gem-quality tourmaline will be recovered from all of these deposits in the future.

References

Dewaele S., De Clercq F., Muchez P., Schneider J., Burgess R., Boyce A. and Fernandez Alonso M., 2010. Geology of the cassiterite mineralisation in the Rutongo area, Rwanda (Central Africa): Current state of knowledge. *Geologica Belgica*, **13**(1-2), 91–112.

Dewaele S., Goethals H. and Thys T., 2013. Mineralogical characterization of cassiterite concentrates from quartz vein and pegmatite mineralization of the Karagwe-Ankole and Kibara Belts, Central Africa. *Geologica Belgica*, **16**(1-2), 66–75.

Fernandez-Alonso M., Cutten H., De Waele B., Tack L., Tahon A., Baudet D. and Barritt S.D., 2012. The Mesoproterozoic Karagwe-Ankole Belt (formerly the NE Kibara Belt): The result of prolonged extensional intracratonic basin development punctuated by two short-lived far-field compressional events. *Precambrian Research*, **216**, 63–86, http://dx.doi.org/10.1016/j.precamres.2012.06.007.

Henn U., 2010. Turmaline aus dem Kongo. *Gemmologie: Zeitschrift der Deutschen Gemmologischen Gesellschaft*, **59**, 111–113.

Henn U., 2013. Grüne und rosafarbene Turmaline aus Ruanda. *Gemmologie: Zeitschrift der Deutschen Gemmologischen Gesellschaft*, **62**, 105–110.

Henn U., Bank H. and Bank F.H., 1990. Gem quality pink and green tourmaline, supposedly from Malawi. *Canadian Gemmologist*, **11**(3), 74–77.

Keller P.C., 1992. *Gemstones of East Africa*. Geoscience Press, Tucson, Arizona.

Krzemnicki M.S., Hänni H.A., Guggenheim R. and Mathys D., 1996. Investigations on sapphires from an alkali basalt, South West Rwanda. *Journal of Gemmology*, **25**(2), 90–106, http://dx.doi.org/10.15506/jog.1996.25.2.90.

Laurs B.M., Simmons W. and Falster A., 2004. Gem News International: Gem tourmaline from Congo. *Gems & Gemology*, **40**(3), 263–265.

Manning P.G., 1969. An optical absorption study of colour and pleochroism in pink and brown tourmaline. *Canadian Mineralogist,* **9**, 678–690.

Manning P.G., 1973. Effect of second-nearest-neighbour interaction on Mn^{3+} absorption in pink and black tourmalines. *Canadian Mineralogist,* **11**, 971–977.

Milisenda C.C., 2003. Gemmologie Aktuell: Saphir aus Ruanda. *Gemmologie: Zeitschrift der Deutschen Gemmologischen Gesellschaft*, **52**, 5–6.

Milisenda C.C., Malango V. and Taupitz K.C., 2000. Edelsteine aus Sambia – Teil 2: Turmalin und Aquamarin. *Gemmologie: Zeitschrift der Deutschen Gemmologischen Gesellschaft*, **49**(1), 31–48.

Ngaruye J.-C., 2011. Petrographic and Geochemical Investigation of Sn-W-Nb-Ta Pegmatites and Mineralized Quartz Veins in Southeastern Rwanda. MS thesis, University of the Free State, Bloemfontein, South Africa, 328 pp.

Selway J.B., Novak M., Hawthorne F.C., Černý P., Ottolini L. and Kyser T.K., 1998. Rossmanite, $\square(Li,Al_2)Al_6(Si_6O_{18})(BO_3)_3(OH)_4$, a new alkali-deficient tourmaline: Description and crystal structure. *American Mineralogist*, **83**, 896–900.

Simmons W.B., Falster A. and Laurs B., 2011. A survey of Mn-rich yellow tourmaline from worldwide localities and implications for the petrogenesis of granitic pegmatites. *Canadian Mineralogist*, **48**, 301–319, http://dx.doi.org/10.3749/canmin.49.1.301.

Simmons W.B., Pezzotta F. and Shigley J.E., 2012. Granitic pegmatites as sources of colored gemstones. *Elements*, **8**, 281–287, http://dx.doi.org/10.2113/gselements.8.4.281.

Smith G., 1978. A reassessment of the role of iron in the 5,000–30,000 cm^{-1} region of the electronic absorption spectra of tourmaline. *Physics and Chemistry of Minerals*, **3**, 343–373, http://dx.doi.org/10.1007/bf00311847.

The Authors

Dr Ulrich Henn FGA and Dipl.-Min. Fabian Schmitz
German Gemmological Association (DGemG)
Prof.-Schlossmacher-Str. 1
D-55743 Idar-Oberstein, Germany
Email: ulihenn@dgemg.com

Acknowledgements

The authors thank the firm Groh & Ripp in Idar-Oberstein for supplying the tourmaline crystals and cabochons that were studied for this report.

Conferences

Gem-A Conference 2014

The annual Gem-A Conference and associated events took place 1–4 November in London. Attended by nearly 190 people from 26 countries, the conference featured 13 speakers, four seminars and a tour of the Natural History Museum in London.

Bruce Bridges (Bridges Tsavorite, Tucson Arizona, USA) described the prospecting, mining, processing and marketing of tsavorite from his family's mines in Kenya, as well as the important contributions by his father, Campbell Bridges (see his recent article in *The Journal*, Vol. 34, No. 3, 2014, pages 230–241). At the conclusion of his talk, he announced that the Scorpion mine will be reopened in January 2015.

Edward Boehm (RareSource, Chattanooga, Tennessee, USA) provided numerous tips for analysing gems while in the field. His preferred instruments are the darkfield loupe and the dichroscope, and he emphasized the need to become proficient at using them in a laboratory setting before setting out for the field. When examining inclusions, it is important to observe the whole scene in a stone, rather than just isolated features.

Dr Thomas Hainschwang (GGTL Laboratories, Balzers, Liechtenstein) described the mechanisms for creating green to greenish blue coloration in diamond, and the challenges in identifying the natural vs. artificial origin of the colour. Irradiation using radium salts can result in dangerous amounts of residual radioactivity, whereas neutron-irradiated stones typically remain radioactive for only a couple of hours—although they may contain inclusions that remain 'hot' for a longer period of time.

Figure 1: In Bahia State (Brazil), gem-quality rutilated quartz is extracted from tunnels such as this one at the Pyramid mine, owned by Brian Cook. Photo © Brian Cook.

Alan Hart (Natural History Museum, London) described the history and future plans for the gem and mineral collection at the Natural History Museum. There are currently about 10,000 specimens on display of the ~180,000 samples in the collection; of these, 5,500 of them are gems. During the next 10 years, there are plans to renovate the display in a new Earth and Planetary Sciences wing.

Dr Ulrich Henn (German Gemmological Association, Idar-Oberstein, Germany) compared the properties of moonstone from Sri Lanka, India and Tanzania. The Sri Lankan material is K-feldspar (cryptoperthite), while the Tanzanian moonstone consists of albite. Indian samples typically are K-feldspar, while a 'rainbow' variety is andesine-labradorite.

Brian Cook (Nature's Geometry, Tucson, Arizona, USA) reviewed the history of Paraíba tourmaline from the São Jose da Batalha deposit in Brazil. Mining efforts are currently focused on an area below the hill where the material was originally discovered, and a 3-cm-long crystal of this valuable tourmaline was recently found in the 40-m-deep shaft. Another mine in neighbouring Rio Grande do Norte State (operated by Mineraçao Terra Branca) continues to produce blue Cu-bearing tourmaline in mostly small sizes. Cook also provided an update on gem-quality rutilated quartz from the Novo Horizonte area, Bahia State, Brazil. Miners search for crystal-bearing cavities that are hosted by quartz veins within volcanic rocks (Figure 1). About 15,000 people are affected by the mining and trading of this material, and after nearly a decade of effort to formalize the claims, they are finally being legalized and environmental permits obtained.

Vincent Pardieu (GIA Laboratory, Bangkok, Thailand) reviewed global localities for gem spinel, including Tajikistan, Myanmar, Vietnam, Tanzania, Sri Lanka, Pakistan and Kenya. His presentation highlighted bright red spinel from secondary deposits at Man Sin, near Pyin Pyit in the Mogok area of Myanmar.

Craig Lynch (Ouellet and Lynch, Phoenix, Arizona, USA) described jewellery recovered from the famous RMS Titanic, which sank on 15 April 1912. Of the approximately 6,000 objects recovered from the wreckage during 25 years of salvage operations, 75–85 pieces consist of jewellery and watches. These

represent the Victorian, Edwardian, Art Nouveau and Belle Époque movements. Many of the artefacts are in poor condition after being submerged in saltwater for many decades.

Dr Laurent Cartier (Swiss Gemmological Institute SSEF, Basel, Switzerland) provided an update on worldwide cultured pearl production. He emphasized that for a farm to be profitable, it must attain both high-quality cultured pearl production and low mortality of the host molluscs.

Chris Smith (American Gemological Laboratories Inc., New York, New York, USA) explained his ruby and sapphire source-type classification system. This objective process helps make country-of-origin determinations more consistent by combining both geological and gemmological considerations. Macroscopic and microscopic observations are used to narrow possible origins and are supported by UV-Vis-NIR spectra and chemical data.

Menahem Sevdermish (Gemewizard Inc., Ramat Gan, Israel) described developments of his Gemewizard software package in the areas of digital colour analysis, grading, pricing and trading of gems. A colour converter is now available that gives equivalent terminology for RGB, CMYK, Munsell, CIELAB and GIA colour descriptions.

Terry Coldham (Gemmological Association of Australia, Normanhurst, Australia) described how Thai developments in the late 1960s in using heat treatment to remove the 'silk' and therefore improve the clarity of Australian sapphire resulted in a huge increase of rough exports to Thailand. This material contributed enormously to the growth of the Thai gem processing and cutting industries. Coldham indicated that Thai experience with heating Australian sapphire facilitated their discovery of how to treat Sri Lankan geuda sapphire in 1979.

Richard Hughes (Lotus Gemology Co. Ltd., Bangkok, Thailand) discussed a variety of gemmological misconceptions. He also encouraged experimentation in gemmology, rather than simply observation. Hughes advocated a more 'right-brained' approach to help bring passion back to the trade.

Dr Franz Herzog (Oltingen, Switzerland) provided an informative seminar on portable EDXRF spectroscopy using a Thermo Nitron analyser. Although such devices do not currently provide quantitative data without extensive calibration procedures, they can give trace-element chemical signatures that are useful for geographic origin determination, chromophore evaluation, and natural vs. synthetic vs. treated identifications.

Other seminars covered coloured stone grading and pricing (with **Richard Drucker**, Gemworld International Inc., Glenview, Illinois, USA), gemmological applications of Raman and photoluminescence spectroscopy (with **Mikko Åström** and **Alberto Scarani** of M&A Gemological Instruments, Järvenpää, Finland and Rome, Italy) and ethical challenges in the gem industry (with **Greg Valerio** of Cred Jewellery and Fair Jewellery Action, London; **Vivien Johnston** of Gem-A, London; and **Dana Schorr** of Schorr Marketing, Santa Barbara, California, USA).

Brendan M. Laurs

GSSA Kimberley Diamond Symposium

The second Geological Society of South Africa Kimberley Diamond Symposium & Trade Show was held in Kimberley from 11 to 13 September 2014, seven years after the first one took place in August 2007. It was attended by 270 people, mainly from the Republic of South Africa (RSA) and neighbouring Botswana, Lesotho and Namibia, but also about a dozen each from Canada and Russia, and a few from Australia, Brazil, Germany, UK and USA. The conference was chaired and organized by Drs John Bristow and Mike de Wit. There were 20 oral and 26 poster presentations during the first two days, and visits to several alluvial deposits and two underground mines (Finsch and Kimberley) were made on the third day. A selection of the many interesting talks and posters is provided below.

Dr Mike de Wit (Tsodilo Resources, Toronto, Canada) indicated that most (or all) of the world's easier-to-find large-sized primary diamond deposits have been discovered. He said that geophysical methods will become more important for detecting deposits through superficial strata (i.e. younger than Cretaceous or Eocene) to find additional kimberlites. Thus, target-area selection must be improved, and this was also discussed by **Dr Hielke Jelsma** (De Beers Exploration, Johannesburg), who showed the periodicity of kimberlite intrusion and the formation of cratons and continents. In addition, **Dr Charles Skinner** (De Beers Exploration, Johannesburg) emphasized the importance of correct area selection combined with geographic accessibility, political

stability, and appropriate environmental and transparency regulations. **Dr Barbara Scott Smith** (Scott Smith Petrology, Vancouver, Canada) previewed of a new glossary of descriptive terms for the precise definition of features observed in kimberlites (both in hand specimens and under the microscope), which are grouped into five stages increasing in detail and related to diamond content.

Dr John Bristow (previously of Rockwell Diamonds and now with Incubex Mineral Consultants, Gauteng, RSA) described the geology of the Middle Orange River alluvial diamond deposits. The Early Mesozoic Ghaap Plateau escarpment funnelled the discharge from the Vaal, Harts and Orange Rivers through a wide valley to form the diamond-bearing gravels. The deposits are of low grade but contain many diamonds larger than 100 ct, and Bourevestnik X-ray luminescence equipment (manufactured in Russia) has improved the recovery of large stones. This theme was also discussed by **James Campbell** (Rockwell Diamonds, Johannesburg, RSA), and specific examples of alluvial gravel deposits were presented in three other talks and 11 posters by geologists from Rockwell Diamonds. **Dr Jürgen Jacob** (Namdeb Diamond Corp., Oranjemund, Namibia) described the various forms of beach gravel (linear, pocket and pothole), aeolian and fluvial deposits in Namibia, and concluded that after 106 years of mining there are at least another 50 years of reserves left in this important megaplacer. Four posters by other Namdeb workers described specific examples of various coastal placer deposits.

Hilde Cronwright (MSA Group, Johannesburg) showed that the analysis of microdiamonds at the Karowe mine (AK6 pipe, Botswana) results in a better prediction of the occurrence of large type IIa diamonds than results derived from large drill or bulk samples. **Dr Mike Lynn** (MSA Group, Johannesburg) described the phlogopite-rich, macrocrystic Moteti kimberlite dyke, a new diamond occurrence in Lesotho that may contain 1.5 million tonnes (Mt) of ore at 65 carats per 100 tonnes (cpht), yielding 1 million carats (Mct) of diamonds valued at $62/ct. This presents a new target for diamond exploration in Lesotho (i.e. small size, small volume, medium grade and medium diamond value).

Dr J. P. Donatti-Filho (Lipari Mineração Ltda., Nordestina, Brazil) described the Braúna 3 project, which is destined to become the first kimberlite diamond mine in Brazil. With a surface area of 2 ha, the Braúna 3 pipe is the largest in a 17-km-long zone of 22 occurrences of dykes, 'blows' and small pipes extending south of Nordestina in Bahia State. Estimated reserves (indicated and inferred) are 4.92 Mt with a grade of 53 cpht, yielding 2.57 Mct valued at US$284/ct.

This symposium provided a nice prelude to a diamond/kimberlite session that will be held at the 35th International Geological Conference in Cape Town in mid-2016, and also the 11th International Kimberlite Conference scheduled for June 2017 in Gaborone, Botswana.

A. J. A. (Bram) Janse (archonexpl@iinet.net.au)
Archon Exploration Pty. Ltd., Carine, Western Australia

NAJA Mid-Year Conference 2014

The National Association of Jewelry Appraisers' mid-year conference took place right after the World of Gems Conference (see following report) on 22–23 September in Rosemont, Illinois. There were 150 people in attendance, and Gail Brett Levine and her team put on a great event.

Tammy Cohen (Diamonds International, New York, New York, USA) explained the valuation of the Crown of Light proprietary diamond cut. She and her team shared retail price lists to help with appraisals. The Crown of Light has 90 facets with a domed top and a very small table, like a modified rose cut.

Carl Schutze and his father-in-law **Manuel Marcial de Gomar** of Emeralds International (Key West, Florida, USA) discussed emeralds from the Atocha, a Spanish galleon that sunk off Key West in 1622. The wreck was salvaged by Mel Fisher, who recovered millions in gold, silver, artefacts and emeralds. These 'shipwreck emeralds' are thought to be from the Tequendama mine in the Muzo area of Colombia.

Dr Paul Downing, an author from Fountain Hills, Arizona, USA, hosted an Ethiopian opal workshop, and examples showing various characteristics were available for examination. The hydrophane characteristic of Ethiopian opal can be revealed by its sticky feel when touched with a dampened finger.

Arthur Skuratowicz (Jewelry Training Center, Colorado Springs, Colorado, USA) held a workshop on the identification of non-traditional metals by non-destructive testing. Many cost-effective metals found

in today's market lack accurate markings, creating a challenge for valuers and appraisers. X-ray fluorescence analysis can give an accurate determination of metal composition, but this technique is beyond the reach of most appraisers.

Day two began with what might have been perceived as a dry topic: Internal Revenue Service appraisal rules for charitable contributions of jewellery. **Karin Gross** (IRS, Washington D.C., USA) gave a clear and concise presentation, with references to IRS publications to make the process flow smoothly.

Schutze and **Marcial de Gomar** returned for a second presentation on another treasure found off Key West (and elsewhere in the Caribbean Sea region): the conch pearl. The process of formation within the shell to the finished piece of jewellery was discussed. They stated that only one in 10,000 conch shells may produce a pearl, with no guarantee of quality.

Jeff Ira (Metro Jewelry Appraisers, Medford, Massachusetts, USA) shared 50 ways to energize an appraisal business. He reviewed and introduced timely tips that were broken down into daily organization, quality of life, networking, promoting and perception.

Dr Cigdem Lule and **Stuart Robertson** of Gemworld International (Glenview, Illinois, USA) discussed appraising natural untreated gems. *Natural* in the true sense of the world means nothing has been done to the material besides cutting and fashioning. Value depends not only on visual appearance but on what treatments a stone has undergone. They indicated that an untreated ruby may command a 200–300+% premium in today's market.

Eric W. Fritz (EricFritz@gem-a.com)
Gem-A Regional Manager, North America
Tucson, Arizona, USA

World of Gems Conference IV

This biennial conference was held in Rosemont, Illinois, USA, on 20–21 September 2014. More than 230 people from 12 countries were in attendance. The talks were moderated by **Richard Drucker** (Gemworld International, Glenview, Illinois), who also began the conference with a historical retrospective of the GemGuide publication, as well as a review of current trends in diamonds and coloured stones.

Dr Thomas Hainschwang (GGTL Laboratories, Balzers, Liechtenstein) reported on his doctoral studies of the coloration and defects in type IB diamonds. In addition to showing yellow coloration as expected from their nitrogen content, such diamonds more typically range from orange to 'olive' green (most common) to brown, as well as showing mixtures of these colours.

Dr James Shigley (Gemological Institute of America [GIA], Carlsbad, California, USA) examined diamond fluorescence. He stated that 80% of the diamonds submitted to GIA's laboratories show very faint to no fluorescence, and only 0.1% show very strong fluorescence. Of those diamonds that do luminesce, 97% show blue fluorescence. He also indicated that this blue fluorescence may influence the diamond's face-up colour appearance only in extreme cases. **Richard Drucker** followed with a presentation on the effect of diamond fluorescence on pricing. He pointed out that until the late 1970s (during the diamond investment boom), it was common for observers to prefer some fluorescence, but subsequently it was perceived that fluorescence creates a 'hazy' appearance in a diamond. Prices of fluorescent diamonds continue to be discounted, making them an attractive option for buyers who don't mind fluorescence.

Stuart Robertson of Gemworld International researched the effect of colour modifiers on the pricing of fancy-colour diamonds. By compiling the prices of numerous GIA-graded diamonds (0.5–1.0 ct radiant-cut stones with Fancy colour grades), he found that brown-to-yellow modifiers result in an approximately 20–25% decrease in value, while greenish modifiers of yellow stones correspond to a 100% increase in value.

This author (*Journal of Gemmology*, Gem-A, Encinitas, California, USA) explained the benefits obtained from doing field research of gem deposits. Such expeditions allow one to gain accurate first-hand information on the location, geology, and mining methods at a given deposit, as well as an idea of future reserves. One can also learn about the ore processing techniques and production (gem varieties, quality and quantity), and witness the trading and distribution of the material. Other benefits include obtaining research samples (directly from the mine in some cases) and purchasing hard-to-find maps and publications.

Dr Cigdem Lule of Gemworld International examined the reliability of country-of-origin reports. She stated that origin determinations are an opinion-based practice that relies on scientific data collected by advanced mineralogical testing. Ultimately the locality decision is based on the knowledge and judgement of

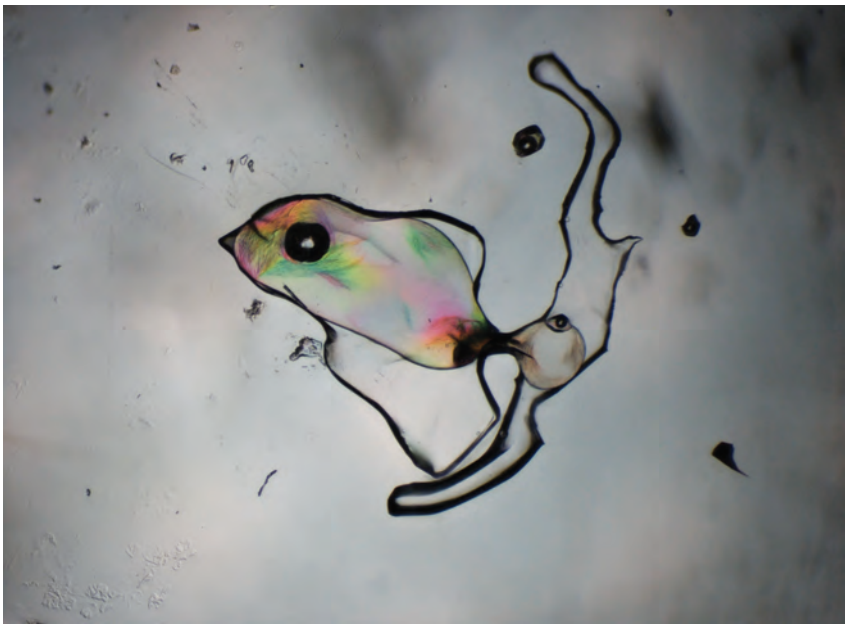

Figure 2: Resembling an abstract fish, this three-phase inclusion in quartz from Bahia, Brazil, was photographed with cross-polarized light to reveal the colourful birefringence in the solid component. A methane gas bubble makes a convincing 'eye' in the petroleum-and-water-filled body. Photomicrograph by Nathan Renfro, © GIA; image width 2.5 mm.

the gemmologist who makes the determination. Due to overlap in the properties of some gems (particularly blue sapphires), the reliability of such determinations would be improved by stating the geologic origin rather than geographic origin, but the latter is preferred by gem merchants.

Eric Braunwart (Columbia Gem House, Vancouver, Washington, USA) highlighted several factors influence the supply and pricing of gems, including: changes in the value of the US dollar; monitoring of gold, diamonds and coloured stones as potential sources of terrorist funding; mine closures due to the global economic recession; the boom in TV/internet sales of gems; China's increased demand for jadeite, as well as diamond, ruby, sapphire and tourmaline, and an increase in the mass production of jewellery in Chinese factories; the prevalence of treated and synthetic gems in coloured stone parcels; and consumers' growing demand for corporate social responsibility in the gem and jewellery industry.

Jeffrey Bergman (Primagem, Bangkok, Thailand) explored trapiche gems in a well-illustrated presentation covering 'true' trapiche stones (e.g. emerald, ruby, sapphire and tourmaline) as well as some gems showing star-like patterns that are not due to a skeletal growth pattern (e.g. garnet, quartz, chalcedony and diamond). In a separate presentation, Bergman described the value factors of star, cat's-eye and trapiche gems: colour, clarity, stone size, and the intensity, sharpness, completeness and centring of the star or eye.

Jon Phillips (Corona Jewellery, Vancouver, British Columbia, Canada) covered recent developments in diamond mining and marketing. He believes that Russia will surpass De Beers' production of rough (by value) in the next five years. He noted that the best-selling shapes of faceted diamonds are pear, round and marquise, and he indicated that branded diamonds may provide better margins—if there is a good story to accompany them.

Dr John Emmett (Crystal Chemistry, Brush Prairie, Washington) and **Stuart Robertson** gave a two-part presentation on how treatments have historically altered the supply and pricing of gem corundum. Dr Emmett reviewed how various heat treatments (with and without added elements) have been critical to boosting the commercial availability of sapphires from localities such as Sri Lanka, Australia, USA (Montana), Madagascar and Tanzania (Songea), as well as rubies from Mong Hsu (Myanmar). Robertson explained that during the past two decades, the proportion of heated corundum in the gem market has grown from approximately 40% to nearly 100%. During this time, the industry has been operating under of the principle of detection, rather than disclosure.

Nathan Renfro (GIA, Carlsbad) illustrated many examples of 'microart' in gems, particularly by using fibre-optic lighting and oblique illumination to highlight interesting inclusion characteristics. With the clever use of a microscope and camera, he showed the beauty associated with gemstone 'imperfections' (e.g. Figure 2).

Gail Brett Levine (National Association of Jewelry Appraisers, Rego Park, New York) described the styles, motifs and pricing of jewellery from the Late Georgian and Victorian movements. She highlighted the variable quality of this jewellery and the fact that some of it is undervalued in today's marketplace.

Brendan M. Laurs

GIT

YOUR GLOBAL PARTNER

Gem Identification Report and Gemstone Memo

GIT, The utmost advanced Gem and Precious Metal Testing Laboratory in Thailand, is recognized by CIBJO (The World Jewellery Confederation) and also a member of LMHC and ICA, we are well equipped with the world's most advanced instruments operated by highly experienced gemologists.

LABORATORY SERVICES

ensuring the authenticity of your valuable gems & jewelry

The Gem and Jewelry Institute of Thailand (Public Organization)
140 ITF Tower, Silom Rd., Bangkok 10500,Thailand
TEL : +66 2634 4999 FAX : +66 2634 4970
http://www.git.or.th E-mail: jewelry.or.th

Gem-A Notices

GEM-A CONFERENCE 2014

The 2014 Gem-A Conference was held on 1–2 November at the Business Design Centre, Islington, London. Originally the Royal Agricultural Hall, the building was the venue for the first Gem-A graduation ceremony in 1913.

A full report of the Conference and events was published in the November/December 2014 issue of *Gems&Jewellery*. Highlights of the presentations are given in the Conferences section, pages 350–351.

Conference Events

Seminars and workshops were presented on 3-4 November at the Gem-A headquarters by Richard Drucker FGA GG, Mikko Åström FGA and Alberto Scarani GG, Dr Franz Herzog, and Greg Valerio, Vivien Johnston and Dana Schorr.

Also on 4 November a guided tour was held of the Mineral Galley at the Natural History Museum hosted by Alan Hart FGA DGA.

Conference Sponsors and Supporters

The Association is most grateful to the following for their support:

Major Sponsor

Jewelry Television (JTV)
www.jtv.com

Sponsors

CIBJO
www.cibjo.org

The Company of Master Jewellers
http://masterjewellers.co.uk

GemmoRaman
www.gemmoraman.com

Supporters

AnchorCert Gem Lab
www.anchorcert.co.uk

Gemworld
www.gemguide.com

Marcus McCallum FGA
www.marcusmccallum.com

National Association of Goldsmiths' Institute of Registered Valuers
www.jewelleryvaluers.org

C W Sellors
www.cwsellors.co.uk

Associate Supporters

AGIL
www.agil.com.hk/tc/index.php

Apsara Gems
www.apsara.co.uk

British Jewellers' Association
www.bja.org.uk

T.H. March, Insurance Brokers
www.thmarch.co.uk

We would also like to thank **DG3 Diversified Global Graphics Group** for sponsoring conference materials.
www.dg3.com

GRADUATION CEREMONY

The Graduation Ceremony and Presentation of Awards was held at Goldsmiths' Hall on 3 November. Gem-A CEO James Riley opened the proceeding by welcoming those present. The guest speaker, Tim Matthews, president of Jewelry Television (JTV), then presented the diplomas and awards.

James Riley announced the special awards. In recognition of their outstanding contributions to the gem and jewellery industry, Dr Gaetano Cavalieri of Bern, Switzerland, and Terry Coldham of Normanhurst, New South Wales, Australia, were each awarded an Honorary Fellowship.

Two members were awarded Fellowship status in recognition of their significant contribution to the field of gemmology for no less than 10 years. They were Edward Boehm of Chatanooga, Tennessee, USA, and Dr Ulrich Henn of Idar-Oberstein, Germany.

Two former members of the Gem-A staff, Dr Jack Ogden and Mary Burland, were awarded Honorary Lifetime Memberships.

Tim Matthews, president of JTV, giving the address. Photo © vips event photography.

The award winners who attended the Graduation Ceremony at Goldsmiths' Hall. From left: Doerte Herold (Diamond Practical Prize), Elie-Anne Caya (Christie's Prize for Gemmology), Ching Man Wong (Deeks Diamond Prize) and Andrea Von Allmen (Bruton Medal). Photo © vips event photography.

Tim Matthews gave the address, congratulating the graduates on their great achievement. He outlined his own career with JTV, before questioning where their careers would take them. He stated: "With your great accomplishment, evidenced by the diplomas conferred this evening, you are now equipped for a great journey in the gemstone business." Tim concluded his address by saying: "I wish you well and trust that your career in the jewellery and gemstone trade will be interesting, exciting and rewarding. Look forward to great destinations and memories of a lifetime. And allow your newfound knowledge and influence to flourish into profound personal leadership to have a positive impact on others in your path."

The ceremony was followed by a reception for graduates and guests in the Drawing Room.

GIFTS TO THE ASSOCIATION

The Association is most grateful to the following for their gifts for research and teaching purposes:

John Bradshaw, Nashua, New Hampshire, USA, for pieces of rough Mexican hyalite opal.

Terry Coldham FGAA FGA, Normanhurst, New South Wales, Australia, for a 0.74 ct natural orange sapphire and six issues of *The Australian Gemmologist* from October 2013 to March 2014.

Brian Davies of Percy Davies Jewellers, Gerrards Cross, Buckinghamshire, for a collection of rough and cut material including emeralds in schist, pegmatite minerals and African gemstones, and photos and negatives from 13 study tours organized by *Retail Jeweller*.

Prof. Dr Henry Hänni FGA, Basel, Switzerland, for fashioned spheres of quartz, olivine and orthoclase.

Bronwen Harman-Jones FGA DGA, Reading, Berkshire, for a selection of faceted diamond simulants including CZ, GGG, quartz, paste, strontium titanate, synthetic corundum, synthetic spinel, YAG and zircon.

Nirijan Khalsa, Beverly Hills, California, USA, for a collection of Oregon sunstones including two large pieces of crystals in matrix, rough stones and oval cabochons, as well as nine fancy-cut stones, each over 10 mm in diameter.

Grenville A. Millington FGA, Knowle, West Midlands, for the 0.03 ct diamond that was used for the winning trigons photograph in the 2014 Gem-A Photographic Competition.

Dominic Mok FGA DGA, Hong Kong, for 35 rough and fashioned gemstones (all showing inclusions), including amber, beryl, corundum, danburite, enstatite, fluorite, garnet, iceland spar, kyanite, moonstone, peridot, phenakite, quartz, scapolite, spinel, topaz, tourmaline and zircon.

Dr John M. Saul, Paris, France, for a copy of his book *The Tale Told in All Lands: The Heavens as Blueprint for Civilization* (2013, Les 3 Colonnes, Paris).

Antonio Silva, London, for approximately 227 g of rough tanzanite (gravel), a blue/green diamond crystal slice and a copy of *Brazil: Paradise of Gemstones* by Jules Roger Sauer (1982, J. R. Sauer, Rio de Janeiro, Brazil).

PHOTOGRAPHIC COMPETITION 2014

Joint Winners

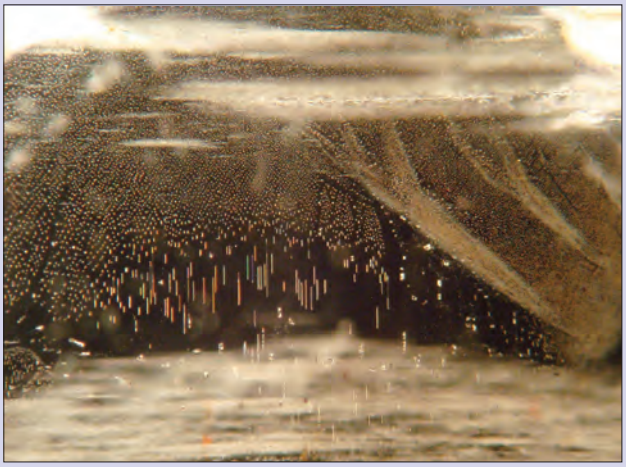

Dayananda Dillimuni FGA. *'Rainy day'. Inclusions in natural beryl, showing flat tabular cavities parallel to basal pinacoid, short tube-like cavities parallel to c-axis and liquid feathers.*

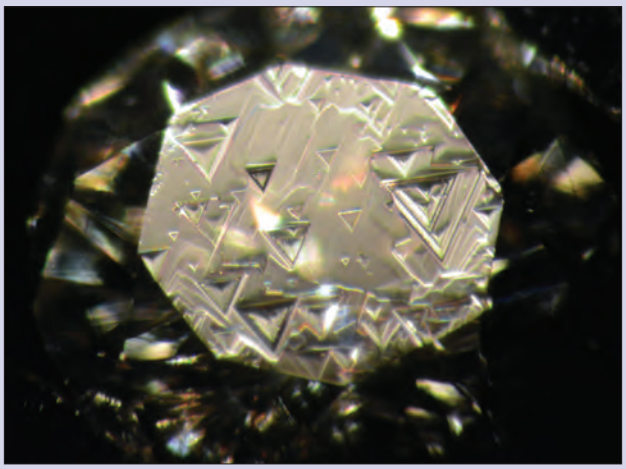

Grenville Millington FGA. *Trigons across the table facet of a 0.03 ct round brilliant diamond (2.01–2.06 × 1.19 mm). Magnification 80×.*

Second Prize

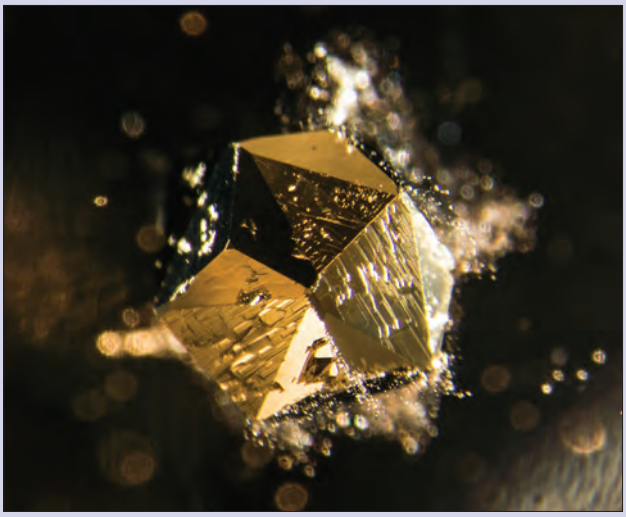

E. Billie Hughes FGA. *Pyrite inclusion in quartz.*

Third Prize

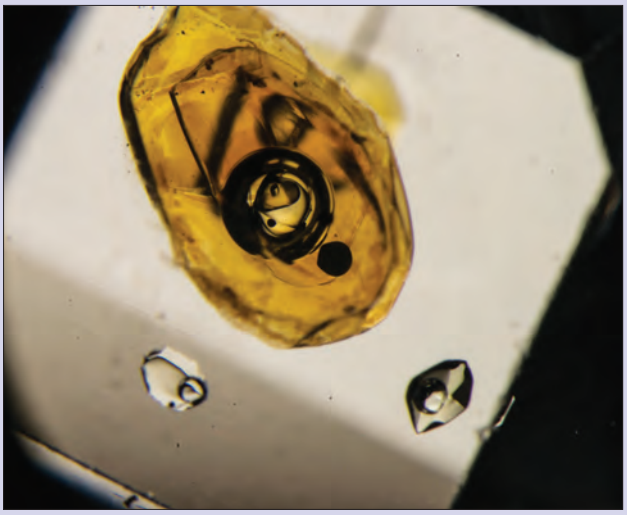

E. Billie Hughes FGA. *Petroleum inclusion in quartz, including a bubble that has the appearance of a 'yin-yang' symbol.*

Honourable Mentions

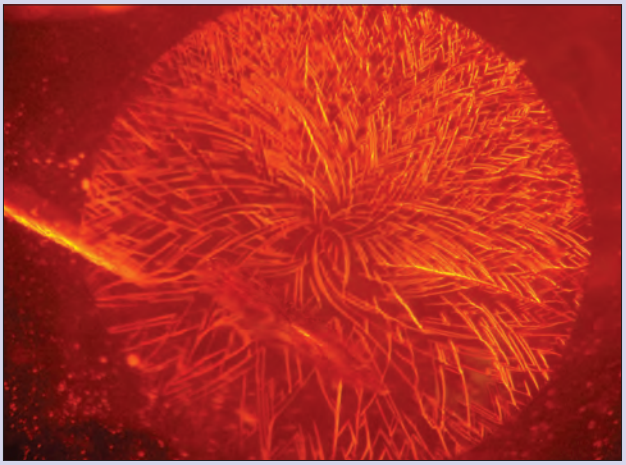

Dayananda Dillimuni FGA. *Sun spangle in amber; the characteristic pattern produced after heat treatment showing curved radiating lines in two directions.*

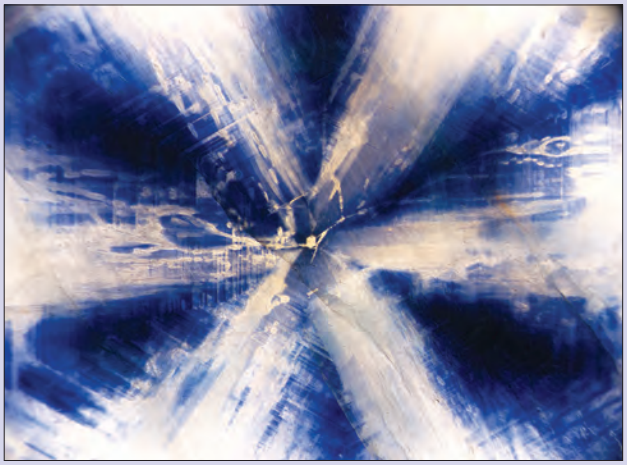

Richard Hughes FGA. *Trapiche sapphire from Mogok, Myanmar. Magnification approximately 7×.*

GEMMOLOGICAL ASSOCIATION OF AUSTRALIA

During the Graduation Ceremony held at Goldsmiths' Hall on 3 November, Gem-A and the Gemmological Association of Australia (GAA) signed an agreement recognizing the equivalent status of the associations' two gemmology diplomas and allowing fully paid-up Fellows of either association to apply for Fellowship of their sister association. The agreement was signed by Gem-A Chairman Jason Williams and President Harry Levy, and GAA President Katrina Marchioni and Patron Terry Coldham. As both organizations are members of CIBJO the agreement was witnessed by CIBJO President Dr Gaetano Cavalieri.

MEMBERSHIP

At a meeting of the Council of the Association held on 3 November 2014, the following were elected to membership:

Fellowship and Diamond Membership (FGA DGA)

Khinvasara, Sunil, *Monroe Township, New Jersey, USA*
Li Man Kit, *Shatin, Hong Kong*
Peshall, Jessica, *Pimlico, London*
Sokkalingam, Visvanathan, *Singapore*
Von Allmen, Andrea, *Münsingen, Switzerland*

Fellowship (FGA)

Carr, Susan, *Thornhaugh, Cambridgeshire*
Chant, Francesca, *Worcester Park, Surrey*
Cheer, Peter, *Somerton, Somerset,*
Elazzouzi, Celine, *Ile de la Réunion, France*
Graff, Elliott, *London*
Griffon, Denise, *Montreal, Quebec, Canada*
Heilio, Saara, *Orpington, Kent*
Kenyon, Janelle, *Auckland, New Zealand*
Kim Dong Hui, *Daegu, South Korea*
Kyle, Jennifer, *Montreal, Quebec, Canada*
Leedham, Laura, *Oldbury, West Midlands*
Lineker-Mobberley, Maryanne, *Bridgnorth, Shropshire*
Liu Hongwei, *Nankai District, Tianjin, P.R. China*
Mustsaers, Gerard, *Dieren, The Netherlands*
Nigam, Pooja, *New Delhi, India*
O'Sullivan Walter, Lauren, *San Francisco, California, USA*
Ramanasse, Anthony, *Paris, France*
Richbourg, Carole, *Los Altos, California, USA*
Roelofse, Frederick, *Bloemfontein, South Africa*
Routledge, Susannah, *Reading, Berkshire*
Schuch-Des Forges, Vanessa, *North Littleton, Worcestershire*
Siritheerakul, Piradee, *Bangkok, Thailand*
Stead, Heather, *Wigginton, North Yorkshire*
Tjioe Ay Djoen, *Montreal, Quebec, Canada*
Tsang, Kim, *Tai Kok Tsui, Hong Kong*

Diamond Membership (DGA)

Acklam, Sharon, *Hull, East Yorkshire*
Fung, Yan Yan, *Yuen Long, Hong Kong*
Hrustic, Ibrahim, *Marieholm, Sweden*
Kuebler-Tesch, Joachim, *Ludwigsburg, Germany*
Lansley, Juliette, *Heathfield, East Sussex*
Lumb, Sarah, *London*
Nadal, Cynthia, *London*
Rice, James, *Hull, East Yorkshire*
Rice, Max, *Hull, East Yorkshire*
Sharpley-Fanner, Harriet, *London*
Wong Yee Wai, *Yuen Long, Hong Kong*

Associate Membership

Appadoo, Vijay, *Croydon, London*
Bohlin, Anne, *Stockholm, Sweden*
Bratton, Tim, *Farnborough, Kent*
Harrison, Peter, *Darlington, County Durham*
Johnson, Mark, *Ryde, Isle of Wight*
McAlpine, Ross, *Liverpool, Merseyside*
McCullough, Lesley-Ann, *Belfast*
McLauchlan, Duncan, *London*
Milliner, Sean, *Scottsdale, Arizona, USA*
Pughe, Marianne, *Corbridge, Northumberland*
Radatzaun, Ramtin, *London*
Risstad Bohlin, Anne, *Stockholm, Sweden*
Rodrigues, Suelle, *Breukeleveen, Utrecht, The Netherlands*
Sathanantharaja, A., *London*
Sergei, Michael, *London*
Sergent, Shelly, *Scottsdale, Arizona, USA*
Shepherd, Drina, *Rude, Isle of White*
Snell, Simon, *Bournemouth, Dorset*
Weerawardana, Sagarika, *Kurunagala, Sri Lanka*

Corporate Gold Membership

Stone Group Laboratories, *Jefferson City, Missouri, USA*
Studley Jewellers, *Wells, Somerset*

Corporate Membership

Fred J Malcolm Ltd, *Belfast*
Serendipity Diamonds, *Ryde, Isle of Wight*
Somewhere in the Rainbow, *Scottsdale, Arizona, USA*

Subscriptions 2015

The Associate, Fellow and Diamond membership subscriptions for 2015 are £135 or £110 if paying by direct debit. Corporate and Corporate Gold Membership subscriptions are £300 or £275 if paying by direct debit.

GEM-A AWARDS

In the Gem-A examinations held in June 2014, 181 students qualified in the Gemmology Diploma examination, including nine with Distinction and 29 with Merit, and in the Foundation Certificate in Gemmology examination 366 qualified. In the Gem Diamond examination 66 qualified, including nine with Distinction and eight with Merit.

In the **Gemmology Diploma** examinations held in January and June 2014, the **Christie's Prize for Gemmology** for the best candidate of the year was awarded to **Elie-Anne Caya** of Quebec City, Canada. The **Anderson Bank Prize** for the best set of theory papers was awarded to **Dilyara Khabrieva** of London. The **Read Practical Prize** for excellence in the practical examination was awarded to **Claire Ito** of Carlsbad, California, USA.

In the **Foundation Certificate in Gemmology** examination, the **Anderson Medal** for the candidate who submitted the best set of answers which, in the opinion of the examiners, were of sufficiently high standard, was awarded to **Andrew Barrett** of Sliema, Malta.

In the **Diamond Diploma** examination, the **Bruton Medal** for the best set of theory answer papers of the year was awarded to **Andrea Von Allmen** of Münsingen, Switzerland.

The **Deeks Diamond Prize** for the best candidate of the year was awarded to **Ching Man Wong** of Discovery Bay, Hong Kong.

The **Diamond Practical Prize** for excellence in the Diamond Practical examination, sponsored by Dominic Mok from AGIL, Hong Kong, was awarded to **Doerte Herold** of Zürich, Switzerland.

The **Tully Medal** was not awarded.

The names of the successful candidates are listed below.

Examinations in Gemmology

Gemmology Diploma

Qualified with Distinction

Jiang Rongxian, *Guangzhou, Guangdong, P.R. China*
Lescuyer, Loic, *Francheville, France*
Li Zhixiang, *Guangzhou, Guangdong, P.R. China*
Liscouet, Marie-Solène, *Saint-Cloud, France*
Platis, Alexandros, *Nafpaktos, Greece*
Wang Jiaying, *Beijing, P.R. China*
Wang Yanjing, *Beijing, P.R. China*
Williams, Kathryn, *Dover, Kent*
Yu Hui, *Beijing, P.R. China*

Qualified with Merit

Borreill, Daniel, *Serralongue, France*
Caya, Elie-Anne, *Quebec City, Quebec, Canada*
Clark, Bryan, *Brooklyn, New York, USA*
Deng Xia, *Beijing, P.R. China*
Dunn, Lauren, *Trowbridge, Wiltshire*
Föge, Kerstin, *Dijon, France*
Fox, Rosanna, *Kennington, London*
Goots, Pauline, *Liège, Belgium*
Lai Cheng, *Guilin, Guangxi, P.R. China*
Li Haoyue, *Beijing, P.R. China*
Liu Jiamin, *Guilin, Guangxi, P.R. China*
Mutsaers, Gerard, *Dieren, The Netherlands*
Na Xiuxi, *Beijing, P.R. China*
Ni Fang, *Qingdao, Shandong, P.R. China*
Nigam, Pooja, *New Delhi, India*
Ramaroarivo, Jerry-Son, *Antananarivo, Madagascar*
Song Shuang, *Beijing, P.R. China*
Tsang Kim Po, *Tai Kok Tsui, Hong Kong*
Tsao Wen Ting, *Taipei City, Taiwan, R.O. China*
Wang Boyu, *Beijing, P.R. China*
Wang Jiaxin, *Beijing, P.R. China*
Wu Jiahui, *Beijing, P.R. China*
Xiao Ya, *Beijing, P.R. China*
Xie Jiajia, *Beijing, P.R. China*
Xu Xiaodan, *Beijing, P.R. China*
Yan Wei, *Beijing, P.R. China*
Yu Xinyuan, *Changsha, Hunan, P.R. China*
Zhang Jing, *Tianjin, P.R. China*
Zhang Shi, *Guilin, Guangxi, P.R. China*

Qualified

Amiel, Chantal, *Marseille, France*
Attanayake, Rochana, *Pilimathalawa, Sri Lanka*
Bailey, Anneabell, *Rotherhithe, London*
Boubouillon, Yasmine, *Crétail, France*
Carr, Susan, *Thornhaugh, Cambridgeshire*
Cazanescu, Cristina, *Genoa, Italy*
Chan Ya-Ting, *Taipei City, Taiwan, R.O. China*
Chen Yin, *Shanghai, P.R. China*
Chen Xiao, Mei, *Kowloon, Hong Kong*
Chen Xiaobin, *Beijing, P.R. China*
Chen Lei-An, *Taichung, Taiwan, R.O. China*
Chen Zhiling, *Fuzhou, Fujian, P.R. China*
Cheung Tak Yee, *Tsoeung Kwan O, Hong Kong*
Cimon, Loic, *Villefontaine, France*
Clark, Christopher, *Knoxville, Tennessee, USA*
Cole, Stephanie, *Bournemouth, Dorset*
Crowther, Lucy, *London*
Desile-Dejean, Celine, *Yangon, Myanmar*
Durocher, Beatrice, *Marseille, France*
Egre, Virginie, *Paris, France*
Fang Xiang, *Shanghai, P.R. China*
Feng Weiyan, *Guangzhou, Guangdong, P.R. China*

Flipo, Laurence Marie Chantal, *Antananarivo, Madagascar*
Fuchs, Alice, *Vaud, Switzerland*
Gao Yunyi, *Guangzhou, Guangdong, P.R. China*
Grezet, Antoine, *Cadillac, France*
Guo Xiaocheng, *Longyan, Fujian, P.R. China*
Hancock, Nancy, *London*
Holland, Katherine, *Liverpool, Merseyside*
Hou Fei-Feng, *Taipei City, Taiwan, R.O. China*
Hsu Yen Hsin, *Taipei City, Taiwan, R.O. China*
Huang Yue, *Nanning, Guangxi, P.R. China*
Huang Jiajun, *Guangzhou, Guangdong, P.R. China*
Huang Xudong, *Beijing, P.R. China*
Hubley, Kathleen, *Pointe-Claire, Quebec, Canada*
Indorf, Paul D., *Chester, Connecticut, USA*
Jiamanusorn, Siriwat, *Bangkok, Thailand*
Jin, Apple, *London*
Kang Xiaofeng, *Shanghai, P.R. China*
Kang Zhiyuan, *Shanghai, P.R. China*
Khinvasara, Sunil, *Monroe Township, New Jersey, USA*
Kitching, Laura, *Northampton, Northamptonshire*
Ko Chih-Li, *Taichung, Taiwan, R.O. China*
Kwok Lai Kwan, *Kowloon, Hong Kong*
Kyle, Jennifer, *Montreal, Quebec, Canada*
Lachambre, Francoise, *Frouzins, France*
Lai Ka Man, *Mayfair, London*
Lam Ching Fei, *Shatin, Hong Kong*
Lancaster, Sonya, *Sutton, Surrey*
Li Wenjie, *Guangzhou, Guangdong, P.R. China*
Li Guo Yi, *Beijing, P.R. China*
Li Chen Xi, *Beijing, P.R. China*
Li Cong, *Xi'an, Shaanxi, P.R. China*
Li Meng, *Montreal, Quebec, Canada*
Li Pingping, *Beijing, P.R. China*
Lin Yu Ping, *Taoyuan, Taiwan, R.O. China*
Lineker-Mobberley, Maryanne, *Bridgnorth, Shropshire*
Liu Bingjie, *Shanghai, P.R. China*
Liu Can, *Shanghai, P.R. China*
Lixi Qin, *Guilin, P.R. China*
Lloyd, Samantha, *Leicester, Leicestershire*
Lu Bin, *Wulumuqi, Xinjiang, P.R. China*
Lv Yijin, *Ordos City, Inner Mongolia, P.R. China*
Matthews, Kate, *Auchenblae, Aberdeenshire*
Mdamu, Harrison Lengube, *Voi, Kenya*
Minelli, Adriana, *Toronto, Ontario, Canada*
Molon, Valentina, *London*
Moorhead, Lisa, *London*
Nyambu, Emmanuel Mwazighe, *Wundanyi, Kenya*
Ootani, Wakana, *Tokyo, Japan*
Ouahed, Daniel, *Montreal, Quebec, Canada*
Ounorn, Papawarin, *Bangkok, Thailand*
Oz, Iryna, *Kiev, Ukraine*
Piccini, Angelo, *Genoa, Italy*
Qian Xiaotong, *Bole, Xinjiang, P.R. China*
Qiu Dongjun, *Heyuan, Guangdong, P.R. China*
Quan Hong, *Tongxiang, Zhejiang, P.R. China*
Raymond, Isabelle, *Saint-Hyacinthe, Quebec, Canada*
Razafindraholy, Claude Willy, *Fianarantsoa, Madagascar*
Recchi, Jean-Noel, *Marseille, France*
Renfer, Alice, *Annemasse, Haute-Savoie, France*
Rexworthy, Simon, *Market Drayton, Shropshire*
Rochambeau, David, *Montreal, Canada*
Roelofse, Frederick, *Bloemfontein, South Africa*
Rojas, Jorge, *Montreal, Quebec, Canada*
Rong Zhen, *Preston, Lancashire*
Sampson, Suzanne, *Leicester, Leicestershire*
San, Thinzar, *Yangon, Myanmar*
Schuch-des Forges, Vanessa E. M., *North Littleton, Worcestershire*
Seto, Kuriko, *Setagaya-ku, Tokyo, Japan*
Shaw, Stephanie, *Walthamstow, London*
Shen Fangqing, *Shanghai, P.R. China*
Shen Qi, *Shanghai, P.R. China*
Shen Tao, *Zhuhai, Guangdong, P.R. China*
Sheng Yumo, *Beijing, P.R. China*
Shi Tianze, *Ningbo, Zhejiang, P.R. China*
Sholo, Peter Chozi, *Wundany, Kenya*
Slootweg, Peter, *Nootdorp, Zuid-Holland, The Netherlands*
Smith, Jennifer, *Stourport-on-Severn, Worcestershire*
Song Ziyi, *Beijing, P.R. China*
Soukvila, Felix Vixay, *Bangkok, Thailand*
Stancliffe, Sarah, *London*
Su Liping, *Guangxi, Guilin, P.R. China*
Sugawara, Naoyuki, *Saitama, Japan*
Sun I-Shan, *Taichung, Taiwan, R.O. China*
Takebayashi, Maya, *Yokohama City, Kanagawa, Japan*
Tang Tse Shan, *Sai Kung, Hong Kong*
Tang Ying, *Shanghai, P.R. China*
Timms, Andrew, *Lancaster, Lancashire*
Tseng Yi Ming, *Taipei City, Taiwan, R.O. China*
Walter, Yuna, *Montreal, Quebec, Canada*
Wei Zijun, *Beijing, P.R. China*
Wong Nga Sze, *Auckland, New Zealand*
Wong Fang, *Singapore*
Wu Bin, *Guilin, Guangxi, P.R. China*
Wu Langqiong, *Beijing, P.R. China*
Xie Ting Ye, *Beijing, P.R. China*
Xin Cuihong, *Shanghai, P.R. China*
Xu Li, *Guyuan, Ningxia, P.R. China*
Yalin Zhu, *Guilin, Guangxi, P.R. China*
Yamazaki, Junichi, *Kamihei-gun, Iwate, Japan*
Yan Yuxi, *West Vancouver, British Columbia, Canada*
Yang Qiankun, *Shanghai, P.R. China*
Yang Jingwen, *Shanghai, P.R. China*
Yang Jia Sin, *Taipei City, Taiwan, R.O. China*
Yang Yizi, *Chongqing, P.R. China*
Ye Yishi, *Dongwan, Guangdong, P.R. China*
Yu Ning, *Foshan, Guangdong, P.R. China*
Zandy, Farhad, *Tehran, Iran*
Hang Ming, *Guangzhou, Guangdong, P.R. China*
Zhang Zhen Zhang, *Beijing, P.R. China*
Zhang Jia, *Guilin, Guangxi, P.R. China*
Zhang Pinglin, *Beijing, P.R. China*
Zhang Baijie, *Shanghai, P.R. China*
Zhang Meng, *Shanghai, P.R. China*

Zhang Hanlin, *Taiyuan, Shanxi, P.R. China*
Zhang Ge, *Beijing, P.R. China*
Zheng Long, *Guangzhou, Guangdong, P.R. China*
Zhong Chunyu, *Shenzhen, Guangdong, P.R. China*
Zhou Xinyi, *Guilin, Guangxi, P.R. China*
Zhu Ying, *Shanghai, P.R. China*
Zhu Chenwen, *Shenzhen, Guangdong, P.R. China*
Zuo Tenglong, *Zhengzhou, Henan, P.R. China*

Foundation Certificate in Gemmology

Qualified

Addeo-Proechel, Juanita, *Lake Mary/Heathrow, Florida, USA*
Aggarwal, Luxmi, *Ludhiana, Punjab, India*
Akira, Oomatsu, *Tokyo, Japan*
Akshay, Vibakar, *Antananarivo, Madagascar*
Arredondo, Gabriel, *Geneva, Switzerland*
Ayako, Okuda, *Tokyo, Japan*
Azad, Anfas, *Colombo, Sri Lanka*
Azusa, Taki, *Kanagawa, Japan*
Badjan de Junnemann, Johanna, *Doussard, France*
Bailey, Rachel, *Edinburgh, Midlothian*
Barrett, Andrew, *Sliema, Malta*
Beard, Thomas, *Eastbourne, East Sussex*
Beaumont, Elizabeth, *Montreal, Quebec, Canada*
Bergamin, Irene, *Zurich, Switzerland*
Bernard, Edmund, *Clanfield, Oxfordshire*
Brahmbhatt, Radha, *Northwood, Middlesex*
Brukås, Silje, *Bergen, Norway*
Buldanlioglu, Gulgun, *Istanbul, Turkey*
Bullmore, Elizabeth, *Birmingham, West Midlands*
Busuttil, Marie, *Tarbes, France*
Buxton, Conner, *Missoula, Montana, USA*
Caldicott, Gary, *Rowley Regis, West Midlands*
Canovas, Ana, *London*
Cao Ying, *Beijing, P.R. China*
Carral, Manon, *Vitrolles, France*
Carriere, Laurence, *Montreal, Quebec, Canada*
Castelino, Rennie, *San Mateo, California, USA*
Caya, Elie-Anne, *Quebec City, Quebec, Canada*
Chai Jing, *Guangzhou, Guangdong, P.R. China*
Chamberlain-Adams, Jemima, *London*
Chan Im Fan, *Ion Han, Macau*
Chan Kai Man, *Kowloon, Hong Kong*
Chan Men Fung, *Sai Wan Ho, Hong Kong*
Chan Wai Ping, *Tsuen Wan, Hong Kong*
Chang Shu-Hua, *New Taipei City, Taiwan, R.O. China*
Chang Yupin, *Taichung, Taiwan, R.O. China*
Chapoutot, Jeanne-Eglantine, *La Rochelle, France*
Charanas, Georgios, *Athens, Greece*
Chee Chi Hang, *Shatin, Hong Kong*
Chen Lu, *Shanghai, P.R. China*
Chen Wai Ching Sylvin, *Kowloon, Hong Kong*
Chen Wei, *Taoyuan, Taiwan, R.O. China*
Chen Xiaoxi, *London*
Chen Yu-Cheng, *New Taipei City, Taiwan, R.O. China*
Chen Yueh Shan, *Taipei City, Taiwan, R.O. China*
Cheng Tsoek Yan, Iris, *Sai Kung, Hong Kong*
Cheng Tzu Shan, *New Taipei City, Taiwan, R.O. China*
Cheng Wai Yin, *Mei Foo, Hong Kong*
Cheng Zhilu, *Birmingham, West Midlands*
Chiang Kai-Hsin, *New Taipei City, Taiwan, R.O. China*
Choi Ka Hei, *Tuen Mun, Hong Kong*
Choi Tsz Ling, *Kowloon, Hong Kong*
Chow Wing, *Tai Po, Hong Kong*
Chu Szu-Yin, *Taipei City, Taiwan, R.O. China*
Chui Chi Fai, *Shatin, Hong Kong*
Chung Man Hei, *Tai Po, Hong Kong*
Cimon, Loic, *Villefontaine, France*
Cornelius, Victoria, *London*
Courrance, Maxence, *Aix-en-Provence, France*
Cutler, Gary, *Bangkok, Thailand*
Dai Jun, *Kunshan, Jiangsu, P.R. China*
Davenport, Nicholas Tristan Barritt, *Hereford, Herefordshire*
Davison, Alexander, *Southend-on-Sea, Essex*
De Bourgues, Ayena, *Oron-la-Ville, Switzerland*
Deng Yihong, *Beijing, P.R. China*
Dimond, Kate, *Enfield, Middlesex*
Dong Yiyuan, *Beijing, P.R. China*
Dufour, Jean Yves, *Velaux, France*
Eaton, Alex, *Richmond, Surrey*
Elkington, Edwina, *London*
Emanuelli, Odile, *Ivry-sur-Seine, France*
Emi, Okubo, *Kanagawa, Japan*
Evans, Charlotte, *Leeds, West Yorkshire*
Fan Mingyue, *Shanghai, P.R. China*
Fan Deng, *Guilin, Guangxi, P.R. China*
Fan Hing Wan, *Kowloon, Hong Kong*
Fauquet, Richard, *Courbevoie, France*
Flipo, Laurence Marie Chantal, *Antananarivo, Madagascar*
Francey, Jacob, *Auckland, New Zealand*
Friend, Hiroko Hara, *Singapore*
Frisnes, Marte, *Bridgnorth, Shropshire,*
Fwa, Christopher, *Yola, Adamawa, Nigeria*
Gao Qi Xin, *Chifeng, Inner Mongolia, P.R. China*
Gao Siyao, *Beijing, P.R. China*
Garvey, Francesca, *Rochdale, Greater Manchester*
Gauthier, Diane, *Montreal, Quebec, Canada*
Geijsen, Lara, *Haarlem, The Netherlands*
Girardet, Marine, *Paris, France*
Girardot, Caroline, *Marseille, France*
Goots, Pauline, *Liège, Belgium*
Graczer, Richard, *Cogoleto, Italy*
Gray, Joanna, *Bishops Stortford, Essex*
Grezet, Antoine, *Cadillac, France*
Griziot, David, *Marseille, France*
Gu Li Fang, *Shanghai, P.R. China*
Gui Fu, *Guilin, Guangxi, P.R. China*
Guljé, Maxime, *Ouderkerk aan de Amstel, The Netherlands*
Haley, Mitchell, *Birmingham, West Midlands*
Han Jie, *Nanchang, Jiangxi, P.R. China*
Han Shuo, *Luoyang, Henan, P.R. China*
He Chin Ju, *Kaohsiung, Taiwan, R.O. China*

Hergott, Laurianne, *Obernai, France*
Ho Lam Ho, Ingrid, *North Point, Hong Kong*
Ho Soi I, *Chai Wan, Hong Kong*
Ho Wingyan, *Brooklyn, New York, USA*
Honda, Takuya, *Sapporo City, Hokkaido, Japan*
Hsu Yen Hsin, *Taipei City, Taiwan, R.O. China*
Huang I-Ping, *New Taipei City, Taiwan, R.O. China*
Huang Shitong, *Shanghai, P.R. China*
Huang Shiying, *Shanghai, P.R. China*
Huang Shu, *Beijing, P.R. China*
Huang Ying, *Beijing, P.R. China*
Hui Xue, *Beijing, P.R. China*
Hui Yee Mei, *Kowloon, Hong Kong*
Hung Tzu Chun, *Hsinchu City, Taiwan, R.O. China*
Hung Yu-Cheng, *Erlin Township, Taiwan, R.O. China*
Iseki, Ayako, *London*
Jackson, Katherine, *Sutton, Surrey*
Ji Ang, *Chatham, Kent*
Jiang Dong, *Beijing, P.R. China*
Jiang Haiyan, *Shanghai, P.R. China*
Jiang Xiaowen, *Shanghai, P.R. China*
Jiang Xueqin, *Shanghai, P.R. China*
Jivabhai, Anuj, *Harrow, Middlesex*
Johnson, Daniel, *Wolverhampton, West Midlands*
Johnson, Amy, *Ruddington, Nottinghamshire*
Jonas, Helen, *Stansted Mountfitchet, Essex*
Kagan, Thierry, *Neuilly-sur-Seine, France*
Kankanamge, Mahindadasa, *Nanterre, France*
Kayo, Akiyama, *Kami City, Kochi, Japan*
Keiko, Gotoh, *Tokyo, Japan*
Khaing Win Sandar, *Yangon, Myanmar*
Kotoe, Hoshino, *Tokyo, Japan*
Kuo Nai Lun, *Kaoshiung City, Taiwan, R.O. China*
Kuo Yupi, *New Taipei City, Taiwan, R.O. China*
Kyaw Ei Khine, *Yangon, Myanmar*
Lachambre, Francoise, *Frouzins, France*
Lai Hsin Han, *Kaohsiung City, Taiwan, R.O. China*
Lai Kar Wai, Maria, *North Point, Hong Kong*
Lai Shuk Yu, *Kwun Tong, Hong Kong*
Lai Yuet Ching, *Yuen Long, Hong Kong*
Lam King Chiu, *Tseung Kwan O, Hong Kong*
Lam Tai Wai, *Aberdeen, Hong Kong*
Lam Wai Chun, *Tuen Mun, Hong Kong*
Lassau, Clothilde, *Cartigny, Switzerland*
Law Kit Fung, *Tseung Kwan O, Hong Kong*
Layton, Janina, *London*
Lee Ji-Eun, *Montreal, Quebec, Canada*
Lee Ka Wo, *Kwai Chung, Hong Kong*
Lee Kun Tai, *Kaohsiung City, Taiwan, R.O. China*
Lemoine, Mathilde, *Vouziers, France*
Lescuyer, Loic, *Francheville, France*
Leung Hoi Yee, *Kowloon, Hong Kong*
Leung Kam Fai, *Yau Tong, Hong Kong*
Leung Sin Man, *Shau Kei Wan, Hong Kong*
Leung Wai Kai, Alexander, *Macau*
Lewis, Rhiannon, *Birmingham, West Midlands*
Li, Claudia, *Central, Hong Kong*
Li Kaifei, *Beijing, P.R. China*
Li Meng, *Montreal, Quebec, Canada*
Li Rong, *Beijing, P.R. China*
Li Shanshan, *Beijing, P.R. China*
Li Ting, *Beijing, P.R. China*
Li Wei Li, *Dalian, Liaoning, P.R. China*
Li Yuan, *Beijing, P.R. China*
Li Zhechen, *Beijing, P.R. China*
Li Zhenjia, *Beijing, P.R. China*
Liechti, Rupa, *Elstree, Hertfordshire,*
Lin Jia Cih, *Yunlin County, Taiwan, R.O. China*
Lin Ming, *Fuzhou, Fujian, P.R. China*
Lin Xuanxuan, *Shanghai, P.R. China*
Lin Yu-Jie, *New Taipei City, Taiwan, R.O. China*
Ling Tung-Wei, *Taipei City, Taiwan, R.O. China*
Liu Cheng Fang, *Kaosiung City, Taiwan, R.O. China*
Liu Jia Hong, *Bangkok, Thailand*
Liu Ka Lai, Athene, *Tai Wai, Hong Kong*
Liu Kaichao, *Beijing, P.R. China*
Liu Lu, *Beijing, P.R. China*
Liu Na, *Shanghai, P.R. China*
Liu Shu, *Tianjin, P.R. China*
Liu-Murphy, Vanessa, *Tividale, West Midlands*
Lixi Qin, *Guilin, Guangxi, P.R. China*
Lo Man Yi, *Chai Wan, Hong Kong*
Lo Nga Man, *Kowloon, Hong Kong*
Luan Dongqi, *Beijing, P.R. China*
Luo Jinglang, *Beijing, P.R. China*
Ma Chunao, *Beijing, P.R. China*
Ma Suk Fong, Cecilia, *Shatin, Hong Kong*
Madoka, Akimoto, *Tokyo, Japan*
Maghni, Karim Christophe, *Laval, Quebec, Canada*
Makriadis, Athanasios, *Athens, Greece*
Man Ka Yi, *Kowloon, Hong Kong*
Mari, Suzuki, *Ginowan, Okinawa, Japan*
Marzo, Jonathan, *Peseux, Switzerland*
Masini, Chiara, *Florence, Tuscany, Italy*
Mdamu, Harrison Lengube, *Voi, Kenya*
Mei, Yamashita, *Miura City, Kanagawa, Japan*
Meidong Zhu, *Guilin, Guangxi, P.R. China*
Meoni, Annabella, *Montreal, Quebec, Canada*
Michelou, Zoe, *Paris, France*
Milton, Monica, *Crossgates, Fife*
Ming Zeng, *Guilin, Guangxi, P.R. China*
Mingyue Chen, *Guilin, Guangxi, P.R. China*
Mo Yu Xin, *Taizhou, Zhejiang, P.R. China*
Mohammed, Osama Salman Taqi, *Manama, Bahrain*
Mohiyadeen Mawzoon, Abdul Razak, *Malwana, Sri Lanka*
Mooney, Suzanne, *Worcester, Worcestershire*
Moug, Rebecca, *Lightwater, Surrey*
Mowle, Holly, *Newport-on-Tay, Fife*
Nacht, Coralie, *Vich, Switzerland*
Nadal, Cynthia, *London*
Nash-Wilson, Jake, *Bristol*
Nenzen, Charlotte, *London*
Ng, Jayne, *Singapore*
Nian Bofeng, *Shanghai, P.R. China*
Niu Tianju, *London*

Noriko, Fukuda, *Tokyo, Japan*
Nyambu, Emmanuel Mwazighe, *Wundanyi, Kenya*
Nyambu, Lucy Mshai, *Taveta, Kenya*
O'Doherty, Brigid, *Belfast, Antrim*
Ouahed, Daniel, *Montreal, Quebec, Canada*
Ounorn, Papawarin, *Bangkok, Thailand*
Page, Barry, *Hove, East Sussex*
Peebles-Brown, Ludmila, *London*
Peng Chien Shen, *Taipei City, Taiwan, R.O. China*
Proler, Rose, *Houston, Texas, USA*
Pui Oi Ip, *Kowloon, Hong Kong*
Qiu Ze Hong, *Xiamen, Fujian, P.R. China*
Quan Xiaoyun, *Beijing, P.R. China*
Rabetokotany, Andrimandimby Lantomanantsoa, *Antananarivo, Madagascar*
Ramaroarivo, Jerry-Son, *Antananarivo, Madagascar*
Raniga, Jaynend, *Greenlane, Auckland, New Zealand*
Rathod, Alpa, *London*
Ratnamalala, Inoka Kumuduni, *Ja-Ela, Sri Lanka*
Raymond, Isabelle, *Saint-Hyacinthe, Quebec, Canada*
Razafindraholy, Claude Willy, *Fianarantsoa, Madagascar*
Redjem, Sihame, *Nanterre, France*
Renfer, Alice, *Annemasse, Haute-Savoie, France*
Richard, Genevieve, *Brossard, Quebec, Canada*
Rieger, Alexis, *Le Puy-en-Velay, France*
Risa, Ito, *Tokorozawa City, Saitama, Japan*
Rochambeau, David, *Montreal, Quebec, Canada*
Rojas, Jorge, *Montreal, Quebec, Canada*
Rol, Emmanuelle, *Marseille, France*
Romanenko, Roxana, *London*
Roos, Maarten, *The Netherlands*
Roux, Zongqi, *Le Pontet, France*
Roux, Edouard, *Montbrisson, France*
Ryan, Christopher, *London*
Sandison, Amanda, *Camberley, Surrey*
Sauvager, Gwénaelle, *Vence, France*
Seroussi, Claudine, *London*
Shajaie, Ahmad, *Montreal, Quebec, Canada*
Shen Tao, *Zhuhai City, Guangdong, P.R. China*
Shi Jiaqing, *Beijing, P.R. China*
Shi Shuang, *Beijing, P.R. China*
Sholo, Peter Chozi, *Kenya*
Si Cheng, *Guilin, Guangxi, P.R. China*
Simonis, Alexandra, *Maarssen, The Netherlands*
Smith, Fiona, *Hoddesdon, Hertfordshire*
Smith, Kerry-Kate, *London*
Soukvilay, Felix Vixay, *Bangkok, Thailand*
Steffens, Hounaida, *Nanterre, France*
Su Bin, *Xinyang City. Henan, P.R. China*
Su Kuo-Hao, *Yuanlin Township, Taiwan, R.O. China*
Su Yung-Han, *Taipei City, Taiwan, R.O. China*
Synnott, Suzie, *Outremont, Canada*
Sze Ching Man Suki, *Shatin, Hong Kong*
Tabak, Simon, *London*
Tang Chung Fu, *Kowloon, Hong Kong*
Tang Kit Yui Jo Jo, *Shatin, Hong Kong*
Testill, Emma, *Cannock, Staffordshire*
Timanova, Desislava, *Sofia, Bulgaria*
Tong Hoi Yum, Louise, *Kowloon, Hong Kong*
Tonkin, Jennifer, *Croydon, Surrey*
Toque, Nathalie, *Montreal, Quebec, Canada*
Tsai Ya Ni, *New Taipei City, Taiwan, R.O. China*
Turkman, Claudine, *Montreal, Quebec, Canada*
Valyraki, Athina, *Glyfada, Greece*
Van Der Wouden-Kuling, Elisabeth Margriet, *Doha, Qatar*
Viguier, Murielle, *Massy, France*
Wachsmann, Elliott, *London*
Wakayo, Tsukui, *Tokyo, Japan*
Walter, Yuna, *Montreal, Quebec, Canada*
Wang Dan, *Beijing, P.R. China*
Wang Hsiao Ling, *Taipei City, Taiwan, R.O. China*
Wang Juan, *Shanghai, P.R. China*
Wang Ling, *Shantou City. Guangdong, P.R. China*
Wang Yiying, *Beijing, P.R. China*
Wang Yu Qi, *Guiyang, Guizhou, P.R. China*
Wang Yujue, *London*
Wei Tian Min, *Nanjing, Jiangsu, P.R. China*
Welch, Trevor, *Enfield, Middlesex*
Wen Yan Ting, *Xian, Shaanxi, P.R. China*
Weng Chunyan, *Beijing, P.R. China*
Weng Ruizhi, *Beijing, P.R. China*
Westmoreland, Samantha, *Burntwood, Staffordshire*
Wong Chak Yan, Bryan, *Kowloon, Hong Kong*
Wong Hiu Moon, *Kowloon, Hong Kong*
Wong Pak Leung, *Tseung Kwan O, Hong Kong*
Wong Tik, *Kwai Chung, Hong Kong*
Wong Yuk Kwo, *North Point, Hong Kong*
Woodfine, Jennifer, *Montreal, Quebec, Canada*
Wu Chia Jung, *Kaohsiung City, Taiwan, R.O. China*
Wu Oi Lam, *Kwai Chung, Hong Kong*
Wu Xuxu, *Beijing, P.R. China*
Wu Yong, *Hangzhou City, Zhejiang, P.R. China*
Xiaorong Jiang, *Guilin, Guangxi, P.R. China*
Xie Danhong, *Enfield, Middlesex*
Xin Wen, *Beijing, P.R. China*
Xu Jian Mei, *Shenzhen, Guangdong, P.R. China*
Xu Qinzi, *Beijing, P.R. China*
Xu Sijia, *London*
Xue Jie, *Ma On Shan, Hong Kong*
Yalin Zhu, *Guilin, Guangxi, P.R. China*
Yan Juan, *Xiamen City, Fujian, P.R. China*
Yan Meng, *Vaughan, Ontario, Canada*
Yan Yan, *Guilin, Guangxi, P.R. China*
Yan Yuxi, *West Vancouver, British Columbia, Canada*
Yanan Fan, *Colombo, Sri Lanka*
Yang Bai, *Colombo, Sri Lanka*
Yang Chen-Yu, *Taipei City, Taiwan, R.O. China*
Yang Dong Wen, *Kowloon, Hong Kong*
Yang Hsiao-Chu, *Taipei City, Taiwan, R.O. China*
Yang Su Fan, *New Taipei City, Taiwan, R.O. China*
Yang Xiao, *Beijing, P.R. China*
Yang Xue-Chang, *New Taipei City, Taiwan, R.O. China*
Yang Yang, *Guilin, Guangxi, P.R. China*
Yang Yong, *Ningbo, Zhejiang, P.R. China*
Yang Yuling, *Beijing, P.R. China*

Ye Run Ling, *Shenzhen, Guangdong, P.R. China*
Ye Shan, *Shanghai, P.R. China*
Yeung Ka Ling, Sophia, *Kennedy Town, Hong Kong*
Yi Nannan, *Beijing, P.R. China*
Yiying Su, *Guilin, Guangxi, P.R. China*
Yong Chenying, *Beijing, P.R. China*
Yoong, Rachel, *Birmingham, West Midlands*
Yoshiaki, Uchida, *Tokyo, Japan*
Yu Hsien-Lung, *New Taipei City, Taiwan, R.O. China*
Yu Menglin, *London*
Yuan Rui Feng, *Shenzhen, Guangdong, P.R. China*
Zerhouni, Yousra, *Montreal, Quebec, Canada*
Zhai Mengqi, *Beijing, P.R. China*
Zhang Lei, *Beijing, P.R. China*
Zhang Lingjie, *Beijing, P.R. China*
Zhang Menglin, *Beijing, P.R. China*
Zhang Nan, *London*
Zhang Peng, *Shanghai, P.R. China*
Zhang Shengdi, *Guangzhou, Guangdong, P.R. China*
Zhang Ting, *Montreal, Quebec, Canada*
Zhang Xiao, *Shanghai, P.R. China*
Zhang Xiaole, *Solihull, West Midlands*
Zhang Yan, *Shanghai, P.R. China*
Zhang Yang, *Shenzhen, Guangdong, P.R. China*
Zhang Yiwen, *Beijing, P.R. China*
Zhao Yi, *Beijing, P.R. China*
Zhao Zhiyang, *Shanghai, P.R. China*
Zhen Wang, *Guilin, Guangxi, P.R. China*
Zheng Bingyu, *Beijing, P.R. China*
Zhong Hua, Anna, *Tsuen Wan, Hong Kong*
Zhou Ziwei, *Beijing, P.R. China*
Zhu Xiaofei, *Shanghai, P.R. China*
Zhu Yuenan, *Hangzhou City, Zhejiang, P.R. China*
Zirogiannis, Athanasios, *Athens, Greece*
Zisis, Vasilis, *Marousi, Greece*
Zou Ran, *Beijing, P.R. China*

Diamond Diploma Examination

Qualified with Distinction

Dixon, Emily, *London*
Harris, Natalie, *Merstham, Surrey*
Hillcoat, Cathryn, *St. Albans, Hertfordshire*
Khinvasara, Sunil, *Monroe Township, New Jersey, USA*
Marek, Genia, *Putney, London*
Marshall, Angela, *Cambridge, Cambridgeshire*
Pei Yu, *Beijing, P.R. China*
Simonsson, Kim, *Stockholm, Sweden*
Von Allmen, Andrea, *Münsingen, Switzerland*

Qualified with Merit

Arioli, Elena, *London*
Backhouse, Theodora, *Battersea, London*
Bevans-Royston, Aston, *Billericay, Essex*
Hrustic, Ibrahim, *Marieholm, Sweden*
Li Man Kit, *Shatin, Hong Kong*
Liu Huan, *Beijing, P.R. China*
Lumb, Sarah, *London*
Soon, Alexis, *London*

Qualified

An Meilan, *Beijing, P.R. China*
Cai Jing, *North Point, Hong Kong*
Chan Lai Ping, *Tai Po, Hong Kong*
Chan Chi Fung, *Tai Po, Hong Kong*
Chen Xiaoxi, *Brockley, London*
Cheung Ka Yan, Michiele, *Sai Kung, Hong Kong*
Chiu Ying Ying, *Tseung Kwan O, Hong Kong*
Chow Yee Man, *Shatin, Hong Kong*
Coppin, Daisy, *Corsham, Wiltshire*
Doyle, Helen, *London*
Du Yu, *Beijing, P.R. China*
Duan Wei Ju, *Chai Wan, Hong Kong*
Fan Sze Man, Ellie, *North Point, Hong Kong*
Fu Qidi, *Beijing, P.R. China*
Fung Yan Yan, *Yuen Long, Hong Kong*
Hao Yun, *Beijing, P.R. China*
Harper, Kate, *Edgbaston, West Midlands*
Jones, Oliver, *Bern, Switzerland*
Kübler-Tesch, Joachim, *Ludwigsburg, Germany*
Lai Kar Wai, Maria, *North Point, Hong Kong*
Lam Ching Wa, *Kowloon, Hong Kong*
Landmann, Juliana, *London*
Lansley, Juliette Elizabeth, *Heathfield, East Sussex*
Lau King Yiu, *Tuen Mun, Hong Kong*
Lee Hao Wen, *Tuen Mun, Hong Kong*
Leung Po Wa, *Ma On Shan, Hong Kong*
Li Jiahao, *Shantou, Guangdong, P.R. China*
Li Cheuk Lam, *Shau Kei Wan, Hong Kong*
Liu Tong, *Beijing, P.R. China*
Liu Zijing, *Beijing, P.R. China*
Ng Nga Chi, *Kowloon, Hong Kong*
Ng Koon Hang, *Kowloon, Hong Kong*
Scully, Kerryanne, *Birmingham, West Midlands*
Slingsby, Hazel, *Old Coulsdon, Surrey*
Spicer, Gregory, *Hove, East Sussex*
Stenlund, Emelie Maria Christina, *Strangnas, Sweden*
Tang Chung Fu, *Kowloon, Hong Kong*
Tang Kit Shan, *Kowloon, Hong Kong*
Thung Chi Ming, Herbert, *Kowloon, Hong Kong*
Tsang Shek Fai Tsang, *Kwai Fong, Hong Kong*
Tse Chi Kuen, *North Point, Hong Kong*
Valentini-Orme, Francesca, *Wandsworth, London*
Wong Yee Wai, *Yuen Long, Hong Kong*
Wong Nga Sze, Jennifer, *Fotan, Hong Kong*
Woods, Edward, *Hungerford, Berkshire*
Xiao Mingqi, *Beijing, P.R. China*
Xiao Qiyun, *Beijing, P.R. China*
Yeung Chuek Yan, *Kowloon, Hong Kong*
Yeung Chi Nang, *Lam Tin, Hong Kong*

OBITUARIES

Pierre Vuillet á Ciles

Pierre Vuillet á Ciles FGA of Villards d'Heria, France, died on 2 November 2014.

Pierre was born in 1957 in Jura, France and studied in Belfort and Dijon before becoming an engineer working for leading oil and gas companies.

Pierre became interested in gemstones after trips to South America and decided to study gemmology. He qualified in the Gemmology Diploma examination in 1993, gaining the Anderson Bank Prize.

Having taken Spanish lessons in Salamanca, Pierre travelled extensively in Colombia where he managed to establish contacts and develop an emerald business between Colombia and Europe. Always keen to develop new markets, he explored the natural pearl sector, specializing in conch pearls. Meanwhile he played an important role in Gem-A's course development when he discussed various gem education topics in great detail.

He continued to travel extensively, particularly to Asia where the emerging new markets led him.

Pierre was a brilliant mind and willingly shared his impressive knowledge. He will be sorely missed.

Denis M. Gravier

Felix Sydney Cobden FGA (D.1970), Ramat Gan, Israel, died on 22 July 2014.

Monika Grafin Von Francken Sierstorpff FGA (D.1985), Cologne, Germany, died unexpectedly on 28 August 2014.

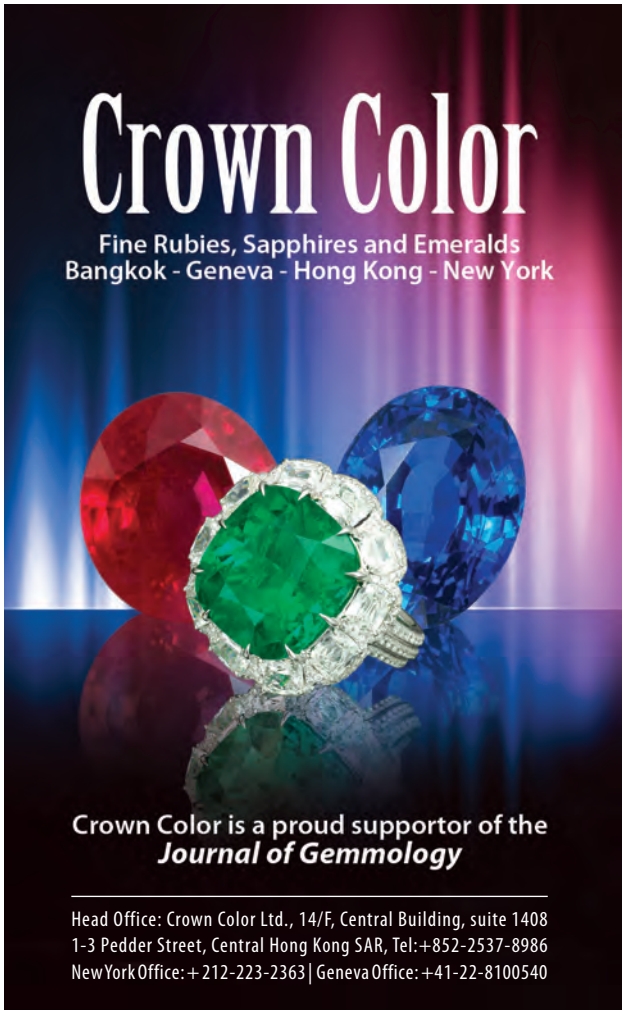

FOR THE FIRST TIME
IN SOUTH AMERICA

cibjo

CONGRESS 2015

SALVADOR - BAHIA
BRAZIL

4-6 MAY 2015

www.cibjo.org

Learning Opportunities

CONFERENCES AND SEMINARS

NAJA 43rd ACE IT Annual Winter Education Conference
1–2 February 2015
Tucson, Arizona, USA
http://najaappraisers.com/html/conferences.html

AGTA GemFair Tucson 2015
3–8 February 2015
Tucson, Arizona, USA
www.agta.org/tradeshows/gft-seminars.html
Note: Gem-A will be exhibiting at booth 29.

AGA Tucson Conference
4 February 2015
Tucson, Arizona, USA
www.accreditedgemologists.org/currevent.php

2015 Tucson Gem and Mineral Show
12–15 February 2015
Tucson, Arizona, USA
www.tgms.org/show-2015
Notes: (1) Lectures and seminars will follow the show theme 'Minerals of Western Europe'.
(2) Gem-A will be exhibiting for the first time at this show: visit booth 1928–1929.

National Council of Jewellery Valuers Conference
15-21 April 2015
Sydney, Australia
www.ncjv.com.au

Mallorca GemQuest Gemmological Conference
18–20 April 2015
Can Pastilla, Mallorca, Spain
www.mallorcagemquest.com

Swiss Gemmological Society Conference
19-21 April 2015
Meisterschwanden, Switzerland
www.gemmologie.ch

AGS International Conclave
22–25 April 2015
New Orleans, Louisiana, USA
www.americangemsociety.org/conclave-2015

Scottish Gemmological Association Annual Conference
1–4 May 2015
Peebles, Scotland
www.scotgem.co.uk/SGAConference2015

Compiled by Georgina Brown and Brendan Laurs

Association for the Study of Jewelry and Related Arts 10th Annual Conference
2–3 May 2015
Chicago, Illinois, USA
www.asjra.net/event.html

CIBJO Congress 2015
4–6 May 2015
Salvador, Brazil
http://tinyurl.com/n8f9utk

3rd Annual New England Mineral Conference
8–10 May 2015
Newry, Maine, USA
www.nemineralconference.org

ICA Congress
16–19 May 2015
Colombo, Sri Lanka
http://congress.gemstone.org

The Santa Fe Symposium
17–20 May 2015
Albuquerque, New Mexico, USA
www.santafesymposium.org

Society of North American Goldsmiths' 44th Annual Conference
20–23 May 2015
Boston, Massachusetts, USA
www.snagmetalsmith.org/conferences/impact-looking-back-forging-forward

9th International Conference on New Diamond and Nano Carbons
24–28 May 2015
Shizuoka, Japan
www.ndnc2015.org

PEG 2015: 7th International Symposium on Granitic Pegmatites
17–21 June 2015
Lover Silesia, Poland
www.peg2015polandczech.us.edu.pl

Sainte-Marie-Aux-Mines Mineral and Gem Show
25–28 June 2015
Sainte-Marie-Aux-Mines, France
www.sainte-marie-mineral.com
Note: Lectures, workshops and gem/mineral-related films will be offered during the show.

1st Mediterranean Gemmological and Jewellery Conference
27–28 June 2015
Athens, Greece
http://cglworld.ca/education

Jewelry Camp 2015: Antique Jewelry & Art Conference
30–31 July 2015
West Harrison, New York, USA
www.jewelrycamp.org

12th International Congress for Applied Mineralogy
10–12 August 2015
Istanbul, Turkey
http://icam2015.org

Northwest Jewelry Conference 2015
14–16 August 2015
Bellevue, Washington, USA
www.nwgem.com

2015 Dallas Mineral Collecting Symposium
21–22 August 2015
Dallas, Texas, USA
www.dallassymposium.org/2015-symposium

SGA 2015: 13th Biennial Meeting of the Society of Geology Applied to Mineral Deposits
24–27 August 2015
Nancy, France
http://sga2015.blog.univ-lorraine.fr
Session of interest: Gems and Industrial Minerals

26th International Conference on Diamond and Carbon Materials
6–10 September 2015
Bad Homburg, Germany
www.diamond-conference.elsevier.com

5th European Conference on Crystal Growth
9–11 September 2015
Bologna, Italy
www.eccg5.eu

Denver Gem & Mineral Show
18–20 September 2015
Denver, Colorado, USA
www.denvermineralshow.com
Note: Lectures and seminars will follow the show theme 'Minerals of the American Southwest'.

Canadian Gemmological Association Gem Conference 2015
16–18 October
Vancouver, British Columbia, Canada
www.gemconference2015.com

EXHIBITS

Europe

Daily Life—Luxury—Protection. Jewellery in Ancient Egypt
Until 25 January 2015
Neues Museum, Berlin, Germany
www.smb.museum/en/museums-and-institutions/neues-museum/exhibitions

The Treasures of the Fondazione Bucellati
Until 22 February 2015
Museo degli Argenti, Florence, Italy
www.polomuseale.firenze.it/mostre/mostra.php?t=547de14a29644508130000b9

With their Heads Held High—Headgear from All Over the World
Until 8 February 2015
Schmuckmuseum, Pforzheim, Germany
http://klimt02.net/institutions/museums/pforzheim-jewellery-museum-2014

Anton Cepka—Kinetic Jewellery
14 March – 7 June 2015
Pinakothek der Moderne, Munich, Germany
www.pinakothek.de/kalender/2015-03-14/49068/anton-cepka-kinetischer-schmuck

Gold of the Gods from Java
Until 6 April 2015
Wereldmuseum, Rotterdam, Netherlands
www.wereldmuseum.nl/en/tentoonstellingen/goud-der-goden.html

An Adaptable Trade: The Jewellery Quarter at War
Until 27 June 2015
Museum of the Jewellery Quarter, Birmingham
www.birminghammuseums.org.uk/jewellery/whats-on/an-adaptable-trade-the-jewellery-quarter-at-war

Middle East

Urartian Jewellery Collection
Until 31 July 2015
Rezan Has Museum, Istanbul, Turkey
www.rhm.org.tr/en/event/rezan-has-museum-urartian-jewellery-collection

North America

Treasures from India: Jewels from the Al-Thani Collection
Until 25 January 2015
Metropolitan Museum of Art, New York, New York, USA
http://tinyurl.com/kw3qafs

Maker & Muse: Women and Early Twentieth Century Art Jewelry
14 February 2015 – 1 January 2016
The Richard H. Driehaus Museum, Chicago, Illinois, USA
www.driehausmuseum.org/maker-and-muse

Colors of the Universe: Chinese Hardstone Carvings
Until 8 March 2015
Metropolitan Museum of Art, New York, New York, USA
www.metmuseum.org/exhibitions/listings/2013/chinese-carving

Hollywood Glamour: Fashion and Jewelry from the Silver Screen
Until 8 March 2015
Museum of Fine Arts, Boston, Massachusetts, USA
www.mfa.org/exhibitions/hollywood-glamour

Brilliant: Cartier in the 20th Century
Until 15 March 2015
Denver Art Museum, Colorado, USA
www.denverartmuseum.org/exhibitions/brilliant-cartier-20th-century

The Greeks – Agamemnon to Alexander the Great
Until 26 April 2015
Montréal Museum of Archaeology and History, Old Montréal, Québec, Canada
www.pacmusee.qc.ca/en/exhibitions/the-greeks-agamemnon-to-alexander-the-great

Ancient Luxury and the Roman Silver Treasure from Berthouville
Until 17 August 2015
The Getty Villa, Pacific Palisades, California, USA
www.getty.edu/art/exhibitions/ancient_luxury

Glittering World: Navajo Jewelry of the Yazzie Family
Until 10 January 2016
National Museum of the American Indian, New York, New York, USA
http://nmai.si.edu/explore/exhibitions/item/?id=890

Gold and the Gods: Jewels of Ancient Nubia
Until 14 May 2017
Museum of Fine Arts, Boston, Massachusetts, USA
www.mfa.org/exhibitions/gold-and-gods

Bulgari: 130 Years of Masterpieces
On display (closing date to be determined)
Houston Museum of Natural Science, Texas, USA
www.hmns.org/index.php?option=com_content&view=article&id=687&Itemid=722

City of Silver and Gold: From Tiffany to Cartier
On display (closing date to be determined)
Newark Museum, New Jersey, USA
www.newarkmuseum.org/SilverAndGold.html

Fabergé: From a Snowflake to an Iceberg
On display (closing date to be determined)
Houston Museum of Natural Science, Texas, USA
www.hmns.org/index.php?option=com_content&view=article&id=594&Itemid=621

Gemstone Carvings: Crystals Transformed Through Vision & Skill
On display (closing date to be determined)
Houston Museum of Natural Science, Houston, Texas, USA
www.hmns.org/index.php?option=com_content&view=article&id=481&Itemid=502

Australia and New Zealand

Fine Possession: Jewellery & Identity
Until 20 September 2015
Powerhouse Museum, Sydney, Australia
www.powerhousemuseum.com/exhibitions/jewellery

OTHER EDUCATIONAL OPPORTUNITIES

Gem-A Workshops and Courses
Gem-A, London
www.gem-a.com/education/course-prices-and-dates.aspx

Gem-A Trip to Idar-Oberstein
13–20 June 2015
Idar-Oberstein, Germany
www.gem-a.com/news--events/events/idar-oberstein-2015.aspx

Montreal School of Gemmology Gem and Jewellery Appraisal Course
6–29 July 2015 (in English and French)
Montreal, Quebec, Canada
www.ecoledegemmologie.com/en/c/10

Gemstone Safari to Tanzania
13–30 July 2015
Arusha, Merelani and Lake Manyara, Tanzania
www.free-form.ch/tanzania/gemstonesafari.html

New Media

Crystal Mountains

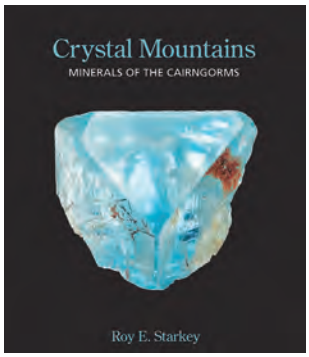

Roy Starkey, 2014. British Mineralogy Publications, Worcestershire, 184 pages, illus., softcover, ISBN 978-0993018213, http://britishmineralogy.com. £25.00.

In this book, the reader is drawn into the granite heights of the Cairngorm Mountains which, rising to over 4,000 feet (1,220 m), host an array of fine crystals and gems. Prominent from this treasure house are the smoky quartz specimens that have traded as 'cairngorm' for some 300 years. The author distinguishes the 1,245 m Cairn Gorm (*blue mountain* in Gaelic) as part of this mountainous terrain known as 'The Cairngorms'.

The area's gems and minerals and their historical background have been assiduously researched by Starkey, and the 184 pages make for an enjoyable journey, without the physical strains the author endured over the years in exploring this wilderness in all types of weather. The reader is treated to some natural history along the way, with mention of the birds (i.e. ptarmigan, capercaillie, dotterel and golden eagle) and red deer that live there.

Starkey has tracked down the earliest reports on the area, such as one from novelist and poet James Hogg who, before Queen Victoria's active interest in the area and its gems, describes "the fields trenched on the height in search of 'Cairngorm Topazes'". The first mention of this famous locality appeared in a jeweller's advertisement in 1769, in the *Aberdeen Journal*, which listed among various gems for sale 'Scots Topazes' and 'Cairngorum seals'.

Topaz continues to be collected from the area, and a 62 g blue crystal is featured on the book's cover (and another one is shown in the book that weighs 164 g). Sadly these are overshadowed today by the tons of blue topaz that occupy the jewellery world's window spaces without a mention of their treated colour.

The reader is further regaled with photos of green and yellow beryls from the region, as well as blue aquamarines. An array of other finds are recorded that extend the gemmological content.

Many Cairngorm gem discoveries came to light in Victorian times, encouraged by the interest of the Queen and her inquisitive consort Albert in all things scientific—a hallmark of the age. The interest intensified after the royal couple's purchase of Balmoral Castle, their Scottish home in the foothills of the Cairngorms. An emerging study of minerals was led by Prof. Matthew Forster Heddle, the defining figure of Scottish mineralogy. This was also the age of Sir David Brewster's discoveries in optics and his enquiries into the multi-phase fluid inclusions in Cairngorm's gems.

The book is overflowing with photos of this alpine massif, deeply scarred by glaciers, which have laid bare the scenery and its mineral delights. Numerous images show gemmy crystal specimens, faceted gems and jewellery, and may tempt the reader to pack a rucksack and head for this Scottish El Dorado. The author achieves a good balance between all the facts assembled and a narrative that takes the reader comfortably to these less accessible parts of Scotland.

The entire area is now the Cairngorms National Park and a Site of Special Scientific Interest with its surrounding remnants of the great Caledonian Forest. All must be treated with respect, and approval to collect gems and minerals should first be sought from landowners or relevant authorities.

Alan Hodgkinson

The Eduard Josef Gübelin Story: The Art and Science of Gems

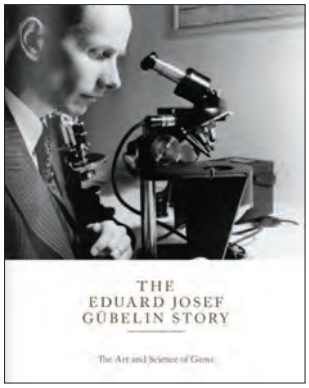

The Gübelin Foundation, 2014. Gübelin Group, Lucerne, and Unicorn Press, London, 306 pages, illus., hardcover, ISBN 978-1910065402, www.guebelin.ch/gemfairhk. £40.00.

"Used to be an Experience meant making you a bit older. This one makes you wider."

– Liner notes to 'Are You Experienced', Jimi Hendrix Experience, 1967

Eduard Gübelin needs little introduction. Arguably the most influential gemmologist of the 20th century, his work spans the transition of the field from 'tradecraft' to a forensic science. But it is actually so much more, as the current book details.

The son of a Swiss watchmaking family, he developed a keen interest in stones at an early age; this was to blossom into a passion for precious stones as

his family's business branched into jewellery. His early scholarly interests were in languages and poetry, but the family eventually steered him towards mineralogy as it was thought this would be more useful in the business. These twin interests in the humanities, fused to exacting science, would give birth to some of the greatest gemmological works in history.

Published 101 years after his birth, *The Eduard Josef Gübelin Story* is a richly illustrated document of this man's amazing life. It is filled with photographs of Gübelin on his various adventures in Burma and Sri Lanka, as well as selections from his vast correspondence, and anecdotes from relatives and colleagues. As such it is a history of gemmology itself and deserves a place on the shelves of anyone wishing to understand the development of the field. It is also studded with photos of his lab and family, which paint a full and personal picture of the man.

The book is divided into logical sections, beginning with the family history. It then continues with Gübelin's early life, his career and accomplishments, with a generous portion devoted to his travels. Completing it is a massive bibliography of Eduard Gübelin's published works and a shorter section on his awards.

This volume is printed on heavy paper and, unlike the *Photoatlas* series, is well bound. An earlier edition (*Enduring Values: In Celebration of Eduard Joseph Gübelin*) appeared briefly in 2013, but had a number of shortcomings. These have been corrected, resulting in a much more professional production. In addition to English, the book is also available in German and Mandarin.

I will close this review with a personal story. When I began my gemmological studies in 1979, a youthful Santpal Singh invited me up to his personal laboratory in Bangkok. I noticed a number of books on gemmology and asked which was his favourite. Without hesitation, he pulled one off the shelf and said: "This." It was Eduard Gübelin's 1973 masterpiece, *Internal World of Gemstones*. Peeking inside, I felt like Harry Potter transported through a brick wall at King's Cross station to a magical world on the other side. This was a work that not only changed my life, but that of virtually all gemmologists who have followed.

In every field, on rare occasions there appears someone with the vision to allow us to see with new eyes. Be it the prose of Morrissey or the guitar of Jimi Hendrix, once heard, nothing is the same. Eduard Gübelin did not simply pass along his experience. He made us wider. We are all better for it.

R. W. Hughes

Gemstones in Victoria

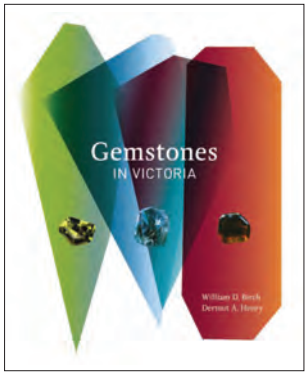

William D. Birch and Dermot A. Henry, 2013. Museum Victoria, Carlton, Victoria, Australia, 232 pages, illus., softcover, ISBN 978-1921833069, http://museumvictoria.com.au/shop. AUS$29.95.

This compilation of gemstone riches from Australia's Victoria State is dedicated to Reverend John Bleasdale (1822–1884), a priest, chemist, mineralogist and former president of the Royal Society of Victoria, who stated in 1868, "…as yet no one country on the broad earth has yielded such an assemblage of varieties of rare and precious gemstones as Victoria".

Following a historic account of gem discoveries in Victoria, the authors launch into specific chapters covering: diamond; sapphire, ruby and zircon; olivine and anorthoclase; topaz, tourmaline and beryl; garnet; quartz; chalcedony and opal; and other gem materials (including banded calcite-ankerite, cassiterite, corundum, chrysoberyl, dumortierite, moonstone, 'selwynite' and turquoise), and round-off each with a brief description of important localities in other Australian states. Each chapter is colour coded to compliment the principal colour of those gemstones, and for easy 'thumbing in' to that section of the book. The chapters each begin with a bold title page and, where available, a historical quotation from the Rev. Bleasdale. For example, on the title page for 'Topaz, Tourmaline & Beryl', he boldly states: "I may venture to say that there is not in the world a stone fit for brooches, of size and fire, and lustre, and suited to both day and candlelight, equal to some of the blue topazes which I have known to be found in Victoria."

The gem photography in the book, credited largely to Museum Victoria staff, is superb both in clarity and detail. The gems are individually photographed or painstakingly arrayed in cascades of colour—loose crystals, fine matrix specimens, or beautiful faceted and polished examples. Each page is adorned with these images plus supporting colour geological locality maps. The layout gives the feel of a fine arts book with strong emphasis placed on its visual presentation; the photos and maps are of ample size, are highlighted by generous white page borders, and are offset by minimal supporting text (printed in a non-distracting neutral grey colour and small font size). The only negative aspect to this presentation, however, was that I found the text somewhat difficult to read under low lighting conditions.

The book is painstakingly comprehensive in its coverage of various Victorian historical occurrences and fossicking localities. To test this, I jumped straight into the 'Sapphires, Rubies & Zircons' chapter, searching under the heading 'Mornington Peninsula and Western Port' for one of my favourite childhood hunting grounds—and there it was, Point Leo, where sapphires and zircons are found 'in a layer about 1 m below the beach' and in 'the matrix of pebble conglomerates at the high-tide level on the beach, and on the rock platform of the point itself'. Following that, I searched the 'Olivine & Anorthoclase' chapter for another favourite, Mt Leura, a 'volcanic complex on the eastern outskirts of Camperdown' where olivine nodules (lherzolite xenoliths) literally fall out at your feet from the walls of the 'scoria and tuff quarries on the northern edge of the volcano'.

Gemstones in Victoria concludes with reference, resource and index sections, conveniently divided into Victorian and other Australian states, as well as a general index, glossary of terms, mineral property data and acknowledgements.

Gemstones in Victoria has been a significant part of the authors' lives for close to two decades now, and no two people could be more fitting to produce such a work than William Birch and Dermott Henry. Birch is curator of minerals, and Henry is manager of the Natural Sciences collections, at Museum Victoria. Both men have worked at the Museum for decades and are avid field collectors of rocks and minerals. They have both spoken to me about countless hours spent on the meticulous collection of gem locality data from museum records, company reports, gem and lapidary club journals and word-of-mouth from prospectors, followed by personal verification of these localities though field visits. This extensive research culminated in the publication of the first edition of *Gemstones in Victoria* in 1997 which, as testimony to its popularity, had completely sold out by 2009, leading Museum Victoria to commission this thoroughly updated second edition.

The publication has been printed in softcover to keep it affordable; however I am pleased to note that a limited run of a hardcover edition was produced and will be considered for future printings depending on demand. The book can be purchased via the internet from Booktopia, Angus & Robertson and CSIRO Publishing, and is available in the Museum Victoria bookshop.

Dr Robert R. Coenraads

Reply to a Review

In response to Jaroslav Hyršl's review of my book *Wonders within Gemstones II* (*Journal of Gemmology*, 2014, **34**(3), 271), I would like to point out a few corrections:

- Regarding the 'silica outcrop' in moldavite on p. 11 of my book, lechatelierite is another word for silica glass. However, I deliberately used the simpler term 'silica outcrop'.
- I have often seen whitish rutile needles in quartz, so why assume the needles shown on p. 54 are tourmaline?
- At least two of the inclusions in the topaz specimen on p. 38 contained several daughter crystals and are indeed multi-phase.

Anthony de Goutière GG, CG
Victoria, British Columbia, Canada
http://anthonydegoutiere.com/the-book

OTHER BOOK TITLES*

Coloured Stones

Jadeite: Identification & Price Guide, 4th edn.

This book should not have been listed since it deals with glassware and not jadeite gem material.

Rhodochrosite: Crystals of Drama and Nuance
By William S. Logan, 2013. Self-published by Spectrum Minerals, Charlotte, North Carolina, USA, 159 pages. US$78 hardcover, $55 softcover or $10 eBook.

* Compiled by Georgina Brown and Brendan Laurs

Diamond

Beyond the Four C's: What You Should REALLY Know Before You Buy a Diamond
By Joshua Fishman, 2014. CreateSpace Independent Publishing Platform, 138 pages, ISBN 978-1497509962. US$9.39 softcover or $4.29 eBook.

Novel Aspects of Diamond: From Growth to Applications
Ed. by Nianjun Yang, 2014. Springer, Heidelberg, Germany, Topics in Applied Physics 121, 292 pages, ISBN 978-3319098333. US$199.00 hardcover.

Organic Gems

***Pearls of Creation: A-Z of Pearls,* 2nd edn.**
By Marjorie M. Dawson, 2014. Self-published, 332 pages, ISBN 978-0615477640. £22.50 softcover.

Gem Localities

***The Collector's Guide to Herkimer Diamonds* [New York, USA]**
By Michael R. Walter, 2014. Schiffer Publishing Ltd., Atglen, Pennsylvania, USA, 96 pages, ISBN 978-0764347108. US$19.99 softcover.

***Gemstones and Minerals of Australia,* updated edn.**
By Lin and Gayle Sutherland, 2014. New Holland, Chatswood, New South Wales, Australia, 144 pages, ISBN 978-1921517297. AUS$24.95 softcover.

Mineral Treasures of the Ozarks
By Bruce L. Stinchcomb, 2014. Schiffer Publishing Ltd., Atglen, Pennsylvania, USA, 160 pages, ISBN 978-0764347153. $29.99 softcover.

General Reference

Comprehensive Hard Materials
Ed. by Vinod K. Sarin, 2014. Elsevier, Oxford, 1,806 pages, ISBN 978-0080965284. £785.00 hardcover.

***The Retail Jeweller's Guide,* 7th revised edn.**
By Kenneth Blakemore and Eddie Stanley, 2014. N.A.G. Press, London, 336 pages, ISBN 978-0719800436. £32.00 softcover.

Rocks and Minerals—A Photographic Field Guide
By Chris and Helen Pellant, 2014. Bloomsbury, London, 192 pages, ISBN 978-1472909930. £12.99 softcover or £9.43 eBook.

Jewellery and *Objets d'Art*

Answers to Questions about Old Jewelry, 1840–1950: Identification and Value Guide
By C. Jeanenne Bell, 2014. Krause Publications, New York, New York, USA, 400 pages, ISBN 978-1440240188. US$32.99 softcover.

Art Jewelry Today: Europe
By Catherine Mallette, 2014. Schiffer Publishing, Atglen, Pennsylvania, USA, 256 pages, ISBN 978-0764346781. US$50.00 hardcover.

The Berthouville Silver Treasure and Roman Luxury
Ed. by Kenneth Lapatin, 2014. J. Paul Getty Museum, Los Angeles, California, USA, 224 pages, ISBN 978-1606064207. US$50.00 hardcover.

Bright Lights in the Dark Ages: The Thaw Collection of Early Medieval Ornaments
By Noel Adams, 2014. D Giles Ltd., London, 408 pages, ISBN 978-1907804250. £65.00 hardcover.

Cartier in the 20th Century
By Margaret Young-Sánchez, 2014. Thames and Hudson, London, England, 272 pages, ISBN 978-0500517673. £45 hardcover.

Contemporary Jewelry Design
By Li Puman and Liu Xiao, 2014. CYPI Press, Harrow, 208 pages, ISBN 978-1908175489. £12.26 softcover.

Cosmic Debris: Meteorites and Jewellery Objects by Reinhold Ziegler
By Halvor Nordby and André Gali, 2014. Arnoldsche Art Publishers, Stuttgart, Germany, 80 pages, ISBN 978-3897904057. £20.00 hardcover.

Glittering World: Navajo Jewelry of the Yazzie Family
Ed. by Lois Sherr Dubin, 2014. Smithsonian Books, Washington D.C., USA, 252 pages, ISBN 978-1588344779. US$50.00 hardcover.

Floral Jewels: From the World's Leading Designers
By Carol Woolton, 2014. Prestel Publishing, New York, New York, USA, 176 pages, ISBN 978-3791381145. US$55.00 hardcover.

Heavenly Bodies: Cult Treasures and Spectacular Saints from the Catacombs
By Paul Koudounaris, 2013. Thames and Hudson Ltd., London, 192 pages, ISBN 978-0500251959. £18.95 hardcover.

A History of Contemporary Jewellery in Australia and New Zealand: Place and Adornment
By Damian Skinner and Kevin Murray, 2014. University of Hawaii Press, Honolulu, USA, 248 pages, ISBN 978-0824846879. US$50.00 hardcover.

Hopi Gold, Hopi Silver: 12 Contemporary Jewelers
By Zena Pearlstone, 2014. Schiffer Publishing, Atglen, Pennsylvania, USA, 144 pages, ISBN 978-0764346835. US$34.99 hardcover.

India—Jewels that Enchanted the World
Ed. by Ekaterina Shcherbina, 2014. Indo-Russian Jewellery Foundation, Moscow, Russia, 428 pages, ISBN 978-0992840419. €200 hardcover.

Jewellery in Israel: Multicultural Diversity 1948 to the Present
By Iris Fishof, 2013. Arnoldsche Art Publishers, Stuttgart, Germany, 224 pages, ISBN 978-3897903968. €39.80 hardcover.

Jewels of Ancient Nubia
By Yvonne Markowitz and Denise Doxey, 2014. MFA Publications, Museum of Fine Arts, Boston,

Massachusetts, USA, 240 pages, ISBN 978-0878468072. US$45.00 hardcover.

Legacy: Jewelry Techniques of West Africa
By Matthieu Cheminée, 2014. Brynmorgen Press, Brunswick, Maine, USA, 232 pages, ISBN 978-1929565528. US$45.00 hardcover.

Maison Goossens: Haute Couture Jewelry
By Patrick Mauriès, 2014. Thames & Hudson, London, 224 pages, ISBN 978-0500517703. £40.00 hardcover.

Mastering Torch-fired Enamel Jewelry: The Next Steps in Painting with Fire
By Barbara Lewis, 2014. North Light Books, New York, New York, USA, 144 pages, ISBN 978-1440311741. US$26.99 softcover.

Metal Clay Jewellery
By Natalia Colman, 2014. Search Press Ltd., Tunbridge Wells, Kent, 144 pages, ISBN 978-1782210443. £14.99 softcover.

Michele della Valle: Jewels and Myths
By Michele della Valle, 2014. Antique Collectors' Club, Suffolk, 352 pages, ISBN 978-1851497713. £125.00 hardcover.

Multiple Exposures: Jewelry and Photography
By Ursula Ilse-Neuman, 2014. Officina Libraria, Milan, Italy, 256 pages, ISBN 978-8897737292. £35.00 hardcover.

Navajo Silversmith Fred Peshlakai: His Life & Art
By Steven Curtis, 2014. Schiffer Publishing, Atglen, Pennsylvania, USA, 224 pages, ISBN 978-0764347450. US$50.00 hardcover.

Russian Decorative Arts
By Cynthia Coleman Sparke, 2014. Antique Collectors' Club, Suffolk, 304 pages, ISBN 978-1851497225. £55.00 hardcover.

Sevan Bicakci
By Vivienne Becker, 2014. Assouline Publishing, New York, New York, USA, 192 pages, ISBN 978-1614281924. US$165.00 hardcover.

Silver Treasures from the Land of Sheba: Regional Styles of Yemeni Jewelry
By Marjorie Ransom, 2014. The American University in Cairo Press, Cairo, Egypt, 224 pages, ISBN 978-9774166006. US$49.50 hardcover.

Traditional Jewellery in Nineteenth-Century Europe
By Jane Perry, 2013. V&A Publishing, London, 144 pages, ISBN 978-1851777297. £63.00 hardcover.

Treasures from India: Jewels from the Al-Thani Collection
By Navina Najat Haidar, 2014. Metropolitan Museum of Art, New York, New York, USA, 144 pages, ISBN 978-0300208870. US$40.00 hardcover.

Unique by Design: Contemporary Jewelry in the Donna Schneier Collection
By Suzanne Ramljak, 2014. Metropolitan Museum of Art, New York, New York, USA, 136 pages, ISBN 978-0300208764. US$24.95 softcover.

Untamed Encounters: Contemporary Jewelry from Extraordinary Gemstones
By Mimi Lipton, 2014. Thames & Hudson, London, 245 pages, ISBN 978-0500970638. £60.00 hardcover.

Van Cleef & Arpels
By Berenice Geoffroy-Schneiter, 2014. Assouline Publishing, New York, New York, USA, 80 pages, ISBN 978-1614282181. US$30.00 hardcover.

Precious Metals

Gold
By Kathryn Jones and Lauren Porter, 2014. Royal Collection Trust, London, 120 pages, ISBN 978-1909741102. £25.00 hardcover.

Gold: The Race for the World's Most Seductive Metal
By Matthew Hart, 2014. Simon & Schuster, New York, New York, USA, 304 pages, ISBN 978-1451650037. US$26 hardcover and $16.00 softcover or eBook.

Jackson's Hallmarks
Ed. by Ian Pickford, 2014. Antique Collectors' Club, Suffolk, 184 pages, ISBN 978-1851497751. £9.95 softcover.

Social Studies

Conflict Minerals: Responsible Sourcing Issues and Factors Impacting SEC Rule
Ed. by Gary L. Simmons, 2014. Nova Science Publishers, Hauppauge, New York, USA, 103 pages, ISBN 978-1634633260. US$120.00 hardcover.

The World Came to Tucson
By Katherine Rambo, 2014. Stanegate Press, Tucson, Arizona, USA, 107 pages, ISBN 978-0984754861. US$20 softcover.

DVD

AGTA GemFair Tucson Seminar DVD
2014. American Gem Trade Association, Dallas, Texas, USA. US$50.00.

Shine Bright

Celebrating 20 Years of Opening the World of Jewelry and Gemstones to Everyone!

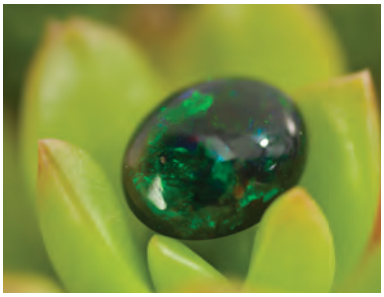

As the largest retailer of loose gemstones in the world, Jewelry Television is committed to offering more of the naturally beautiful treasures that our customers adore.

Education, Expertise & Entertainment

We take pride in our longstanding commitment to education. With programs like our web-based GEM-A course and our on-air Jewel School® series, our partnerships bring industry luminaries straight into the homes of jewelry and gemstone aficionados everywhere.

Educational videos, professional tools of the trade, plus live programming with knowledgeable hosts place Jewelry Television and jtv.com at the forefront of a dynamic learning and shopping environment.

Into the Future

At the heart of our vision is a continuing quest to deliver the rarest of gemstones, plus educational resources and world-class gemstone authorities to our customers. We believe this is the ultimate way to enlighten, inform and entertain, as we take flight into our next decade.

20 yrs
jewelry television®

JTV Your Way

To order call +1 800-619-3000 or visit jtv.com

Literature of Interest

Coloured Stones

Considerations for pricing colored stones. S.M. Robertson and C. Lule, *GemGuide,* **33**(5), 2014, 2–6.

Discussion on the main composition jadeite in jade. T. Ji, M. Sun and W. Chen, *Superhard Material Engineering,* **26**(1), 2014, 52–54 (in Chinese with English abstract).

La Luminescence UV dans les Apatites [UV Luminescence in Apatites]. S. Seguin-Leblan, Diplome d'Universite de Gemmologie, University of Nantes, France, 2014, 78 pp., www.gemnantes.fr/documents/pdf/DUGs/Leblan_DUG.pdf (in French).*

New typology and origin of tsavorite. J. Feneyrol, G. Giuliani, D. Ohnenstetter, B. Rondeau, E. Fritsch, A.E. Fallick, D. Ichang'i and E. Omito. *InColor,* **26**, 2014, 28–34.

Pleochroism in faceted gems: An introduction. R.W. Hughes, *Gems & Gemology,* **50**(3), 2014, 216–226, http://dx.doi.org/10.5741/GemS.50.3.216.*

Progress in the study of color emerging mechanism of turquoise. Q. Guo and Z. Xu, *Acta Petrologica et Mineralogica,* **33**(Supp.), 2014, 136–140 (in Chinese with English abstract).

Residual pressure distribution and visualization of mineral inclusions in corundum: "Application of photoluminescence spectroscopy in relation to sapphires from New England, New South Wales, Australia". A. Abduriyim, N. Kamegata, N. Noguchi, H. Kagi, F.L. Sutherland and T. Coldham, *Australian Gemmologist,* **25**(6–7), 2014, 245–254.

Valuing crazed opal. R.B. Drucker, *GemGuide,* **33**(5), 2014, 12–13.

Diamonds

Beyond Hope: Some other notable diamonds at the Smithsonian Institution—Part 4. R.C. Feather, *Rocks & Minerals,* **89**(6), 2014, 538–540, http://dx.doi.org/10.1080/00357529.2014.949172.

The development of sintered polycrystalline diamond compact (PCD&PDC). Y. Zhao, S. Zhao and S. Yan, *Superhard Material Engineering,* **25**(6), 2013, 53–56, and **26**(1), 2014, 48-51 (in Chinese with English abstracts).

Different precipitation forms of graphite during growth process of different type large diamond crystals. S. Li, D. Song, S. Liu, S. Wang, T. Su, M. Hu, Q. Hu, H. Ma and X. Jia, *Journal of Synthetic Crystals,* **43**(6), 2014, 1525–1528 (in Chinese with English abstract).

Homoepitaxial growth of diamond single crystal on HPHT substrates. L. Yan, Z. Ma, W. Cao, C. Wu, P. Gao and T. Zhang, *Journal of Synthetic Crystals,* **43**(6), 2014, 1420–1424 (in Chinese with English abstract).

New generation of synthetic diamonds reaches the market, part B: Identification of treated CVD-grown pink diamonds from Orion (PDC). B. Deljanin, F. Herzog, W. Bieri, M. Alessandri, D. Günther, D.A. Frick, E. Cleveland, A.M. Zaitsev and A. Peretti, *Contributions to Gemology,* **14,** 2014, 21–40.

New generation of synthetic diamonds reaches the market, part C: Origin of yellow color in CVD-grown diamonds and treatment experiments. A.M. Zaitsev, B. Deljanin, A. Peretti, M. Alessandri and W. Bieri, *Contributions to Gemology,* **14,** 2014, 41–55.

Properties of the natural and CVD synthetic diamonds for identification. Y. Kim, J. Song, Y. Noh and O. Song, *Journal of the Korean Ceramic Society,* **51**(4), 2014, 350–356, http://dx.doi.org/10.4191/kcers.2014.51.4.350 (in Korean with English abstract).*

Fair Trade

'Constructing' ethical mineral supply chains in Sub-Saharan Africa: The case of Malawian fair trade rubies. G. Hilson, *Development and Change,* **45**(1), 2014, 53–78, http://dx.doi.org/10.1111/dech.12069.*

Gem Localities

Cu- and Mn-bearing tourmalines from Brazil and Mozambique: Crystal structures, chemistry and correlations. A. Ertl, G. Giester, U. Schüssler, H. Brätz, M. Okrusch, E. Tillmanns and H. Bank, *Mineralogy and Petrology,* **107**(2), 2013, 265–279, http://dx.doi.org/10.1007/s00710-012-0234-6.*

Fingerprinting of corundum (ruby) from Fiskenæsset, west Greenland. N. Keulen and P. Kalvig, *Geological Survey of Denmark and Greenland Bulletin,* **28**, 53–56, http://www.geus.dk/publications/bull/nr28/nr28_p53-56.pdf.*

Gemmological and spectroscopic characteristics of haüyne from Germany. T. Lei, Y. Yu and Q. Jiang, *Journal of Gems & Gemmology,* **16**(2), 2014, 32–37 (in Chinese with English abstract).

Compiled by Brendan Laurs

* Article freely available for download, as of press time.

Nephrite jade from Guangxi Province, China. Z. Yin, C. Jiang, M. Santosh, Q. Chen, Y. Chen and Y. Bao, *Gems & Gemology,* **50**(3), 228–235, http://dx.doi.org/10.5741/GEMS.50.3.228.*

Origin of tanzanite and associated gemstone mineralization at Merelani, Tanzania. C. Harris, W. Hlongwane, N. Gule and R. Scheepers, *South African Journal of Geology,* **117**(1), 2014, 15–30, http://dx.doi.org/10.2113/gssajg.117.1.15.

Sarcolite del Vesuvio: Una storia ottocentesca riscoperta dopo il taglio di una favolosa gemma [Sarcolite from Vesuvius: A history of the nineteenth-century rediscovery after cutting a fabulous gem]. A. Guastoni, *Rivista Mineralogica Italiana,* **4**, 2013, 244–252 (in Italian).

Spectroscopic characteristics study of morganite from Mozambique. Z. Yin, X. Li, D. Bao, Q. Chen and M. Zhang, *Spectroscopy and Spectral Analysis,* **34**(8), 2014, 2175–2179 (in Chinese with English abstract).

Sri Lanka: Expedition to the island of jewels. A. Lucas, A. Sammoon, A.P. Jayarajah, T. Hsu and P. Padua, *Gems & Gemology,* **50**(3), 174–201, http://dx.doi.org/10.5741/GEMS.50.3.174.*

A study of ruby (corundum) compositions from the Mogok belt, Myanmar: Searching for chemical fingerprints. G.E. Harlow and W. Bender, *American Mineralogist,* **98**(7), 2013, 1120–1132, http://dx.doi.org/10.2138/am.2013.4388.

Topaz of the Zabytoe deposit, Primorsky Krai, Russia. O.V. Stepanov, V.A. Pakhomova, D.G. Fedoseev, S.Y. Buravleva, O.A. Karas and V.B. Tishkina, *Journal of the Gemmological Association of Hong Kong,* **35**, 2014, 71–72, http://www.gahk.org/journal/GAHK_Journal_2014_v4.pdf.*

The unique attributes of Australian precious opal. A. Smallwood, *Australian Gemmologist,* **25** (6–7), 2014, 207–230.

Vanadium-rich ruby and sapphire within Mogok gemfield, Myanmar: Implications for gem color and genesis. K. Zaw, L. Sutherland, T.F. Yui, S. Meffre and K. Thu, *Mineralium Deposita,* 2014 [no vol. or page no.], 1–15, http://dx.doi.org/10.1007/s00126-014-0545-0.

Yellow gem plagioclase from Cenozoic basalts, eastern Australia, identity and origin. F.L. Sutherland, A. Abduriyim, R.E. Pogson, G.B. Sutherland and R. Wuhrer, *Australian Gemmologist,* **25**(6–7), 2014, 231–238.

Historical Gemmology

Du Turkestan à la Birmanie: La quête du jade dans les sources chinoises, 1ère partie [From Turkestan to Burma: The quest for jade from Chinese sources]. L. Long, *Revue de Gemmologie A.F.G.,* **189,** 2014, 10–17 (in French).

La vente des diamants, perles et pierreries provenant de la collection dite des joyaux de la Couronne de France en mai 1887 [The sale of diamonds, pearls and precious stones said to be from the collection of the French Crown Jewels in May 1887]. G. Riondet, *Revue de Gemmologie A.F.G.,* **189**, 2014, 18–23 (in French).

Mughal gems in context. J. Ogden, *InColor,* **26,** 2014, 36–47.

Instruments

A portable *versus* micro-Raman equipment comparison for gemmological purposes: The case of sapphires and their imitations. G. Barone, D. Bersani, V. Crupi, F. Longo, U. Longobardo, P. Paolo Lottici, I. Aliatis, D. Majolino, P. Mazzoleni, S. Raneri and V. Venuti, *Journal of Raman Spectroscopy,* **45**(11–12), 2014, 1309–1317, http://dx.doi.org/10.1002/jrs.4555.

Presidium Synthetic Ruby Identifier. E.B. Hughes, *InColor,* **26,** 2014, 18–23.

La spectrométrie d'émission accessible à tous, 2nd partie [Portable emission spectrometry, part 2]. D. Peyresaubes, M. Schoor and J.-C. Boulliard, *Revue de Gemmologie,* **189**, 2014, 26–29 (in French).

News Press

Ancients used nanotechnology to make jewellery. The Daily Telegraph (Sydney, Australia), 25 July 2013, http://tinyurl.com/o6gd9j3.*

China's pearl industry: An indicator of ecological stress. L. Cartier and S. Ali, *Our World*, 23 January 2013, http://ourworld.unu.edu/en/chinas-pearl-industry-an-indicator-of-ecological-stress.*

Diamond hunters give up search for gems too hard to find. T. Biesheuvel, *Bloomberg,* 3 October 2014, www.bloomberg.com/news/2014-10-02/diamond-hunters-give-up-search-for-gems-too-hard-to-find.html.*

The rise of eco-friendly pearl farming. B. Howard, *National Geographic,* 11 August 2013, http://news.nationalgeographic.com/news/2013/08/130811-eco-friendly-pearl-farming-kamoka-polynesia-oysters-environment.*

Searching for Burmese jade, and finding misery. D. Levin, *New York Times,*1 December 2014, www.nytimes.com/2014/12/02/world/searching-for-burmese-jade-and-finding-misery.html.*

Synthetics pose a conundrum for world diamond industry. A. Rabinovitch, *Reuters News Agency,* 31 July 2014, http://af.reuters.com/article/topNews/idAFKBN0G01LR20140731?pageNumber=1&virtualBrandChannel=0.*

Organic Gems

Micro-Raman investigation of pigments and carbonate phases in corals and molluscan shells. L. Bergamonti, D. Bersani, S. Mantovan and P. Paolo Lottici, *European Journal of Mineralogy,* **25**(5), 2013, 845–853, http://dx.doi.org/10.1127/0935-1221/2013/0025-2318.

Raman spectroscopic study of the formation of fossil resin analogues. O.R. Montoro, M. Taravillo, M. San Andrés, J.M. de la Roja, A.F. Barrero, P. Arteaga and V.G. Baonza, *Journal of Raman Spectroscopy,* **45**(11–12), 1230–1235, http://dx.doi.org/10.1002/jrs.4588.

Pearls

Characteristics of trace elements in freshwater and seawater cultured pearls. E. Zhang, F. Huang, Z. Wang and Q. Li, *Spectroscopy and Spectral Analysis,* **34**(9), 2014, 2544–2547 (in Chinese with English abstract).

Observations on pearls reportedly from the Pinnidae family (pen pearls). N. Sturman, A. Homkrajae, A. Manustrong and N. Somsa-ard, *Gems & Gemology,* **50**(3), 202–215, http://dx.doi.org/10.5741/GEMS.50.3.202.*

Phase analysis of $CaCO_3$ in gold pearl. Z. Xu, Q. Guo and R. Li, *Acta Petrologica et Mineralogica,* **33**(Supp.), 2014, 157–161 (in Chinese with English abstract).

The unique reflection spectra and IR characteristics of golden-color seawater cultured pearl. J. Yan, J. Tao, X. Deng, X. Hu and X. Wang, *Spectroscopy and Spectral Analysis,* **34**(5), 2014, 1206–1210 (in Chinese with English abstract).

Synthetics and Simulants

Corindons Synthétiques Verneuil entre Polariseurs Croisés suivant l'Axe Optique: les Lignes de Plato [Verneuil Synthetic Corundum between Crossed Polarizers along the Optic Axis: Plato Lines]. C. Vasseur, Diplome d'Universite de Gemmologie, University of Nantes, France, 2014, 138 pp., www.gemnantes.fr/documents/pdf/DUGs/Vasseur_DUG.pdf (in French).*

Fabrication of artificial gemstones from glasses: From waste to jewelry. N. Srisittipokakun, Y. Ruangtaweep, M. Horprathum and J. Kaewkhao, *AIP Conference Proceedings,* **1617**, 2014, 120–125, http://dx.doi.org/10.1063/1.4897119.*

Research on identifications of lapis lazuli imitations. Z. Wu, S. Wang, X. Ling and M. Yuan, *Acta Petrologica et Mineralogica,* **33**(Supp.), 2014 141–145 (in Chinese with English abstract).

Treatments

Effects of heat treatment on red gemstone spinel: Single-crystal X-ray, Raman, and photoluminescence study. R. Widmer, A.-K. Malsy and T. Armbruster, *Physics and Chemistry of Minerals,* 2014 [no vol. or page no.], http://dx.doi.org/10.1007/s00269-014-0716-7.

Influence of temperature on surface colouration of the lead oxide treated natural gem ruby. R.K. Sahoo, B.K. Mohapatra, S.K. Singh and B.K. Mishra, *Advanced Science Letters,* **20**(3–4), 2014, 622–625, http://dx.doi.org/10.1166/asl.2014.5390.

Some problems deserving attention in identifying the filled gems by the 3036 and 3058 cm^{-1} peaks of the FTIR spectra. J. Li, D. Li, G. Shan, X. Ding and Y. Cheng, *Acta Petrologica et Mineralogica,* **33**(Supp.), 2014, 106–110 (in Chinese with English abstract).

Studies of colored varieties of Brazilian quartz produced by gamma radiation. C.T. Enokihara, R.A. Schultz-Güttler, P.R. Rela and W.A.P. Calvo, *Nukleonika,* **58**(4), 2013, 469–474, www.nukleonika.pl/www/back/full/vol58_2013/v58n4p469f.pdf.*

A theoretical and experimental study of the heat treatment of opaque Thai sapphire to transparent blue sapphire. T. Sripoonjan, B. Wanthanachaisaeng and C. Sutthirat, *Australian Gemmologist,* **25**(6–7), 2014, 239–244.

Two pieces of sapphire treated by Be and Ti multiple diffusion. J. Li, Y. Qi, G. Shan and D. Li, *Journal of Gems & Gemmology,* **16**(2), 2014, 27–31 (in Chinese with English abstract).

Compilations

Gem News International. Aquamarine with strong dichroism • Color-changing garnet inclusion in diamond • Topazolite from Mexico • Large baroque *Tridacna gigas* pearl • Coated fire opal • IMA conference report. *Gems & Gemology,* **50**(3), 244–249, www.gia.edu/gems-gemology.*

Lab Notes. Irradiated and coated brown diamond • Mixed-type cape diamond • Yellow diamond with xenotime inclusion • CVD synthetic diamonds—with unusual inclusions, Fancy Dark gray, irradiated • *Spondylus* pearls • Flame-fusion synthetic ruby with flux synthetic ruby overgrowth. *Gems & Gemology,* **50**(3), 236–243, www.gia.edu/gems-gemology.*

Gem-A

THE GEMMOLOGICAL ASSOCIATION
OF GREAT BRITAIN

Changing the world one business decision at a time

Corporate Social Responsibility (CSR) is changing the industry — and the world — for the better. That's why we're offering our NEW **CSR for the Jewellery Professional** course, in collaboration with the World Jewellery Confederation Education Foundation (WJCEF) and Branded Trust.

Specifically tailored to the jewellery industry, this course will provide you and your business with an essential foundation in Corporate Social Responsibility.

Featuring **six online lectures** delivered by experts in ethics and the jewellery industry, **downloadable course notes** and the **ability to study from anywhere**, you can start changing the world for just £595.

For more information or to book, contact **education@gem-a.com.**

Branded Trust
Education

WJCEF

Understanding Gems

Join us.

The Gemmological Association of Great Britain, 21 Ely Place, London, EC1N 6TD, UK. T: +44 (0) 20 7404 3334 F: +44 (0) 20 7404 8843. Registered charity no. 1109555. A company limited by guarantee and registered in England No. 1945780. Registered Office: 3rd Floor, 1-4 Argyll Street, London W1F 7LD.

And I saw as it were

a sea of glass

mingled with fire.

— Revelation 15:2

Pala International

Palagems.com / Palaminerals.com

+1 800 854 1598 / +1 760 728 9121

Aquamarine, Madagascar • 20.36 ct • 14.12 x 14.12 x 9.83 mm

Photo: Mia Dixon